Graz University of Technology

Markus STAUD, BSc
1031556

Modelling the in-vehicle PM2.5-concentration

Master's Thesis

In cooperation with BMW China.

Institute of Automotive Engineering

Supervisor - TU Graz: Ass.Prof. Dipl.-Ing. Dr.techn. Univ.-Doz. Mario Hirz
Supervisor - BMW Group: Dr. Thomas Lindberg

Beijing, September 2015

This document is set in Palatino, compiled with pdfLaTeX2e and `Biber`.

The LaTeX template from Karl Voit is based on KOMA script and can be found online: https://github.com/novoid/LaTeX-KOMA-template

Sperrvermerk

Die Arbeit beinhaltet vertrauliche Informationen, die der Geheimhaltung unterliegen. Aus diesem Grund darf die Arbeit ohne vorherige schriftliche Zustimmung der BMW Group nicht vervielfältigt oder veröffentlicht werden.
Dieser Zustimmungsvorbehalt endet am: 31. 10. 2017.

Acknowledgements

First and foremost I want to express my deep sense of gratitude to my two supervisors from BMW China Services, Dr. Thomas Lindberg and Simo Bian, for their perpetual support and belief in my work. Not only did they inspire and guide me in a vocational way, but they also helped to develop myself personally.
My appreciation also extends to our team of EC-130. They created an invaluable experience for me, both professionally and culturally and I am happy to say that I have not only found competent colleagues but genuine friends. Thanks also go to all the other interns and colleagues at BMW and BBA in China for blessing me with joy aside from work and exploring Asia's hidden secrets and mysteries together with me.
Moreover, I would like to express my appreciation for my supervisor from Graz University of Technology, Dr. Mario Hirz, for enabling me to write this thesis in China and revising its content. In terms of revising, I also want to highlight the efforts of Verena Kremsner, Dr. Ana Torvisco, James Kepner and, above all, Siddarth Sreeram who revised and corrected this paper as proficient English speakers.
Finally, I want to thank my family and friends, for without them I would never have come this far. Your endless support empowers me to thrive for new achievements every day and I cannot emphasize enough how important your company and trust are to me.

非常感谢!
Vielen Dank!
Thank you very much!

Markus Staud

Statutory Declaration

I declare that I have authored this thesis independently, that I have not used other than the declared sources/resources, and that I have explicitly marked all material which has been quoted either literally or by content from the used sources.

Graz, _____ _____

Date Signature

Eidesstattliche Erklärung[1]

Ich erkläre an Eides statt, dass ich die vorliegende Arbeit selbstständig verfasst, andere als die angegebenen Quellen/Hilfsmittel nicht benutzt, und die den benutzten Quellen wörtlich und inhaltlich entnommenen Stellen als solche kenntlich gemacht habe.

Graz, am _____ _____

Datum Unterschrift

[1] Beschluss der Curricula-Kommission für Bachelor-, Master- und Diplomstudien vom 10.11.2008; Genehmigung des Senates am 1.12.2008

Abstract

This thesis provides a feasibility study for modelling the in-vehicle PM2.5 concentration. A generic model is proposed, incorporating various key characteristics of the vehicle, as well as the ambient aerosol the vehicle is exposed to. An approach for modelling the deterioration of the cabin filter was proposed but could not be verified with the given equipment and was therefore not incorporated into the concentration model. Ventilation speed, air circulation mode, window and door openings, and vehicle speed actively influence the in-vehicle PM2.5-concentration and can therefore be seen as inputs of the model. Vehicle-specific parameters that influence the concentration have been identified as air-exchange rate, deposition rate, filter efficiency and filter leakage. A detailed guideline to determine the model's parameters is presented and the obtained results for a specific test vehicle are shown. All experiments were conducted in Beijing, China in the time from April to September 2015. After all the parameters had been obtained, validation test drives were conducted and statistically evaluated. The evaluation shows promising results and indicates that the proposed model can indeed be used in real-world applications. Various use-cases are concluded from the results and presented in the end. In the evaluation of the results, as well as the conclusion, it is assumed that in the future an on-board PM2.5 sensor will be available, measuring the in- and outside concentration of the vehicle. Unfortunately, a prototype of this sensor was not available at the time the experiments in the course of this thesis were conducted. However, in order to commercially exploit the model, further research and investigations, especially using other vehicle types and models, have to be conducted.

Contents

1 Introduction

What is air pollution?
According to the World Health Organisation (WHO), air pollution is defined as *the contamination of the indoor and outdoor environment by any chemical, physical or biological agent that modifies the natural characteristics of the atmosphere* [1]. That said, there is substantial evidence that air pollution causes millions of premature deaths worldwide (see section 2.1). The average American adult spends 101 minutes a day in his or her car [2], in relation to an average lifespan of 79 years [3], that is 5.5 years or 7% of his or her lifetime. To reduce the exposure to air pollution for their customers, BMW is therefore highly interested in offering them a clean air environment by improving the in-vehicle air quality. One of the markets exhibiting particularly bad air quality is, beyond doubt, China. Fuelled by the rapid growth of the Chinese economy in recent years, the increased demand for energy and resources as well as the increase in individual transportation caused shocking levels of air pollution throughout the last few years. Publications on the adverse effects of particulate matter as a pollutant raised the public awareness. PM2.5, the mass concentration of particulate matter smaller than 2.5μm, was introduced and became a publicly known indicator. Companies that offered solutions for indoor air cleaning devices emerged, creating a whole new business field. However, standard configuration solutions for in-vehicle air quality monitoring and improvement are still scarce and rarely provided by the manufacturer itself. A formidable market for after-sales solutions has formed, offering a wide range of products varying in price and quality. Thus, BMW aims to meet the demand for effective, reliable air-quality monitoring and improvement systems by providing a holistic standard equipped solution.
Before attending to an in-depth examination of the physical behaviour of particulate matter, a short target evaluation should verify the need of monitoring and filtering it. A basic understanding of how particles affect the human health is hereby tried to be conveyed. Extremely contaminated areas like China are discussed, to further corroborate a requirement for an in-vehicle air cleaning system. The thesis then explores different ways of obtaining the in-vehicle air pollution level. Different approaches are presented in order to obtain characteristics that influence the in-vehicle concentration of particulate matter. Aside from the practical requirements by BMW, several research questions shall be answered in the course of this thesis.

The following four research questions form the basis of this work:

Is there a way to model the in-vehicle concentration of PM2.5?
An extensive literature research should provide fundamental information on whether there have already been attempts to model the air quality inside vehicles or similar enclosed structures. Based on the findings, the question of feasibility should be answered. If feasible, an improved model should be derived from previously published work.

How can the parameters of that model be determined in practice?
Once the model has been proposed, it is applied to a real use case. Therefore, the parameters of the model have to be obtained numerically and in a simple way that could optimally be reproduced. Several experiments are presented and discussed, providing one or more of the model's parameters when properly executed.

Can the model provide feasible estimates under real conditions?
Having experimentally determined all model parameters, the model has to be validated in a real environment. A statistical evaluation should quantify the quality of the model and illustrate whether it is able to provide feasible estimates when exposed to real input quantities.

How can the obtained model be used in a real-world application?
As the model should perform under real conditions, ways of exploiting it should be found. While every model is constrained and limited to some degree, these limitations and constraints should be pointed out and be subject to further discussion.

With all these questions answered, a further outlook and implications for improvements and future work can be made.
The thesis is divided into five chapters. While this introduction is already the first one, the second chapter elaborates previous work and the contemporary understanding of particulate matter and its properties. Based on this theoretical backing the third chapter elucidates the chosen methodology and explains how the results of this work were obtained. In chapter four, the results of the applied methods from the methodology chapter are presented and interpreted. The last chapter links the obtained results to results from past work and distinguishes them from previous approaches. Limitations and constraining assumptions are discussed and an analysis of applicability to real-world conditions is made. Finally, these conclusions are used for further implications on this topic.

2 Related Work

This chapter provides an overview on relevant research conducted on similar topics in the past. It aims to give the reader a basic understanding of what the current state of the art in aerosol science and engineering is. Nonetheless, the author is trying to incorporate only the basic theory needed to understand the science behind the methodology applied to obtain the results this thesis presents. For further information on these topics, the reader ought to feel encouraged to have a look at the referred literature.

2.1 Health impacts of PM2.5

In a recent article, Kim et al. [4] provide an extensive overview of how airborne particulate matter affects the human health. Also chapter 11 of Hinds extensive book of reference on aerosols provides insightful work on how particulate matter is influencing the human respiratory system. Particles mainly enter the human body through the human respiratory system and it is proven that a particle's size is the key factor for particle induced health problems. A common conception is, that the smaller a particle's size, the more hazardous its impact on human health.
To understand this impact of PM on the human body, the basic functionality of the human respiratory system has to be understood. In general, the respiratory system can be divided into three parts, consisting of different parts of the body and representing somewhat the lines of defence of the body. First, there is the nasopharyngeal zone, including nose, mouth, pharynx and larynx. Then there is the tracheobronchial system, consisting of the airways from trachea to the terminal bronchioles. At last the gas exchange takes place in the respiratory region, consisting of the respiratory bronchioles holding the alveoli. At rest, the respiratory rate of an average adult is between 12 and 20 breaths per minute (inhalation-exhalation-cycles). During heavy workout, this figure can easily triple. For the tidal volume of air (effective volume of air inhaled and exhaled at rest), 0.5 litres are average at rest. However, an average adult man can force inhale up to 3 more litres and force exhale up to 1.1 litres more than during quiet breathing. The minimum residual volume of air that can not be exhaled is 1.2 litres on average. These figures are based on measurements on adult men, women, smokers and obese people tend to have less than that on average, while tall people and people living at high altitudes tend to have more than that.
The deposition of particles can now be divided into the deposition in each zone, nasopharyngeal, tracheobronchial and respiratory. Figure 2.1 illustrates the anatomic structure of the human respiratory system, as well as diagrams showing where

particles deposit, depending on their size.

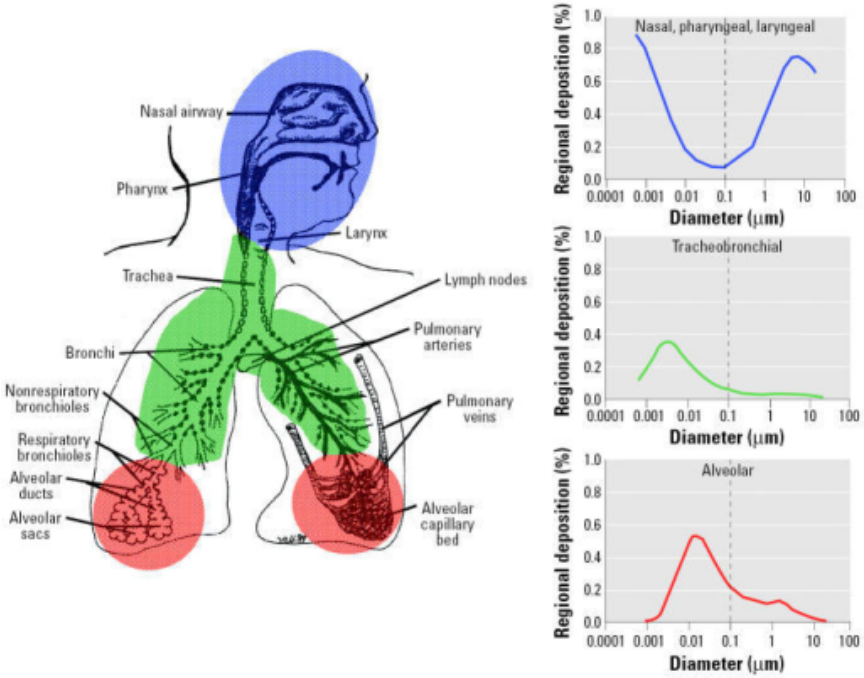

Figure 2.1: Overview of the different regions of the respiratory system. Courtesy of J. Harkema.

Air is inhaled either by nasal or oral breathing. In the nasal cavity, the cilia (microscopic hair-like structures covering the surface of the nasopharyngeal and tracheobronchial region to a large extent) as well as mucus are very effective in removing coarse particulate matter larger than 10μm. The remaining fraction of course particles deposits in the trachea or, at the latest, in the bronchi. In order to transport the deposited particles, the body produces mucus which is then "pumped" up the trachea by the cilia, beating in coordinated waves. This mechanism is also referred to as the "mucociliary escalator". To expectorate mucus, the body is initiating reflexes as sneezing and coughing, mechanically removing the settled particulate matter. Particles in a size range smaller than 1nm are subject to vigorous Brownian motion (see section 2.4.6) thus, they also tend to adhere to a surface before entering the bronchioles. The most important clearance mechanism in the alveolar region is due to macrophages, through phagocytosis of particles. Translated from Greek, macrophage means "big eater", describing the function of this type of white bloods cells very well. In the process of phagocytosis, macrophages devour and digest substances which they identify as foreign to the body. After a macrophage's capacity is saturated, it will move towards the mucociliary escalator, to be expectorated. Comprehensive work on macrophages and other clearance mechanisms has been coined by Oberdörster et al. [5]. In their contribution, they focus on the health impact of ultrafine particles (UFP) which are in a particle size range of below 300nm. In the course of their work they present the results of an interesting in-vivo study, conducted on rodents.

These rodents were exposed to different monodisperse (see section 2.4.2) aerosols. After 24 hours, their stomachs were lavaged, recovering around 80% of alveolar macrophages. As can be seen in figure 2.2, around 80% of 0.5, 3 and 10μm particles could be recovered examining the extracted macrophages. For particles of 15-20 and 80nm in diameter, however, only 20% could be recovered from the macrophages. Thus, Oberdörster et al. conclude, that the rest of the particles translocated either in epithelial cells (the membranous tissue covering the lungs) or even further into the bloodstream. Once in the circulatory system, particles are distributed throughout the body. Here, liver and spleen are the major sites, as they accumulate most of the macrophages in the body. However, translocation to heart, kidney and bone marrow have also been reported, as well as distribution to the central nervous system.

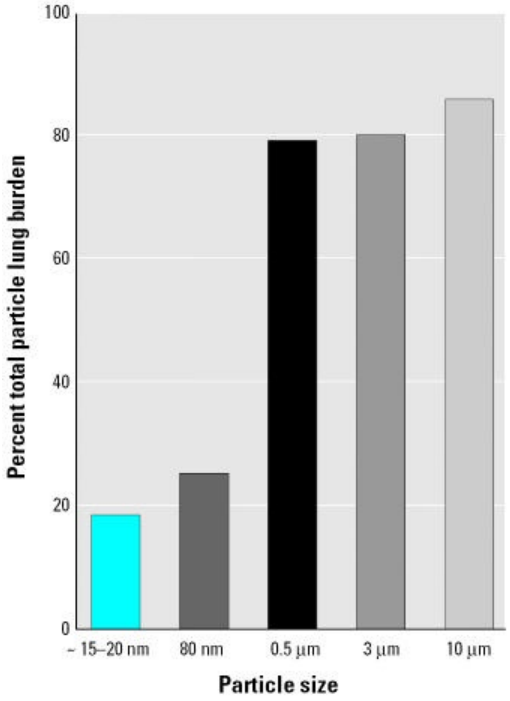

Figure 2.2: Percentage of recovered particulate mass by particle size in the experiments conducted by Oberdörster et al.

Numerous human diseases have been linked to exposure of particulate matter. Kim et al. [4] compiled a multitude of articles exploring noxious effects linked to particulate matter exposure. From these contributions, they list significant correlations of particulate matter exposure to premature death, chronic bronchitis, asthma, pneumonia, diabetes, cardiovascular diseases and cancer.
Regarding the mortality of particulate matter pollution, the WHO conducted a large-scaled study in 2012, with the result that an estimate of 7 million deaths were attributable to air pollution, with an estimate of 3.7 million deaths due to ambient PM2.5 [6]. Around 2.61 of deaths occur in the Western Pacific region and the South-

East Asian region alone, which is about 70% of the total mortality. Figure 2.3 shows the percentage of main mortal diseases caused by ambient PM2.5.

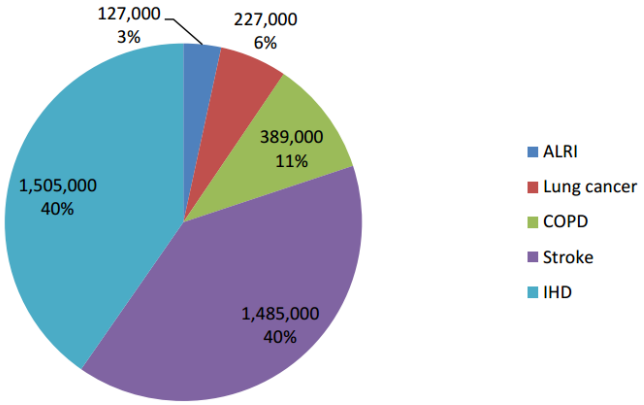

Figure 2.3: Deaths attributable to ambient PM2.5 exposure in 2012, by disease

ALRI . . . Acute lower respiratory disease
COPD . . . Chronic obstructive pulmonary disease
IHD . . . Ischaemic heart disease

To categorize the noxiousness of PM2.5 as a pollutant, the WHO defined certain guideline concentration levels which should not be exceeded.
For PM2.5, the guideline values are:

$$10\mu g/m^3 \text{ annual mean}$$
$$25\mu g/m^3 \text{ 24-hour mean}$$

Based on these values, different national and international institutions defined their own guideline values. In the US, the Environmental Protection Agency (EPA) is the responsible institution for air quality standards. In Europe (i.e. the EU), the European Environment Agency (EEA) is in charge of air quality related standards. For China, the Ministry of Environmental Protection (MEP) defines air quality standards and enforces them.
The following table compares the standards of the US, China and the EU as reported by Kim et al. [4]:

Average -	Country -	PM2.5 $\mu g/m^3$
annual	US	12
	CN	35
	EU	25
daily	US	35
	CN	75
	EU	not defined

2.2 Air quality in China

As aforementioned, 70% of deaths due to ambient air pollution occur in the West Pacific and South-East Asian regions combined. Using the same model as the WHO, a recent study conducted by Rohde and Muller [7] estimates the ambient particulate matter exposure attributed deaths in China even at 1.6 millions per year, or in between 0.7 and 2.2 millions at 95% confidence. Relative to all annual deaths in China, these are around 17%.
The following table shows the Top 15 ranking of annual PM2.5 burden for each country, as compiled by the WHO [8]:

Rank -	Country -	PM2.5 $\mu g/m^3$	PM10 $\mu g/m^3$
1	Pakistan	101	282
2	Qatar	92	165
3	Afghanistan	84	286
4	Bangladesh	79	163
5	Iran	76	127
6	Egypt	74	136
7	Mongolia	64*	140
8	U.A.E	61*	161
9	India	59*	134
10	Bahrain	57	254
11	Nepal	50*	114
12	Ghana	49	98
13	Jordan	48*	128
14	**China**	41*	90
15	Bulgaria	41	58

Figures with an asterisk* are not entirely based on measured data, but partly converted from PM10 to PM2.5, using regional conversion factors.

As can be seen, China ranks at 14^{th} position, but considering the affected number of people, it is in second place only behind India. However, in the most recent issue of "The Little Green Data Book", released annually by the World Bank [9], China is in second spot with an average annual PM2.5 concentration of $73 \mu g/m^3$, only topped by the U.A.E. with an average annual PM2.5 concentration of $90 \mu g/m^3$. Regardless which statistic is more accurate, it can not be denied, that air pollution by particulate matter is a serious issue in China. Especially the region around Beijing is subject to heavy pollution throughout the year. The following table compares the ten most polluted Chinese cities to the Top 5 worldwide, again, according to the WHO [8]:

Rank -	City -	Country -	PM2.5 $\mu g/m^3$	PM10 $\mu g/m^3$
1	India	Delhi	153	286
2	India	Patna	149	164
3	India	Gwalior	144*	329
4	India	Raipur	134*	305
5	Pakistan	Karachi	117	273
36	China	Lanzhou	71*	155
61	China	Urumqi	61*	133
70	China	Xi'An	58*	126
72	China	Xining	57*	124

Figures with an asterisk* are not entirely based on measured data, but partly converted from PM10 to PM2.5, using a regional conversion factor.

According to this list, Beijing is in fifth spot in China, with an annual PM2.5 concentration twice as high as the correspondent WHO guideline value. During the time this thesis was composed (April 1^{st} to September 7^{th} 2015), the average ambient PM2.5 concentration was $56\mu/m^3$. However, the cold seasons tend to have more days with higher concentration, as domestic fuels add to the concentration level. Figure 2.4 shows the trend in China, colour coded using the Chinese AQI standard colours (see next subsection).

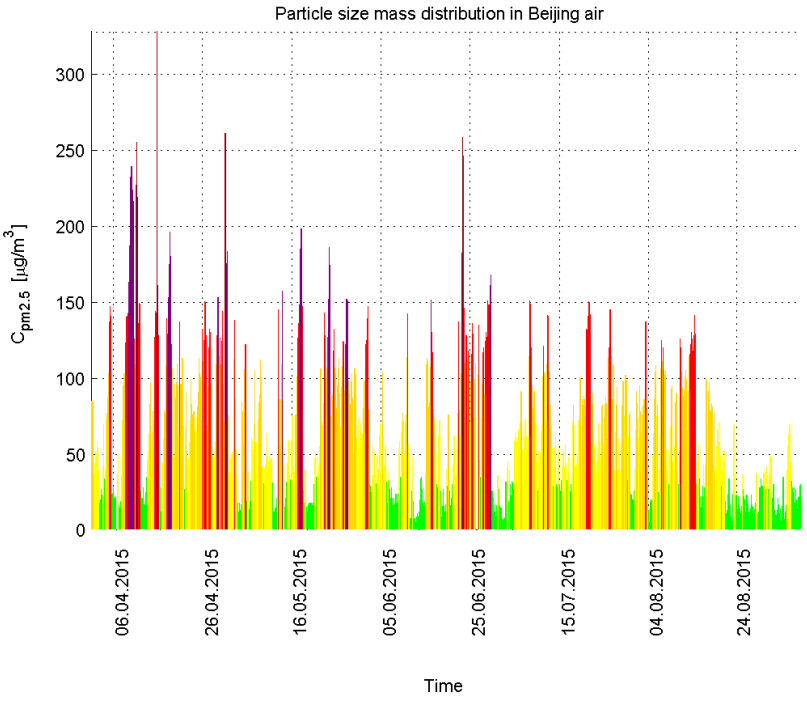

Figure 2.4: Trend of ambient PM2.5 concentrations in Beijing from April 1^{st} to September 7^{th} 2015

To get a better understanding of how heavy local air pollution affects everyday life, figure 2.5 compares the visible effect of two different air pollution levels on different days during summer 2015 in Beijing.

Figure 2.5: The view from the BMW office building in Beijing, at two different ambient pollution levels, courtesy of Ms Anthea Viragh

To improve the situation in Beijing, the government announced certain countermeasures. In 2013 they established "The Airborne Pollution Prevention and Control Action Plan", intending to improve the air quality by defining ten measures such as reducing coal use, installing exhaust gas filters in cars and industrial plants and renewing outdated industrial facilities. The ultimate goal for the Beijing-Tianjin-Hebei Province is to reduce annual PM2.5 pollution by 25% by the year 2017 (see announcement of the MEP [10]). In order to limit the exhaust from combustion engine vehicles in Beijing, a ban-day regulation was imposed. As such, it prohibits conventional fossil fuelled vehicles from entering Beijing's 5^{th} ring road one day a week, depending on the last digit of their license plate. Each working day of the week two digits are banned. During certain events (the APEC meeting in 2014, the 70^{th}

anniversary of the end of WWII in 2015) the government even imposed an even-odd ban-day regulation, reducing the individual traffic by 50%.
A considerable fraction of pollution in Beijing is caused by the emissions of steel factories in the surrounding Hebei province. Based on data provided by the World Steel Association [11], China is by far the world's biggest crude steel manufacturer representing 48% of the global steel market with a total production volume of 822.7 million tons in 2014. According to a recently published article by Reuter's [12], around 23% of those 822.7 million tons were produced in Hebei province (185.3 millions), which is more than twice as much as the entire US and more than the second biggest steel producer worldwide, Japan. However, due to careless treatment of waste emissions resulting from the production process, steel production is a major reason for air pollution in Beijing. Figure 2.6 shows a steel production site in Yuanbaoshan, Hebei, illustrating the grotesque view of exhaust gas being pumped into the atmosphere in billows.

Figure 2.6: Steel plant in Yuanbaoshan, Hebei, copyright by Lu Guang, Greenpeace

The government in Beijing announced to cut down steel production in Hebei province by 60 million tons, as well as closing down smaller, outdated plants and enforcing the use of advanced exhaust-gas systems. Yet, it remains to be seen, whether and in which extent these measures are implemented and enforced.

2.2.1 Air quality index (AQI)

To define a common standard to rate the noxiousness of the concentration of each pollutant present in the regional atmosphere, the AQI was created. The AQI system assigns an index to the concentration level of each pollutant, the so-called Individual Air Quality Index, or simply IAQI.
Currently, the IAQI is evaluated for six major pollutants:

- PM2.5, particulate matter with a particle size smaller or equal to 2.5μm
- PM10, particulate matter with a particle size smaller or equal to 10μm
- O_3, ozone
- SO_2, sulfur dioxide
- NO_2, nitrogen dioxide
- CO, carbon monoxide

The official Chinese standard for the calculation of the IAQI for PM2.5 is defined by the MEP [13]. It is calculated as:

$$IAQI_{PM2.5} = \frac{IAQI_{hi} - IAQI_{lo}}{BP_{hi} - BP_{lo}} (C_{PM2.5} - BP_{lo}) + IAQI_{lo} \tag{2.1}$$

with
$IAQI_{PM2.5}$ being the individual air quality index for PM2.5
$C_{PM2.5}$ being the 24-hours average of PM2.5 concentration
BP_{lo} being the concentration breakpoint that is $\leq C_{PM2.5}$
BP_{hi} being the concentration breakpoint that is $\geq C_{PM2.5}$
$IAQI_{lo}$ being the index breakpoint that is $\leq C_{PM2.5}$
$IAQI_{hi}$ being the index breakpoint that is $\geq C_{PM2.5}$

As the Chinese standard was derived from the US standard [14], the formula to calculate the AQI is the same, however, at lower concentration ranges, the breakpoints are different, resulting in the Chinese AQI being lower than the US AQI for the same PM2.5 concentration in $\mu g/m^3$. The breakpoints for the calculation of the AQI are represented in the following table:

IAQI breakpoints for PM2.5, CN

IAQI	PM2.5 breakpoint
0	0
50	35
100	75
150	115
200	150
300	250
400	350
500	500

IAQI breakpoints for PM2.5, US/EPA

IAQI	PM2.5 breakpoint
0	0
50	12
100	35.5
150	55.5
200	150.5
300	250.5
400	350.5
500	500

As an example, an ambient PM2.5 concentration of $70\mu g/m^3$ would calculate to an IAQI of 158 according to US standard, but would only lead to an IAQI of 94 in the Chinese standard, due to the differently distributed break points. Beside the different breakpoints, the US/EPA standard is also using a different wording to classify the level of air pollution:

AQI	Air Pollution Level CN	Air Pollution Level US/EPA
0-50	Excellent	Good
51-100	Good	Moderate
101-150	Lightly Polluted	Unhealthy for Sensitive Groups
151-200	Moderately Polluted	Unhealthy
201-300	Heavily Polluted	Very Unhealthy
300-400	Severely Polluted	Hazardous
400-500	Severely Polluted	Very Hazardous

These differences in calculating/naming the current level of air pollution can be confusing and are not certain to be known by the general public. Hence, the implementation of a sensor system requires careful thought of how to communicate the current level of PM2.5 to the customer.

2.3 Characteristics of gaseous fluids

Particulate matter is always carried along by some kind of fluid. In the specific case this thesis addresses, the fluid is what is commonly referred to as *air*, a mixture of different gaseous fluids. Per definition standard dry air consists of [15]:

Species	Percentage
Nitrogen	78.02
Oxygen	20.946
Argon	0.916
Rest	0.118

Realistically, a temperature range of -20°C to 40°C covers most of the ambient temperature conditions in a natural environment. Thus, the calculations in this section refer mainly to this range and are only valid within those limits, unless otherwise specified.
Depending on its temperature (and the atmospheric pressure), air can also hold only a certain capacity of water vapor. The so-called relative humidity of air is defined as the ratio of the partial pressure of water vapor in the gaseuos mixture of air, to the equilibrium vapor pressure of water at a given temperature.

$$RH = \frac{P_v}{P_{sv}} \tag{2.2}$$

The partial pressure P_v is defined as the imaginary pressure of water vapor if it was the only gas in the gaseous mixture occupying the mixture's total volume. The equilibrium vapor pressure P_{sv} is the pressure at which the water vapor is in thermodynamic equilibrium with its condensed (liquid or solid) state. For water the Magnus equation is an easy and well-perfoming approximation within a temperature range of -45°C up to 60°C.
According to [16] it defines as:

$$P_{sv}(\vartheta) = 611.2 \cdot \frac{17.62 \cdot \vartheta}{243.12 + \vartheta} \tag{2.3}$$

With ϑ as the gas temperature in °C. Here, the effect of variation of atmospheric pressure P_0 may be neglected, as there are only slight variations in a natural environment.
As the presence of water vapor influences the behaviour of air as a fluid, this thesis aims to consider the relative humidity by incorporating it in the calculation of these characteristics.
The interaction of a particle with its suspending fluid depends very much on the physical characteristics of both particle and fluid. Thus, this section aims to give an overview for the most important characteristics of a fluid, which will later be used to model the filtration process. Kinetic theory assumes, that the behaviour of a gaseous fluid can be described by its temperature, its pressure, its viscosity and its mean free path. Therefore those characteristics will be discussed in the following.

2.3.1 Air density

The density of air is a measure of mass a per volume of air. Considering air with a certain level of relative humidity RH, Tsilingiris [17] proposes the following formula:

$$\rho_m(RH,\vartheta) = \frac{P_0}{R\cdot(\vartheta - 273.15)}\cdot M_a \cdot \left[1 - RH\cdot\left(1-\frac{M_v}{M_a}\right)\cdot\frac{P_{sv}}{P_0}\right] \tag{2.4}$$

With M_a= 28.962458 and M_v= 18.0152 as the molar mass of dry air and pure water respectively and R as the Boltzmann constant. T denotes the gas temperature in K. This formula resembles an alternated form of the ideal gas law, combining the specific gas constants of dry air and water.

2.3.2 Dynamic viscosity

The dynamic viscosity of a fluid is a measure for the fluid's resistance to flow. For gases, viscosity represents the transfer of momentum by collisions of the gases molecules and are thus a measure for molecular motion. Other than for liquids, a gases viscosity increases with temperature. There have been several attempts to coherently derive a relation for the dynamic viscosity of a gas, depending on its temperature as well as its relative humidity. Tsilingiris [17] proposed the following equation:

$$\mu_m(RH,\vartheta) = \frac{\left[1-RH\cdot\left(\frac{P_{sv}}{P_0}\right)\right]\cdot\mu_a}{\left[1-RH\cdot\left(\frac{P_{sv}}{P_0}\right)\right]+RH\cdot\left(\frac{P_{sv}}{P_0}\right)\cdot\Phi_{av}} + \frac{RH\cdot\left(\frac{P_{sv}}{P_0}\right)\cdot\mu_v}{RH\cdot\left(\frac{P_{sv}}{P_0}\right)+\left[1-RH\cdot\left(\frac{P_{sv}}{P_0}\right)\right]\cdot\Phi_{va}} \tag{2.5}$$

where Φ_{av} and Φ_{av} are the so-called "'interaction parameters"' calculated as:

$$\Phi_{av} = \frac{\sqrt{2}}{4}\cdot\left(1+\frac{M_a}{M_v}\right)^{-\frac{1}{2}}\cdot\left[1+\left(\frac{\mu_a}{\mu_v}\right)^{\frac{1}{2}}\cdot\left(\frac{M_v}{M_a}\right)^{\frac{1}{4}}\right]^2 \tag{2.6}$$

$$\Phi_{va} = \frac{\sqrt{2}}{4}\cdot\left(1+\frac{M_v}{M_a}\right)^{-\frac{1}{2}}\cdot\left[1+\left(\frac{\mu_v}{\mu_a}\right)^{\frac{1}{2}}\cdot\left(\frac{M_a}{M_v}\right)^{\frac{1}{4}}\right]^2 \tag{2.7}$$

to obtain the temperature-dependent viscosities for dry and pure water vapor, Tsilingiris uses the following approximation, based on data compiled by Irvine and Liley [18]:

$$\mu_a = c_{a,0} + c_{a,1}\cdot T + c_{a,2}\cdot T^2 + c_{a,3}\cdot T^3 + c_{a,4}\cdot T^4 \tag{2.8}$$

$$\mu_v = c_{v,0} + c_{v,1}\cdot\vartheta \tag{2.9}$$

As a simplification and due to the fact that the temperature range of this thesis' scope is relatively small, the viscosity can also be approximated by a polynomial of 6^{th} order [17]:

$$\mu_{sm}(\vartheta) = c_{m,0} + c_{m,1}\cdot\vartheta + c_{m,2}\cdot\vartheta^2 + c_{m,3}\cdot\vartheta^3 + c_{m,4}\cdot\vartheta^4 \tag{2.10}$$

Using this expression calculates the viscosity at temperature ϑ of fully saturated air or air with an RH of 100%, respectively.

To obtain the viscosity of moist air, a linear interpolation of the following form can be done, using the viscosity of dry and fully saturated air:

$$\mu_m(RH, \vartheta) = \mu_{sm} + (\mu_a - \mu_{sm}) \cdot RH \tag{2.11}$$

The following table shows the used coefficients according to Tsilingiris:

i	$c_{a,i}$	$c_{v,i}$	$c_{m,i}$
0	$-9.8601 \cdot 10^{-1}$	$8.058131868 \cdot 10^{1}$	$1.715747771 \cdot 10^{-5}$
1	$9.080125 \cdot 10^{-2}$	$4.000549451 \cdot 10^{-1}$	$4.722402075 \cdot 10^{-8}$
2	$-1.17635575 \cdot 10^{-4}$	-	$-3.663027156 \cdot 10^{-10}$
3	$1.2349703 \cdot 10^{-7}$	-	$1.873236686 \cdot 10^{-12}$
4	$-5.7971299 \cdot 10^{-11}$	-	$-8.050218737 \cdot 10^{-14}$

2.3.3 Mean free path

The concept of the mean free path λ abandons the idea of gas being a continuous homogeneous fluid again and introduces a measure of how frequently gas molecules collide with dispersed particles. Therefore, the mean free path is defined as the mean distance a single molecule of a gas can travel until it collides with another molecule. As stated before, standard air is a mixture of different gases, with water vapor being a variable part of that mixture. Jennings [19] proposed a relation for the mean free path depending on viscosity, air density and absolute pressure, assuming the gas molecules to be rigid elastic spheres:

$$\lambda(RH, \vartheta) = \sqrt{\frac{\pi}{8}} \cdot \frac{\mu_m(RH, \vartheta)}{0.4987445} \cdot \frac{1}{\sqrt{\rho_m(RH, \vartheta) P_0}} \tag{2.12}$$

A simulation of all the parameters at different temperatures and water vapour saturations (i.e. relative humidities) is presented in section 4.1.

2.4 Characteristics of dispersed particulate matter

Dispersed particulate matter or aerosols, can be described by various characteristics. Physiochemically, an aerosol consists of liquid or solid matter, dispersed in a gaseous fluid. As section 2.3 already described all the relevant characteristics of gaseous fluids, this section aims to give a basic understanding of how to scientifically describe aerosols.

2.4.1 Particle size

The arguably most important parameter, characterizing a single particle is its size. As Hinds [20] states, different particles come in an infinite variety of shapes. Therefore, there have been numerous proposals on how to uniformly describe and categorize a particle. A common practice is to consider each particle as a perfect sphere, defined by its diameter d_p. For liquid particles, this is usually a valid assumption, as they nearly always come in spherical droplets. Solid particles, however, come in the most complex of shapes, making it hard to describe them uniformly. Hence, it is a common practice to define an equivalent diameter, referring to an ideal regular particle with the same, or at last similar physical properties. One widely applied concept for an equivalent diameter is the use of the definition of the so-called aerodynamic diameter d_a. As particles consist of a variety of chemical components with different densities, the concept of the aerodynamic diameter also aims to detach a particle's bulk density from its geometrical dimensions. Thus, for a particle of an arbitrary shape the aerodynamic diameter is defined as the diameter an equivalent spherical particle with standard bulk density would have. The standard bulk density ρ_0 is defined as the density of water as $1000 kg/m^3$.
In this thesis, when referring to a particle's size or diameter, this usually does **not** mean the aerodynamic diameter. This is due to the fact, that the bulk density ρ_p of the particles considered is not equal to 1000 $\frac{kg}{m^3}$. A detailed explanation will be given in section 3.5.1. To calculate the aerodynamic diameter from the particle diameter used, one can apply this formula:

$$d_a = d_p \left(\frac{\rho_p}{\rho_0} \right) \tag{2.13}$$

2.4.2 Particle size distribution

To characterize the composition of an aerosol, a common approach is to describe it as a number, volume or mass distribution among particle size. If an aerosol only consists of particles of one size, it is also referred to as a *monodisperse* aerosol. However, this kind of aerosol only occurs under lab conditions and can hardly be found in a real environment. Here, the aerosol is composed of a multiplicity of particles of different size, accordingly called a *polydisperse* aerosol. As particles of different size behave differently in a flow regime, it can be crucial to possess knowledge of the size

distribution within an aerosol, as it will define how the aerosol will interact with its surroundings. In literature, there are a couple of ways to describe the particle size distribution. The most intuitive approach is to divide the size spectrum in a finite number of bins and define the magnitude of the value of one bin to be total number (or volume, mass, surface ...) of that bin. The more bins, the higher the resolution and the smoother the shape of the distribution curve. Figure 2.7 shows the same particle size distribution, using different numbers of bins:

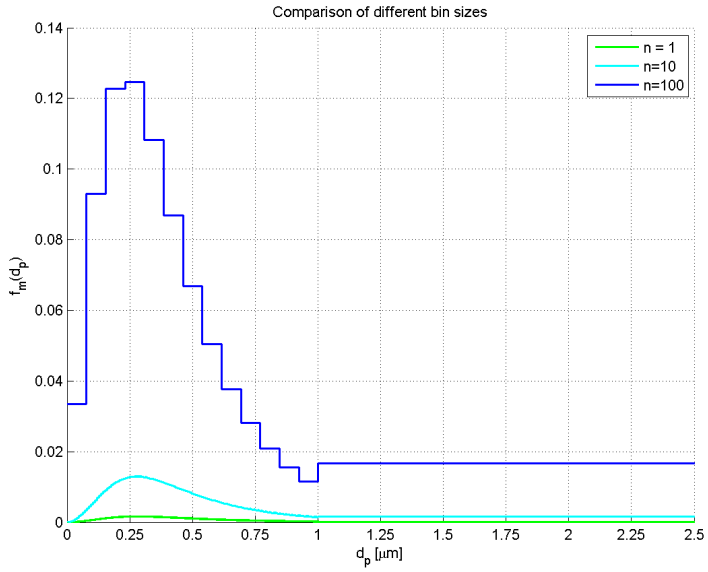

Figure 2.7: Arbitrary particle size distribution

This figure provides a distorted representation though, as by increasing the number of bins and refining the resolution, the fractional share per bin is decreasing. The sum over all bins, however, must always be unity.
Of course, with a higher resolution, the accuracy of calculations using the particle diameter increases, however, the computing complexity increases as well, so that a trade-off has to be found, considering accuracy and computational speed.
For urban aerosols it was found to be useful to distinguish between four different modes, dividing the particle diameter size range into four ranges:

Mode	Particle size range
Nucleation	1nm – 10nm
Aitken	10nm – 100nm
Accumulation	100nm – 1μm
Coarse	>1μm

These definitions may not be the same in every work. Thus, the thresholds are usually also specified in comprehensive literature. Another way of illustrating the particle

distribution is the lognormal distribution. This is due to the empirical observation, that the particle size distribution in a mixed environment tends to have a wide range and a skewed shape. According to Seinfeld and Pandis [21] the lognormal distribution is defined as:

$$n_N^o(logd_p) = \frac{dN}{dlogd_p} = \frac{N_t}{\sqrt{2\pi}\ log\sigma} \cdot e^{-\frac{(logd_p - log\bar{d}_p)^2}{2(log\sigma)^2}} \tag{2.14}$$

Basically, this formula provides an expression for the number of particles per m^3 of aerosol in the size range $logD_p$ to $logD_p$ + $dlogD_p$.
However, this graphic rendition can be deceiving, as it is logarithmic, meaning that the area under the curve is **not** the integral over the aereosol concentration. To obtain the fraction of particles in each bin, Seinfeld and Pandis [21] use the following equations:

$$dN = n_N(d_p)dd_p = n_N^o(logd_p)dlogd_p \tag{2.15}$$

$$dV = n_V(d_p)dd_p = n_V^o(logd_p)dlogd_p \tag{2.16}$$

In their work, Wu et al. [22] measured the concentration of PM1 in Beijing over four years, from 2004 to 2008, and published their results in form of lognormal distributions. They divided the year into its four seasons and fitted lognormal distributions for Nucleation, Aitken and Accumulation mode for each.
The following table presents the parameters for each season in each mode:

Seasons	$N_{t,1}$	σ_1	$\bar{D}_{p_1}$	$N_{t,2}$	σ_2	$\bar{D}_{p_2}$	$N_{t,3}$	σ_3	$\bar{D}_{p_3}$
Spring	10,200	2.0	16	12,400	1.9	50	5700	1.9	126
Summer	6600	1.9	19	10,100	1.8	54	6900	1.8	148
Fall	5800	1.9	20	11,900	1.9	52	8500	1.8	146
Winter	6300	2.0	19	11,500	1.8	53	9400	1.8	117

To merge the results, the total number distribution among particle size is the sum over all modes (Wu et al. [22]):

$$\frac{dN}{dlogD_p} = \sum_{i=1}^{n} \frac{N_{t,i}}{\sqrt{2\pi}\ log\sigma_i} \cdot e^{-\frac{(logD_p - log\bar{D}_p)^2}{2(log\sigma_i)^2}} \tag{2.17}$$

As in this thesis the general concern is the mass distribution among particle size, the number distribution has to be transformed into a volume distribution. This can be done using the assumption of perfectly spherical particles again. Then, the volume distribution calculates as:

$$dV = dN \cdot \frac{\pi}{6} d_p^3 \tag{2.18}$$

To obtain the mass distribution, the particle bulk density has to be used:

$$dm = dV\rho_p \tag{2.19}$$

The simulated results obtained through evaluation and simulation of the work of Wu et al. can be seen in section 4.1.

2.4.3 Reynolds number

To describe the characteristics of a fluid's flow around aerosol particles, the Reynolds number is introduced. As such, it denotes the following properties:

- an index for the flow regime, it provides a benchmark to determine whether the fluid flow is laminar or turbulent.
- the ratio of inertial forces to friction forces within the fluid, thus indicating which flow resistance equation to use in a given situation.
- the path or pattern of streamlines surrounding an object in a flow field. For geometrically similar flow occurring around geometrically similar objects, the Reynold number has to be of equal.

Calculating the Reynolds number can be done in numerous ways, yet the simplest and for the scope of this thesis most useful one is (Hinds [20]):

$$Re = \frac{\rho_g v d}{\mu} \tag{2.20}$$

for the airflow around a particle, d equals the diameter of the particle d_p, here, v does not denote the absolute velocity of the particle, but merely the relative velocity of the particle and the fluid.
For low Reynolds numbers ($Re < 1$), the flow regime is in laminar flow, whereas for high Reynolds numbers the flow regime is in turbulent flow. Laminar is characterized by negligible inertial forces and is thus also referred to as viscous flow, while on the other hand turbulent flow is called inertial flow.

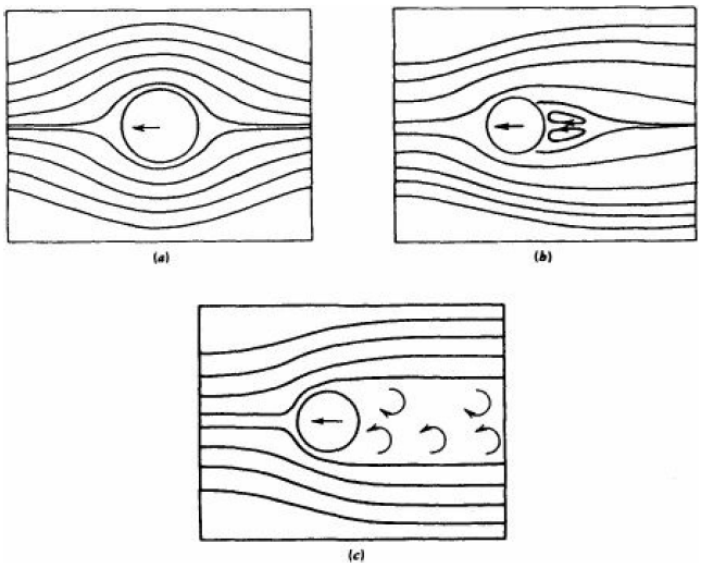

Figure 2.8: Schematic illustration of the streamlines in a flow regime at different Reynolds numbers [20]

Figure 2.8 illustrates the paths of streamlines for Reynolds numbers of (a) Re = 0.1, (b) Re = 2 and (c) Re = 250.

2.4.4 Stokes number

The concept of the Stokes number is used, whenever a particle is in curvilinear motion, i.e. when it follows a curved path. This motion can basically result from two situations:

- In still or uniformly moving air, when forces are applied to it on one or more axes, while accelerating along one axis or when one or more of the forces change over time.
- When the flow of air carrying the particle is converging, changing direction or pass around an obstacle, the resulting curved streamlines cause the suspended particles to have a curvilinear motion.

While the first situation is useful in terms of deposition, the second situation applies for inert particles moving towards a filter fibre. To characterize the curvilinear motion, the Stokes number is introduced. The Stokes number is defined as the ratio of the stopping distance of a particle to a characteristic dimension of the obstacle. The stopping distance S is defined as the total distance a particle would travel, when all external forces acting on the particle are suddenly turned off. Hinds [20] provides mathematical expressions in order to determine stopping distance and Stokes number, all the equations in this section can be found in his work.

$$S = v_0 \tau \tag{2.21}$$

with v_0 being the initial velocity of the particle and τ the relaxation time of a particle, defined as the time required for a particle to adapt or relax into new conditions of forces.
Another situation the concept of the stopping distance applies to is, however, when the flow of air suddenly changes abruptly. In this case the stopping distance is a measure of how far the particle keeps moving in its original direction, or in other words it somehow describes the persistence of a particle in a flow regime.
Accordingly, for particles in laminar flow ($Re < 1$), circulating perpendicularly around a cylindrical object with diameter d_c the Stokes number can be determined as:

$$Stk = \frac{S}{d_c} = \frac{v_0 \tau}{d_c} \tag{2.22}$$

For particles with a Reynolds number greater than unity, a more complicated expression to obtain the stopping distance can be found, where:

$$S = \frac{\rho_p d}{\rho_g} \left[Re_0^{\frac{1}{3}} - \sqrt{6} \arctan \frac{Re_0^{\frac{1}{3}}}{\sqrt{6}} \right] \tag{2.23}$$

This equation provides the stopping distance for particles with an initial Reynolds number $Re_0 < 1500$ with an accuracy of around 3%.

2.4.5 Cunningham correction factor

In order to obtain further comprehension about the necessity of the Cunningham correction factor, Newton's and Stoke's laws of resistance have to be discussed. Hinds demonstrates the calculation of the Cunningham correction factor in his book [20], therefore the expressions used in this section originate from there. Newton evaluated the ballistic characteristics of cannonballs and drew the conclusion that spheres moving through a gas experience a force, caused by the acceleration of the gas that is pushed aside. This so-called drag force is given by

$$F_D = C_D \frac{\pi}{8} \rho_g d^2 v^2 \tag{2.24}$$

as the force is proportional to the volume of gas that is pushed aside. This proportionality is described by C_D, the drag coefficient. For spheres at a Reynolds number $Re > 1000$ C_D is constant at 0.44. However, as small particles usually move in a laminar flow regime at $Re < 1$, C_D is not a constant anymore. In this range, Stoke's law is valid. Stoke expressed the drag coefficient as:

$$C_D = \frac{24\mu}{\rho_g v d} \tag{2.25}$$

as can be observed, C_D is now containing the viscosity of the medium, which is influencing the drag on the suspended particles much more in a laminar flow regime. Finally, it has to be mentioned that Stoke's law assumes the relative velocity at the

surface of the particle itself to be zero. However, this assumption is not correct for small particles, in the range of the mean free path of the carrier gas mixture. Those particles settle faster than suggested by Stoke's law, because of some *slip* on their surface. At standard conditions, the slip has to be taken in account for particles smaller than 1μm. Cunningham's correction factor aims to compensate the effect of slip in the determination of the drag force. His Cunningham factor C_C is always greater than 1 and can be calculated as:

$$C_c = 1 + \frac{\lambda}{d}\left(2.34 + 1.05e^{-0.39\frac{d}{\lambda}}\right) \tag{2.26}$$

This formula is valid even for particles below 0.1 μm. As the slip increases rapidly for particles smaller than 1 μm, the Cunningham slip correction factor must be applied in this range.

2.4.6 Diffusion coefficient

When observing the motion of pollen grains in water in 1827, the botanist Robert Brown could not describe it using conventional methods. Many years later it was Albert Einstein with his theoretical work and Jean Perrin with the experimental proof, who were able to describe the Brownian motion of a particle within a fluid. As such, Brownian motion is the result of a dispersed particle being exposed to a constant bombardment of molecules of the suspending fluid.
To mathematically describe this motion, the concept of diffusion is introduced. Diffusion of aerosol particles is defined as the net transport of particles in between regions of different concentrations. To characterize this transport, the diffusion coefficient D is introduced. A high value of D implies intense Brownian motion and a rapid mass transfer from a region of higher particle concentration to a region of lower particle concentration. A practicable way to obtain the diffusion coefficient is the Stokes-Einstein equation, according to Hinds [20] defined as:

$$D = \frac{k_B T C_c}{3\pi\mu d} \tag{2.27}$$

with k_B being the Boltzmann constant. Analysing this equation, the following statements can be made: D is proportional to the temperature T, as T indicates a more vigorous movement of molecules of the suspending fluid. D is indirectly proportional to the particle size d_p, as smaller particles are influenced more by collisions with the fluid's molecules. Due to an increasing slip correction factor C_c for smaller particles, diffusion is even larger for small particles influenced by surface slip.

2.4.7 Peclet number

An interesting concept to describe the particle transfer process within an aerosol is the Peclet number. As such, it is defined as the ratio of mass transport due to advection of particles to the ratio of mass transport due to diffusion of particles. Advection is defined as the bulk flow rate of the aerosol stream in regard to a characteristic length, determined by the product of flow velocity and the characteristic length. Diffusion is represented by the already discussed diffusion coefficient D. Hence, the Peclet number is defined as (Hinds [20]):

$$Pe = \frac{LU_0}{D} \tag{2.28}$$

2.5 Modelling the in-vehicle concentration of PM2.5

Due to the increased public awareness of the health impact of PM2.5, several researchers have contributed studies in this area. As the average human being spends most of its time indoors, extensive research has been done on how air pollution can be modelled in-house and how the air quality can be improved. However, as already mentioned in the introduction, people tend to spend more and more time using individual or road-bound public transportation. Thus, the need arises to estimate the in-vehicle exposure of each passenger.

Fruin et al. [23], Hudda et al. [24] [25] and Li et al. [26] did extensive research on how to qualitatively model the exposure to PM2.5 and UFP for residents of the Southern Californian area. Particularly Hudda et al.'s most recent article [25] merges the results of their work into a single model, estimating the in-vehicle concentration of PB-PAH (particle bound polycyclic aromatic hydrocarbons), PM2.5 and PM10. In their studies, Hudda et al. use generalized estimating equation (GEE) models, choosing a black-box approach to measure inside and outside concentration and match the logit of the I/O-rates with generalized linear models, incorporating a set of assumed parameters. In their work, they chose age, vehicle speed, fan setting and cabin volume as parameters that influence the I/O-rate of each pollutant. Furthermore, they differentiated between outside air (fresh air intake) and recirculation mode. Their study was conducted using a large representative set of vehicles, all equipped with a coarse particle filter and no dedicated fine dust filter. To determine the cabin volume of each vehicle, they roughly calculated it by taking the dimensions using a tape measure. Another note worth mentioning is, that they didn't evaluate the ventilation speed at each fan setting; instead, they merely took the ventilation level (off, 1, 2, ...) into consideration.

Based on the contributions discussed above, Joodatnia et al. [27] published similar approaches regarding nanoparticles (particle diameter < 300nm). Their mathematical modelling approach is based on a semi-empirical model of the form:

$$N_{ci}(t_{n+1}) = N_{oi}(t_n) \cdot (I/O)_i + (N_{ci}(t_n) - N_{oi}(t_n) \cdot (I/O)_i) \cdot e^{-A_E(\Delta t)} \tag{2.29}$$

Another contribution addressing the in-vehicle concentration of PM2.5 was coined by Liu and Frey [28]. In their work they also want to derive a feasible model to estimate the average exposure of an individual to PM2.5 while using road-bound transportation. Therefore they model the inside concentration of PM2.5 by using a mass-balance model originally proposed by Switzer and Ott [29]:

$$\frac{dC_{in}}{dt} = P \cdot ACH \cdot C_{out} - ACH \cdot C_{in} - C_{in}\delta \tag{2.30}$$

with C_{in} and C_{out} being the in-vehicle and outside concentration of PM2.5, respectively, ACH being the air exchange rate, P being the rate of penetration or penetration efficiency and δ being the deposition rate. A basic assumption made here is that the in-vehicle microenvironment is treated as a well-mixed zone, meaning that the PM2.5 concentration is the same in every spatial point. They also mention that Allen

et al. [30] suggests that a mass-balance model is more reliable than linear regression models (as Hudda et al. used). The approach here is more of a white box model, by trying to model the interaction of the vehicle and its environment based on a physical approach, instead of a statistical one. Considering the influence of the vehicle's heating, ventilation and air conditioning (HVAC) unit with installed particle filter and assuming the pentration efficiency to be approximately 1, they modified the model above as:

$$\frac{dC_{in}}{dt} = ACH \cdot (C_{out} - C_{in}) - \eta\lambda_{HVAC}C_{in} - C_{in}\delta \tag{2.31}$$

with filter efficiency η and λ_{HVAC} being the air exchange rate from the HVAC unit (>1 when receiving air from the outside, fresh air intake mode).

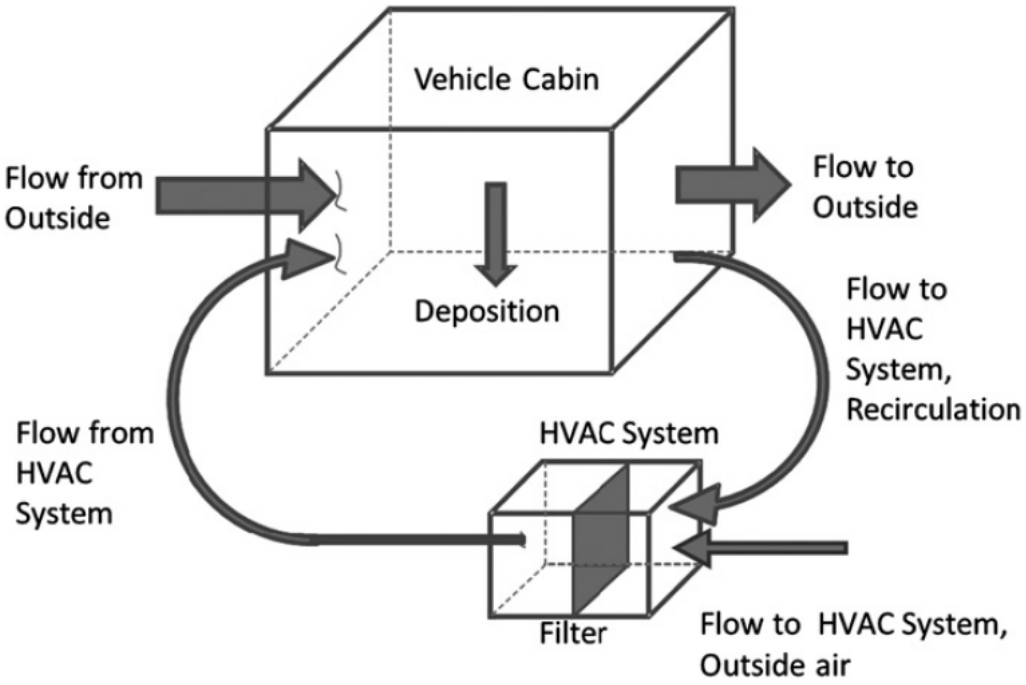

Figure 2.9: Schematic illustration of the mass-balance model used by Liu and Frey.

For the deposition rate δ they suggest it to be dependent of particle size and air exchange rate. Interestingly, they suggest the sensitivity to the deposition rate to be quite low, a statement that this thesis will also try to confirm. Same as Hudda et al., the examined vehicles in Liu's and Frey's work do not use special fine dust filters, but conventional coarse particle filters. In their conclusion they also suggest to further improve their model by including the effect of HVAC settings in the model. One contribution with a very similar approach and setting to this thesis was made by Park et al. [31]. Other than the previous mentioned contributions, they use a

special fine dust filter, a so-called electret filter (more in section 2.6.2). As to their model of the inside concentration they also used a mass-balance model of the form:

$$V_{cab}\frac{dC_{in}}{dt} = C_{out}\left(\dot{Q}_S\left(1-\eta_{filt}\right)\right) - C_{in}\left(\dot{Q}_S+\dot{\delta}\right)+\dot{S} \tag{2.32}$$

with $\dot{Q}_S$ as the air flow rate supplied into the cabin, $\dot{S}$ the generation rate of PM2.5 (which was assumed to be 0, as there is negligibly little resuspension of trapped particles within the cabin)

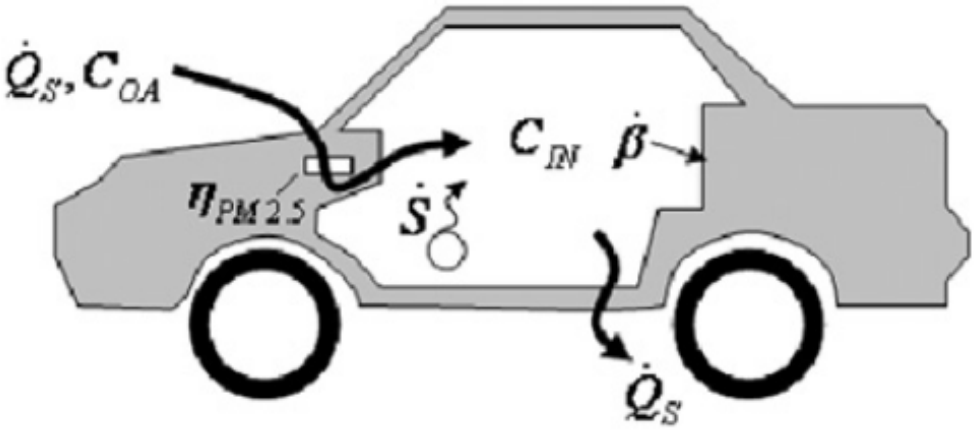

Figure 2.10: Schematic illustration of the mass-balance model used by Park et al.

Another distinction worth mentioning was that they used the actual face velocity at each ventilation level and not the ventilation level itself, as all the previously discussed studies. However, as their main concern was to improve the filter's performance, their interest was only in the steady-state solution as they would derive the filter's performance efficiency from it. Nevertheless, their work provides a useful basis for further research on this subject.

2.6 Filtering

The filtration process of aerosol particles has been topic of extensive research in the past. However, even though the basic underlying principles are well understood, there is still a remarkable gap between theory and reality. Considering atmospheric aerosol concentrations, the most efficient, inexpensive and simple means to achieve a high capture rate are fibrous filters. However, as they also implicate a high pressure drop in order to achieve a high filter efficiency, a recent practice is to additionally apply an electrostatic charge on the fibres, combining mechanical and electrostatic filter effects. Using this technique, it is possible to get rather high capture rates at low pressure drops. The main disadvantage of this practice is, that, in contrary to the mechanical collection efficiency, the electrostatic collection efficiency decreases of lifetime. Also, as will be discussed later in this section, it is very complex to accurately model the electrostatic filter effect, as it is influenced by many parameters. The efficiency of a filter is usually characterized by the ratio of captured particulate mass $m_{up} - m_{down}$ to the applied upstream particulate mass m_{down}.

$$\eta_{filt} = \frac{m_{up} - m_{down}}{m_{up}} \tag{2.33}$$

Another definition for the filter performance is the penetration rate, the ratio of remaining concentration downstream C_{down} to the applied concentration upstream C_{up}.

$$p_{filt} = \frac{C_{down}}{C_{up}} \tag{2.34}$$

Whereas the relation of filter penetration to filter efficiency is defined as:

$$\eta_{filt} = 1 - p_{filt} \tag{2.35}$$

As the aerosol moves through the filter at a certain flow rate $\dot{Q}$, the velocity of the aerosol right at the face of the filter (A being filter surface area, including pleating) is defined as:

$$U_0 = \frac{\dot{Q}}{A} \tag{2.36}$$

As it is referred to the face area of the filter, this quantity is called face velocity U_0. Inside the filter, respectively, the velocity of the aerosol is slightly increased as the volume of the air passage is reduced by the volume of the fibres. The volume of the fibres itself can be described in relation to the total volume of the filter, referred to as the packing density or solidity α. The decreased velocity U is called the interstitial velocity and calculated as:

$$U = \frac{U_0}{(1-\alpha)} = \frac{\dot{Q}}{A(1-\alpha)} \tag{2.37}$$

To obtain the packing density, either volume or bulk density of the filter material have to be known. Alternatively, it can be derived from the porosity of the filter.

$$\alpha = \frac{V_{fibre}}{V_{total}} \approx \frac{\rho_{total}}{\rho_{fibre}} = 1 - porosity \tag{2.38}$$

Regardless of the type of filter, these relations are always valid.

2.6.1 Fibrous filtration

Fibrous filters consist of microscopic fibres made of cellulose, glass or polypropylene. They are arranged so that most of them are perpendicular to the air flow, as to maximize their collection efficiency. Usually they come in the form of mats, immobilized by a pattern of spot welds. Consisting mostly of air, their porosity is usually in a range of 70 to 99%. The shape of the fibres is assumed to be cylindrical, with a fibre diameter d_f typically ranging from between 1 to 20μm. To increase the effective filter area, it is also a common practice to pleat the filter. The following photograph provides an insight into the structure of a fibrous filter.

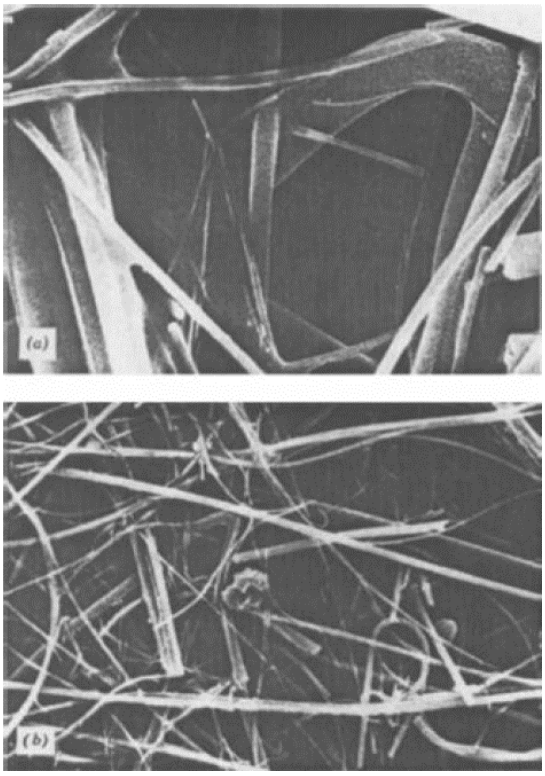

Figure 2.11: Scanning electron microscope photograph of a high-efficiency glass fiber filter [20]

A common misconception about aerosol filtration is the notion of a sieve, capturing particles of all sizes bigger than the pore size and passing all the particles smaller than it. As will be shown in this section, fibrous filters rather capture particles by collision and adhesion. Each fibre has a certain probability of capturing particles, depending numerous characteristics of the aerosol and the fibre itself. This ability is often quantified as the single fibre collection efficiency η. For fibrous filters with no applied electrical charge, the single fibre collection efficiency can be described by

four different *mechanical collection mechanisms*. Hinds [20] defines these for standard conditions of $0.005 < \alpha < 0.2$, $0.001 < U_0 < 2m/s$, $0.1 < d_f < 50\mu m$ and $Re_f < 1$ as the following:

Gravitational settling From largest to smallest, the mechanism effecting particles of larger size most is gravitational settling. The number that represents the number of deposition due to gravitational settling is G.

$$G = \frac{v_{ts}}{U_0} = \frac{\rho_g d_p^2 C_c g}{18\mu U_0} \tag{2.39}$$

Depending on the geometry of the filter system, U_0 and v_{ts} are oriented towards each other in a certain way. Downward airflow means they are in the same direction. In this case the single-fibre efficiency due to gravitational settling can be expressed as:

$$\eta_G = G(1+R) \tag{2.40}$$

When U_0 is directed upwards, this relation becomes:

$$\eta_G = -G(1+R) \tag{2.41}$$

Here, R is a dimensionless parameter describing the ratio of the particle size to the size of the filter fibre d_p/d_f. For every a horizontal flow of air, η_G becomes much less, around G^2. In general η_G is rather small in comparison with other filter mechanisms, other than for large particles and low ventilation speeds.

Inertial impaction If a particle is too inert to quickly adjust to an abrupt change of direction of the streamlines, it crosses those streamlines and collides with the fibre.

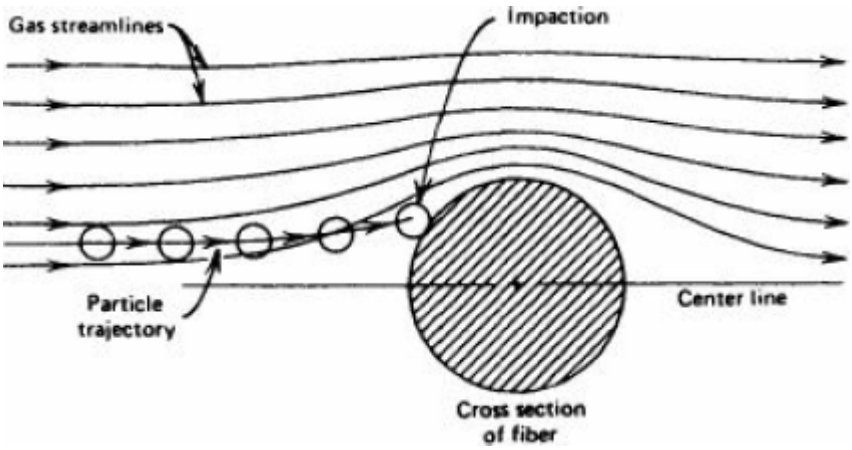

Figure 2.12: Particle collection by impaction [20]

For inertial impaction, the representative parameter is the Stokes number Stk (see 2.4.4):

$$Stk = \frac{\tau U_0}{d_f} = \frac{\rho_p d_p^2 C_c U_0}{18 \eta d_f} \tag{2.42}$$

The single-fibre collection efficiency due to inertial impaction is determined by:

$$\eta_I = \frac{StkJ}{2Ku^2} \tag{2.43}$$

With Ku being the Kuwabara factor, a dimensionless factor, that incorporates the effect of distortion of a flow field around a fibre due to its proximity to other fibres. As such, Ku only depends of the filters packing density α and is obtained by:

$$Ku = -\frac{ln\alpha}{2} - \frac{3}{4} + \alpha - \frac{\alpha^2}{4} \tag{2.44}$$

Here, J is a parameter obtained by numerical simulation as proposed by Stechkina et al. [32] . Depending on α and R it is determined as:

$$J = (29.6 - 28\alpha^{0.62})R^2 - 27.5R^{2.8} \tag{2.45}$$

However, this relation is only valid in a viscous flow regime ($Re_f < 1$) as noted by Hubbard et al. [33] and for $R < 0.4$. As Hinds [20] suggests, J can be set as 2 for approximate analysis when $R > 0.4$. Impaction is the most important mechanism for large particles; however, those particles are also highly affected by the interception mechanism, discussed next.

Interception In contrast to impaction, interception does not result of a particle departing from its streamline, but due to the fact that the streamline it follows comes within one radius of the particle. As a result, the particle is captured by hitting the fibre and adhering to its surface. In conclusion, for a given particle size, certain streamlines will lead to a capture of that particle. As the basic assumption is that the particle follows its streamline perfectly, only particles within a certain size range are captured purely by interception. Therefore particles have to have negligible inertia, settling and Brownian motion, to not depart from its streamline.

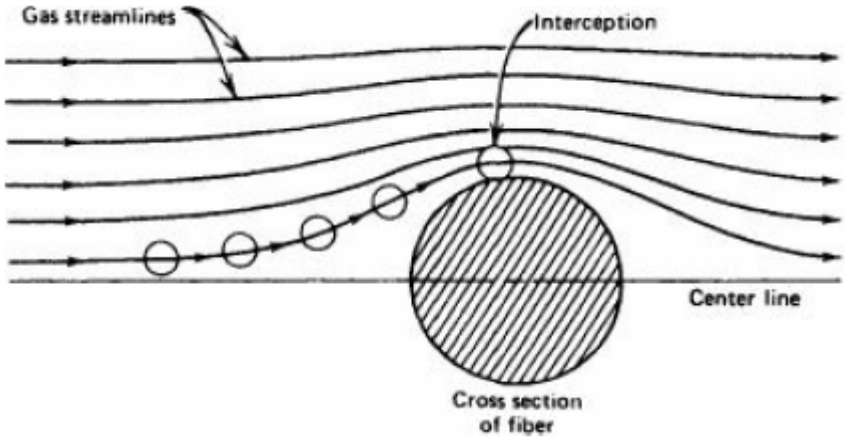

Figure 2.13: Particle collection by interception [20]

In order to calculate the single-fibre efficiency due to interception, Hinds [20] states the following expression:

$$\eta_R = \frac{(1-\alpha)R^2}{Ku(1+R)} \tag{2.46}$$

As can be observed, η_R only depends on the particle-fibre size ratio R, the packing density α and the Kuwabara factor Ku (which, as aforementioned, is also a function of α alone in the scope considered). η_R increases with R and is the only definition of single-fibre efficiency that does not depend on the face velocity U_0.

Diffusion As impaction and interception apply to particles of adequately high inertia, they are still insufficient in describing the movement of particles subject to Brownian movement. Similar to highly inert particles, small particles are not able to follow their streamlines.

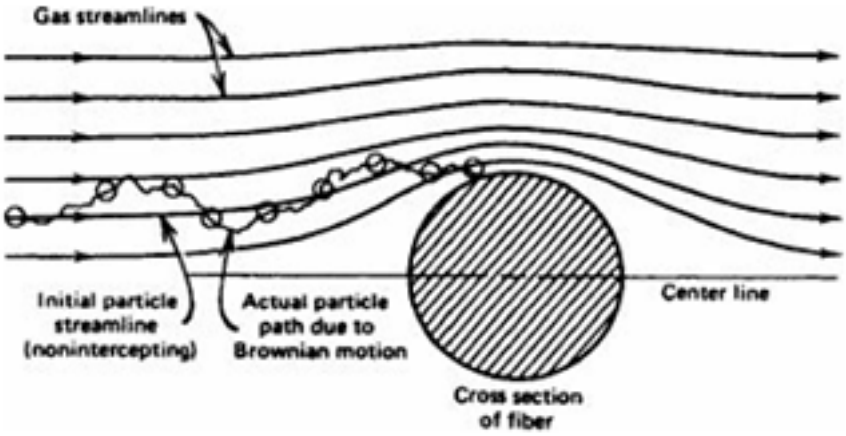

Figure 2.14: Particle collection by interception [20]

This behaviour increases their probability to be captured by a fibre. Using the the concept of the Peclet number with respect to the fibre diameter, the Peclet number is calculated as:

$$Pe_f = \frac{d_f U_0}{D} \tag{2.47}$$

To get the single-fibre efficiency due to diffusion, Kirsch and Fuchs proposed the following expression:

$$\eta_D = 2Pe^{-\frac{2}{3}} \tag{2.48}$$

As the Peclet number increases with higher flow velocities, particle collection due to diffusion is more likely to happen at lower face velocities. The coefficient 2 in the equation for η_D is experimental determined. However, as diffusing particles are also more likely to be captured by interception, an interaction term has to be introduced.

$$\eta_{DR} = \frac{1.24R^{\frac{1}{2}}}{(KuPe)^{\frac{1}{2}}}. \tag{2.49}$$

To merge all the single fibre collection efficiencies the total single-fibre efficiency is introduced

$$\eta_\Sigma = 1 - (1 - \eta_G)(1 - \eta_I)(1 - \eta_R)(1 - \eta_{DR})(1 - \eta_D) \tag{2.50}$$

In order to obtain a model for a fibrous filter element of a certain thickness Z, the overall filter efficiency η_{filt} is introduced. As Hinds [20] states, the overall filter efficiency has clearly to be a function of the combined filter efficiencies. To get the total length of fibres in a unit volume, assuming a single fibre to be a perfect cylinder, the packing density of the filter is divided by the cross-section area of a single fibre with diameter d_f.

$$l_f = \frac{\alpha}{A_f} = \frac{4\alpha}{\pi d_f^2} \tag{2.51}$$

Using this expression provides l_f in m/m^3, to calculate the collection rate of a layer (γ) of fibrous material the overall collection rate of single fibres in this layer has to be considered. As the total single fibre collection efficiency is defined in relation to a fibre of unit length with a diameter d_f, γ can be obtained as:

$$\gamma = \eta_\Sigma l_f d_f \tag{2.52}$$

The number of particles captured passing through that layer can now be determined as:

$$n_c = N\gamma dZ \tag{2.53}$$

with N being the total number of particles entering the layer and dZ being the infinitesimal thickness of the layer. In other words, the decrease of particle number in each layer dN is obtained by:

$$dN = -n_c = -N\gamma dZ \tag{2.54}$$

In order to combine the amount of captured particles in each layer, the integral over the whole thickness of the filter Z has to be determined.

$$\int_{N_{in}}^{N_{out}} \frac{dN}{N} = \int_0^Z (-\gamma)\, dZ \tag{2.55}$$

the solution of this equation is found as:

$$ln\left(\frac{N_{out}}{N_{in}}\right) = -\gamma \tag{2.56}$$

As one can observe, it happens that $\frac{N_{out}}{N_{in}}$ is conform to the previous stated definition of the penetration rate P. As η_{filt} equals 1-P it can be obtained as:

$$\eta_{filt} = 1 - e^{-\gamma} = 1 - e^{\frac{-4\alpha\eta_\Sigma Z}{\pi d_f}} \tag{2.57}$$

This basic model for fibrous filters can be further extended by applying certain refinements. Frising et al. [34] proposed a model that incorporates varying fibre diameters, concluding that a serial approach is best suited as an assumption. Including their model (serial approach), equation 2.57 becomes:

$$\eta_{filt} = 1 - \prod_{i=1}^{n_f} e^{-\gamma_i} = 1 - \prod_{i=1}^{n_f} e^{\frac{-4\alpha_i\eta_{\Sigma,i}Z}{\pi d_i}} \tag{2.58}$$

with d_i being the different fibre diameters ranging from d_0 to d_{n_f}, each of those fibres contributing a fraction of α_i to the total packing density α. This model also involves that the single fibre density $\eta_{\Sigma,i}$ has to be calculated for every fibre diameter d_i, increasing the complexity and thus the required computing power.
Another extension for his model was developed by Joubert et al. [35], as they model the influence of humidity on the cake (i.e. the dust layer forming on the upstream face of the filter). However, the applicability for this thesis is highly doubtable, as

they state themselves, that their correlations are "difficult to use due to the lack of data on the physical parameters, characterizing the filters studied". Hence, their proposal was not taken into consideration and relative humidity is only considered in the calculation of the aerosol's fluid characteristics.
An interesting approach for the modelling of the clogging process of fibrous filters was proposed by Thomas et al. [36]. They model the clogging process in two steps, one is the forming of a cake on the surface facing the upstream air flow, the other is the forming of a cake within the filter. Captured particles form so-called dendrites, shapes that act similar to fibres and are able to capture dust themselves. As more and more particles are trapped in the filter, more and more dendrites form, creating a structure that can be seen as an additional filter. Thomas et al. split the filter virtually into slices, each consisting of one slice of fibres and one slice of dendrites in parallel. The (mechanical) filtration characteristics of the fibrous material is constant, whereas the collection of particles by dendrites increase steadily, as they grow with each captured particle. The captured particulate mass in each slice can thus be modelled as:

$$m_{fj,t} = \left(1 - \frac{\alpha_{pj,t-1}}{1-\alpha} \sum_{i=1}^{n_{d_p}} \left(\eta_{fj,i,t} m_{j,t} f_{uj,i,t}\right)\right) \tag{2.59}$$

$m_{fj,t}$ being the fraction of mass collected by fibres and

$$m_{pj,t} = \left(\frac{\alpha_{pj,t-1}}{1-\alpha} \sum_{i=1}^{n_{d_p}} \left(\eta_{pj,i,t} m_{j,t} f_{uj,i,t}\right)\right) \tag{2.60}$$

$m_{pj,t}$ being the fraction of mass collected by dendrites. $\alpha_{pj,t-1}$ is the additional packing density caused by the collected particles within slice j, n_{d_p} being the total number of particle size ranges i. $f_{uj,i,t}$ is the particle distribution upstream of slice j, depending on the collection efficiency for each range of particle diameter of the previous layer, the distribution has to be calculated accordingly. $\eta_{fj,i,t}$ and $\eta_{pj,i,t}$ are the single fibre collection efficiency and the single dendrite efficiency, respectively. They can be obtained by:

$$\eta_{fj,i,t} = 1 - e^{\frac{-4\alpha\eta_f Z_j}{\pi\left(1-\alpha-\alpha_{pj,t} d_f\right)}} \tag{2.61}$$

and

$$\eta_{pj,i,t} = 1 - e^{\frac{-4\alpha\eta_f Z_j}{\pi\left(1-\alpha-\alpha_{pj,t} d_f\right)}} \tag{2.62}$$

Thus, the total efficiency in each slice can be calculated as:

$$\eta_{j,t} = \frac{\sum_{i=1}^{n_{d_p}} m_{fj,i,t} + m_{pj,i,t}}{m_{j,t}} \tag{2.63}$$

Here, the whole mass entering each slice can be found as:

$$m_{j,t} = \left(1 - \eta_{j-1,t}\right) m_{j-1,t} \tag{2.64}$$

For the new packing density of particles, the expression

$$\alpha_{pj,t} = \alpha_{pj,t-1} + \frac{m_{fj,t} + m_{pj,t}}{\rho_p Z_j} \tag{2.65}$$

provides a recursive solution. Also, as dendrites not only grow in length, but also in diameter, a new average diameter of dendrites has to be determined.

$$\bar{d}_{pj,t} = \frac{\bar{d}_{pj,t-1}\alpha_{pj-1,t}\rho_p Z_j + \sum_{i=1}^{n_{dp}} \left(m_{fj,i,t} + m_{pj,i,t}\right) d_{p,i}}{\alpha_{pj-1,t}\rho_p Z_j + \sum_{i=1}^{n_{dp}} \left(m_{fj,i,t} + m_{pj,i,t}\right) d_{p,i}} \tag{2.66}$$

Furthermore, to model the filter's pressure drop across each slice, Thomas et al. [36] suggest using Bergman's model for each slice:

$$\Delta p_{j,t} = 16\mu U_0 Z_j \left(\frac{4\alpha_{pj,t}}{\bar{d}^2_{pj,t}} \frac{4\alpha}{d_f^2}\right)^{\frac{1}{2}} \left(\frac{2\alpha_{pj,t}}{\bar{d}^2_{pj,t}} \frac{2\alpha}{d_f^2}\right) \cdot \left(1 + 56(\alpha + \alpha_{pj,t})^3\right) \tag{2.67}$$

and obtaining the total pressure drop as the sum of pressure drops across each slice

$$\Delta p_t = \sum_{j}^{n_s} = 1\Delta p_{j,t} \tag{2.68}$$

To illustrate this, on first glance maybe rather complicated, model, the following figure shows the whole process in a graph:

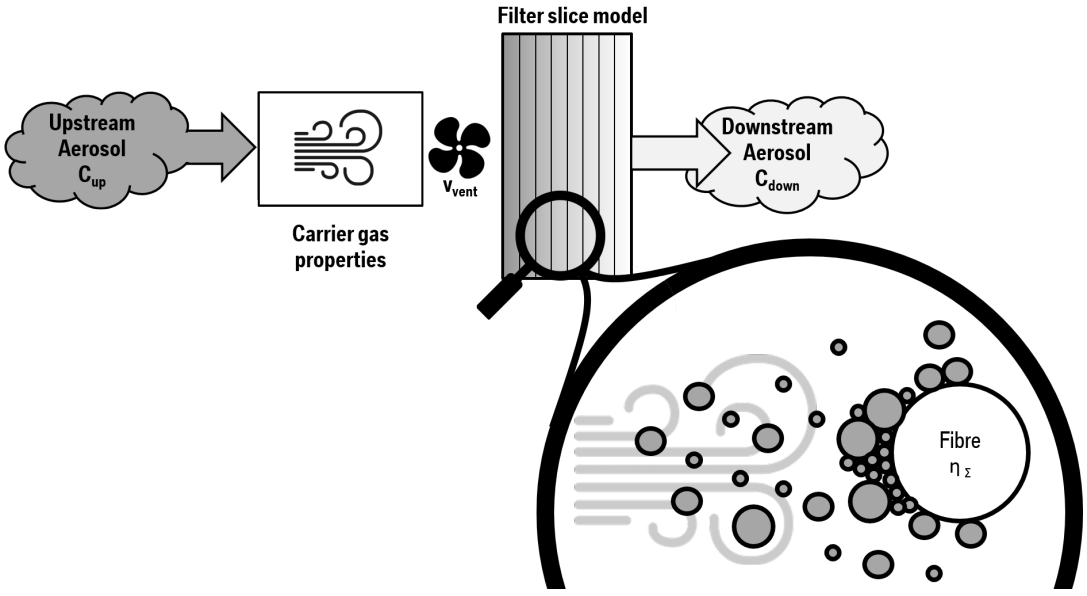

Figure 2.15: Illustration of the filter clogging model.

The last parameter missing is the packing density of the cake α_{pc}. Unfortunately, the approach Thomas et al. [36] are using is deemed not practical for polydisperse aerosols. Also, they did not use pleated filters, which behave quite different to flat filters in case of cake formation.

2.6.2 Electret filters

Fibrous filters are widely used in HEPA (high efficiency particulate arresting) applications, as in indoor air cleaners or in aircrafts. However, achieving high collection efficiencies always comes with the downside of a high pressure drop across the filter, as well as filters large in dimension and expensive in cost. Thus, fibrous filters working only on mechanical principles are hardly practical to use in automotive applications. As an aerosol is not only composed of uncharged particles, applying a charge to the filter's fibres is an auspicious approach to improve the filter's efficiency. This practice is often referred to as electret filters or HPFEF (high performance electret filter), according to the HEPA acronym. As already mentioned in section 2.5, Park et al. contributed not only in research on modelling the in-vehicle PM2.5 concentration, but also in examining the use of electret filtration in vehicles. In fact, their intention was to prove that ionizing (i.e. applying a charge to by-passing particles) the particles from the HVAC unit's intake with carbon fibre ionizers would improve the electret filter's performance. Finally, in comparison to other studies, their study was conducted near Seoul, South Korea, Asia. Thus, it is assumed that the exposure to PM2.5 is comparable to the environment in China, in contrast to all the other studies mentioned before, whiche were conducted in other parts of the world.
Fundamentally, particles have to be distinguished by whether they hold an electrical charge or not. The electrostatic single-fibre efficiency is much smaller for neutral particles, however, these particles also experience a force, due to in-homogeneous field distributions. Brown [37] did extensive work in researching these forces, providing expressions for both the Coulombic attraction parameter N_{pq} and the dielectrophoresis parameter N_{p0}.

Coulombic attraction is the force resulting of electrical charges interacting with each other, usually described by an electric field distribution. As charged particles can hold an integer multiple of the elementary charge e, this force is not the same for each particle in a flow field of aerosol. However, as it is nearly impossible to quantify the charge on each particle of a regional aerosol, this force is hard to estimate. In order to estimate the likelihood of a particle being captured by a fibre due to coulombic attraction, the dimensionless parameter N_{pq} has been introduced. It is defined as:

$$N_{pq} = -\frac{C_c q Q_f}{6\mu(1+\varepsilon_f)U_0\varepsilon_0 d_p} \tag{2.69}$$

Aside from the total charge q of the particle, its size d_p and velocity U_0, as well as the fibre's permittivity ε_f and total charge Q_f influence the likelihood of capture. N_{pq} is also known as the Coulombic force parameter as it governs particle capturing by Coulombic force. Brown chose an exponential approach, incorporating this parameter and fit it to measured single-fibre efficiency rates. Lee et al. [38] then introduced a refined form of Brown's model, proposed by

co-author Otani:

$$\begin{aligned} \eta_C &= 0.78 N_{pq} && : 10^{-3} < N_{pq} < 10^{-1} \\ \eta_C &= 0.59 Ku^{-0.17} N_{pq}^{0.83} && : 10^{-1} < N_{pq} < 10 \end{aligned} \tag{2.70}$$

Every charged particle neutralizes the same quantity of opposite charge inside the fibre. Thus, with more and more charged particles captured, the charge within the fibre is eventually neutralized. Therefore, the electrostatic single-fibre efficiency is decreasing by collected particulate matter, compared to the mechanical single-fibre efficiency, which is increasing.
Various approaches have been made in order to improve this mechanism of electrostatic collection. As aforementioned (Park et al. [31]), pre-filter located ionizers have been installed in order to additionally charge particles, in order to enhance the collection efficiency due to Coulombic attraction. Using this technique, they were able to enhance the collection efficiency up to 21%.

Dielectrophoresis is the electrical phenomenon of exerting a force on particles, due to a non-uniform field distribution. Notably, a particle does **not** have to be charged itself in order to experience a dielectrophoresic force. Brown describes the effect as a force, resulting from an induced dipole moment in a neutral particle, attracting it to a region of high field. The dipole moment occurs because of polarization of a particle residing within an in-homogeneous electrical field. Depending on the orientation of the induced dipole in the particle, the particle either moves into the direction of the higher field, or is repelled. These behaviours are called positive dielectrophoresis (DEP) and negative DEP, respectively. Same as for Coulombic attraction, Brown introduced a dimensionless parameter N_{p0}, in order to quantify the likelihood of suspended particle being captured due to DEP.

$$N_{p0} = -\frac{C_c(\varepsilon_p - 1)\pi^2 Q_f^2 d_p^2}{6\mu(\varepsilon_p + 2)(\varepsilon_f + 1)U_0 \varepsilon_0 d_f} \tag{2.71}$$

with the particle's permittivity ε_p. Again, using N_{p0}, Lee et al. propose an exponential model obtained by a fit over a wide range of data:

$$\begin{aligned} \eta_{dep} &= 1.48 N_{p0}^{0.93} && : 10^{-4} < N_{p0} < 10^{-2} \\ \eta_{dep} &= 0.51 Ku^{-0.35} N_{p0}^{0.73} && : 10^{-2} < N_{p0} < 1 \\ \eta_{dep} &= 0.54 Ku^{-0.60} N_{p0}^{0.40} && : 1 < N_{p0} < 100 \end{aligned} \tag{2.72}$$

Combined, these two effects describe the enhanced collection efficiency of a single fibre due to its charge.

$$\eta_{C,dep} = 1 - (1 - \eta_C)(1 - \eta_{dep}) \tag{2.73}$$

Numerous workers engaged in studying the decay of the electrostatic effect with increasing dust load. However, there is little research on how to practicably model

the decay of the fibre charge. Ji et al. [39] present a semi-empirical approach using the following expression:

$$\eta_{C,dep}(m_l) = \eta_{C,dep}(0)e^{\beta m_l} \tag{2.74}$$

with β as the decay parameter, determined empirically for a certain combination of aerosol and filter material.
The concept of single-fibre efficiency makes it easy to merge the derived mechanical slice model with the electrostatic model. The overall single-fibre efficiency computes as (Hinds [20]):

$$\eta_\Sigma = 1 - (1-\eta_G)(1-\eta_I)(1-\eta_R)(1-\eta_{DR})(1-\eta_D)(1-\eta_C)(1-\eta_{dep}) \tag{2.75}$$

2.7 Measuring PM2.5

There are numerous methods to measure the concentration of particulate matter. Each technology is used for different applications and optimized to determine different characteristics of an aerosol. The company TSI is one of the leading providers for aerosol sampling equipment. In their product range they are offering devices which utilize four different measuring methods to obtain the particle concentration: optical particle counters, photometers, aerodynamic particle sizer spectrometers and condensation particle counters [40]. As mentioned before, each of those devices has a certain field of application. As the experiments conducted in this thesis are focussing on particulate mass concentration, this section elucidates the functionality of optical particle counters and photometers.

2.7.1 Optical particle counters

Optical particle counters are measuring the particle size and number concentration by detecting light, scattered from particles in a constant flow of aerosol. Figure 2.16 shows a graphic illustrating the operation method of a optical particle counter.

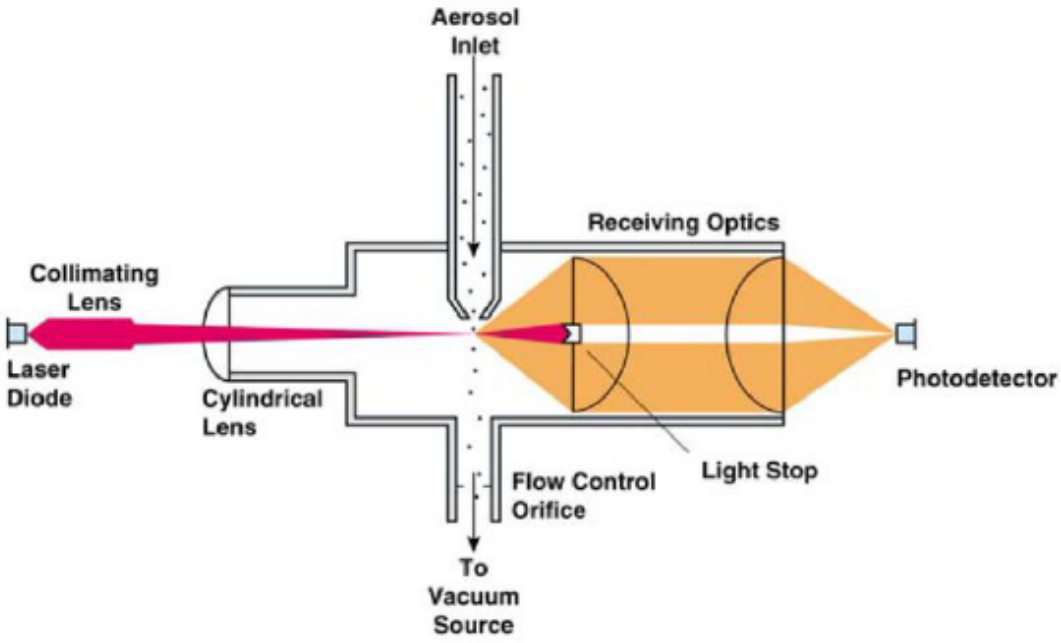

Figure 2.16: Illustration of the measuring principle of optical particle counters [40]

A flow of aerosol is directed into a focussed laser beam, causing the beam to flash. This intensity of the scattered light can then be referred to a count of particles as it is detected by an optical detector and processed using a rather complex algorithm of diameter, shape, refracting index and properties of laser and detector.

The calibration of these devices is usually done with a monodisperse aerosol of well known characteristics. To refer the measured figure to a real world value, this calibration may have to be adjusted by a regional factor. Most instruments count the light pulses induced by single particles passing the laser beam and are thus limited to a maximum concentration as well as a minimal detectable particle size. This range minimum is usually around 0.3μm, below that a drastic increase in laser intensity is required.

2.7.2 Photometers

Photometers are a good and inexpensive choice to measure real time concentrations of particulate matter, as they also use conventional light-scattering technology to estimate the particulate mass concentration of an aerosol. Figure 2.17 illustrates the operation of a photometer.

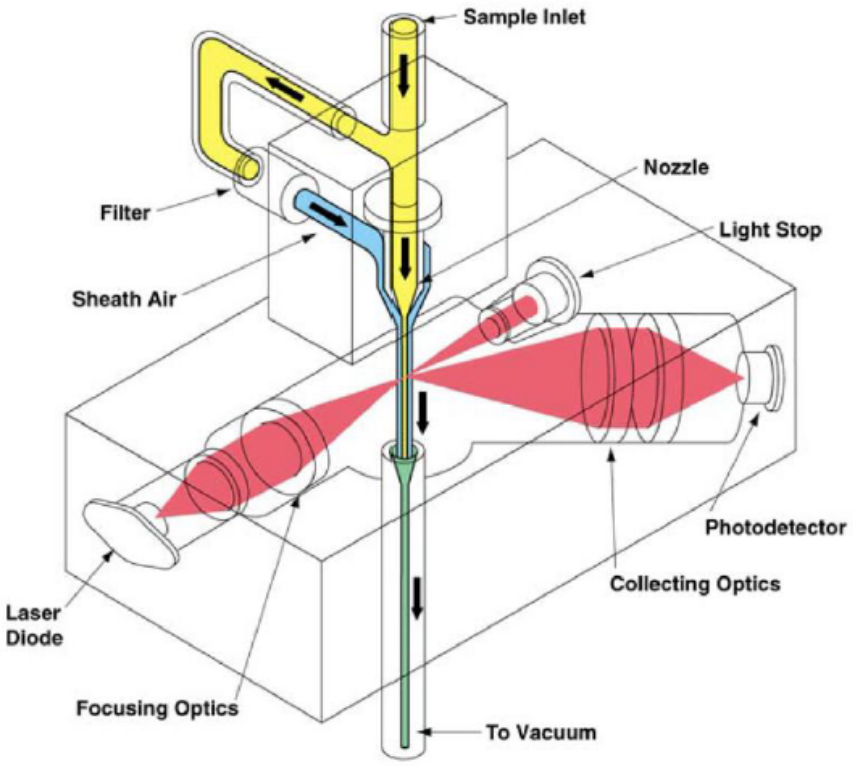

Figure 2.17: Illustration of the measuring principle of a laser photometer [40]

Samples of the measured aerosol are constantly drawn into the instrument by the suction of a pump. Using techniques like a cyclone or impactor, different size fractions of the aerosol can be separated. A sample of known size rage is then focussed by a nozzle and directed into a photodetector chamber. This chamber is composed of a laser diode and a set of focussing optics. The particles passing

through the light beam, scatter it in all directions. A photodetector collects the scattered light and converts it to a calibrated, known mass concentration. As a safety mechanism to protect the instruments from fouling, one part of the drawn aerosol sample is filtered and reinjected as sheath air, to "coat" the measured air stream. Photometers are usually operating within ranges from 0.1 to 10 μm and can handle rather high concentrations up to 100mg/m^3. Detections of UFP is not possible, as these scatter not enough light to be detected. In contrast to optical single particle counters, photometers are measuring a cloud of particles and do no operate well in very low concentrations. The calibration of most photometers is against a defined polydisperse aerosol such as Arizona Road Dust. However, TSI provides and recommends locally determined correction factors.

Typically, photometers can be used in wide ranges of mass concentration, but do not provide any information about particle size. Thus, the input aerosol has to be filtered or conditioned by impactors or similar. Optical particle counters on the other hand, are able to determine the size of single particles but do not work in high concentration.

3 Methodology

Trying to address some of the unresolved problems that emerged in the previous chapter, this chapter elaborates the methodology followed to obtain the results presented in the following chapter. Based on past contributions a new methodology is created by relating different studies and combining their results and proposed mathematical models with new ideas and observations from autonomously conducted experiments.

3.1 Modelling the outside air quality

This thesis does **not** propose a model to estimate the outside ambient air quality. However, in order to verify the measurements and quantify the ambient air conditions during every test cycle, various sources have been used to obtain certain data. Relevant data includes meteorological data, traffic data and air quality data from official public sources. As this data is highly dependent on the geographical location of the test drives, specific sources have to be identified. Thus, this section starts with an overview of the test tracks and elaborates on special geographical circumstances.

3.1.1 Test environment

The experiments in this thesis have all been conducted in the time from July to September 2015. Every experiment was done under real conditions, in other words the vehicle was always exposed to real atmospheric conditions. In terms of realism this is an optimal approach, however, in terms of simplicity this approach can be highly complex. Test drives were conducted at 0, 30, 50, 70 and 100km/h. As the vehicle speed needed to be kept as constant as possible, tracks had to be found where traffic and regulation was appropriate. For standstill measurements, the BMW engineering centre in Beijing was an obvious choice, as the test vehicle that was used was based there. Measurements at 30km/h could also be performed within the so-called Free Trade Zone, an enclosed industrial area with little traffic and no traffic lights. Both of these locations are shown in Figure 3.1.

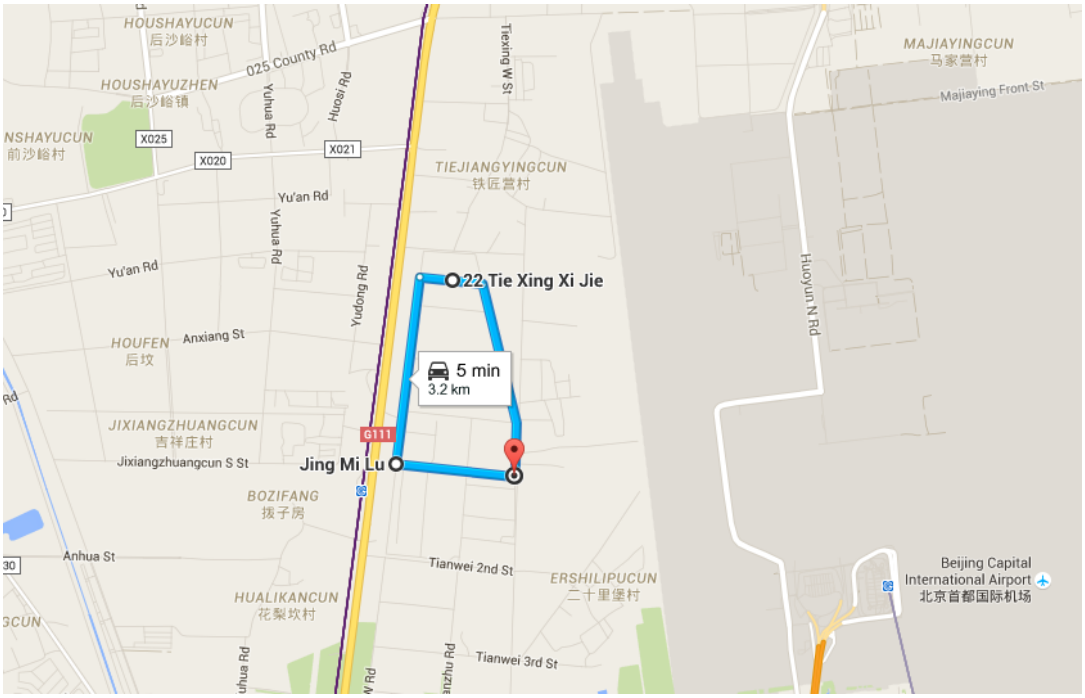

Figure 3.1: The Free Trade Zone in Beijing, location for 0, 30 and 50km/h test drives

The high speed measurements at 70 and 100km/h, respectively, were performed along the Sixth Ring Road in Beijing. As this road is a highway, there were no traffic lights. Also, this ring is the outermost ring road and thus the traffic is usually flowing freely. Figure 3.2 shows the chosen test track.

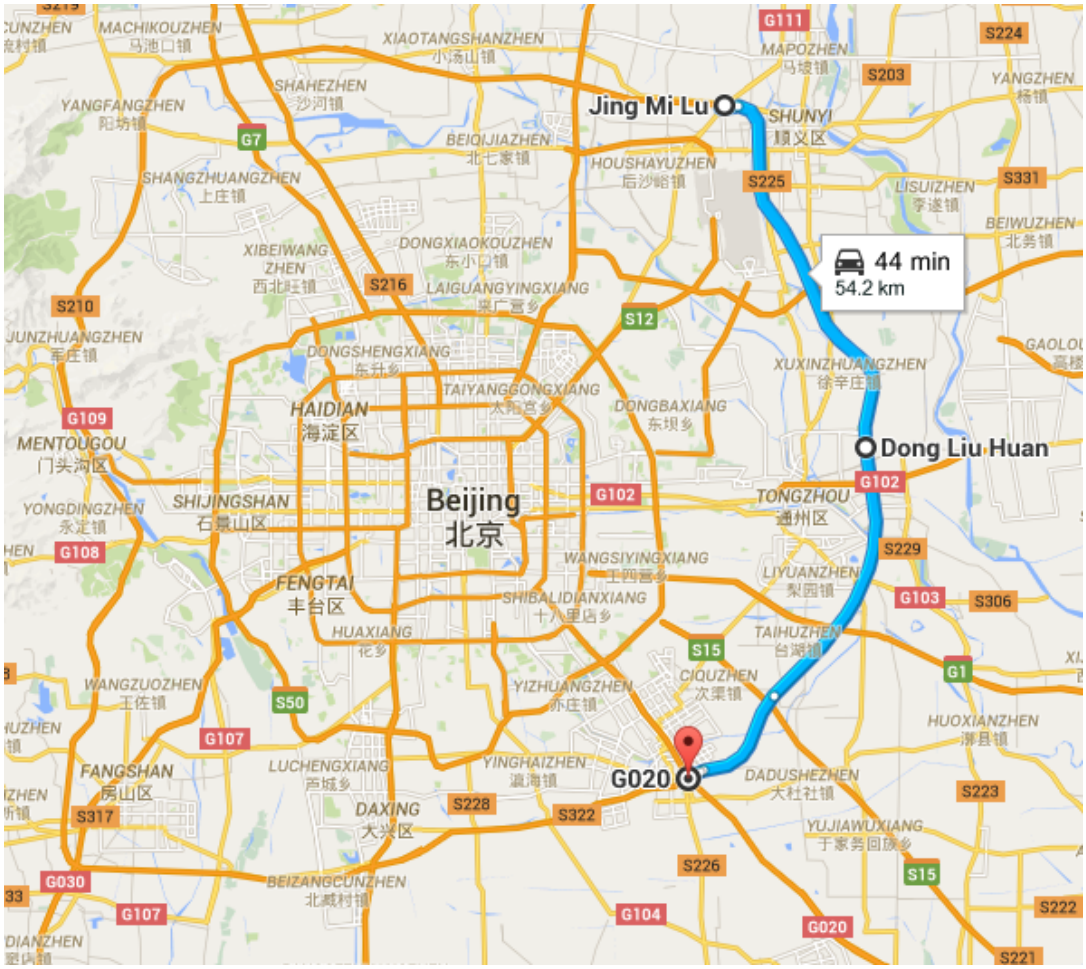

Figure 3.2: The Sixth Ring Road in Beijing, location for 70 and 100k/h test drives

3.1.2 Data sources

As already mentioned, data sources for traffic, weather and official PM2.5 air quality in Beijing had to be obtained.
Several providers were able to supply the data:

wunderground.com is a network of public and private providers of meteorological data. The most important data with respect to the air quality are temperature, wind speed and direction, humidity and atmospheric pressure.

Fresh-Ideas Studio provides hourly AQI data of over 35 air quality measuring stations all over the Beijing metropolitan area. This data can be obtained via App, or http-request, providing the data in JSON-format.

CenNavi provides traffic data every minute via http-request. This data includes road parameters such as lane numbers in both directions but also live traffic data as congestion levels in both directions.

3.2 Modelling the in-vehicle concentration of PM2.5

Concluding from the literature review in section 2.5, the model derived in this section should contribute to get a better understanding of:

- The influence of various HVAC settings on the inside PM2.5-concentration
- Which parameters influence the PM2.5-concentration estimation most
- How to obtain the parameters used in the model

Based on the suggestions of Switzer and Ott [29] as well as Liu and Frey [28] the in-vehicle PM2.5 concentration is modelled using a white-box approach, trying to incorporate physically explicable relations. For better comprehension the derivation of the model is examined in a time discrete domain, which is also easier to implement in the form of a software-based model.
The vehicle's interior microenvironment is represented by its volume, the cabin volume V_{cab}. Within this volume the assumption of a continuous, homogeneous particle distribution is made, leading to a uniform PM2.5 concentration within the vehicle's cabin, C_{in}. Similarly, the outside aerosol is assumed to be of a continuous and homogeneous nature represented by the outside concentration C_{out}. Every vehicle features an air circulation system and most modern cars even boast sophisticated HVAC systems. With ventilation enabled, there is a certain fraction ΔV of air that passes the HVAC unit and is released into the cabin. At the same time, we assume that there is no gas compression inside the vehicle, hence the same volume ΔV of air that enters the cabin, has to leave it. To determine the quantity of ΔV, a couple of parameters have to be considered: the volume of air passing through the HVAC within a timespan Δt is equal to the fan speed of the ventilation fan times the cross-section of the air duct of the HVAC unit. These parameters can be obtained in relation to the filter dimensions and the face velocity of the filter:

$$\Delta V = A_{face} v_{vent} T_d \tag{3.1}$$

with T_d being the discretization or sampling time.
Most cars allow the operator to decide whether to recirculate the in-vehicle air (**RC** mode) or enable the fresh air intake to supply the HVAC unit with outside air (**OA** mode). To achieve this switch-over in modes, one or more flaps are installed in two separate air ducts, to either shut off the inside or outside air intake of the HVAC unit. Expressing the mechanisms discussed so far in a mathematical model, a basic mass balance equation can be derived. This can be done in form of a regression, modelling the change in in-vehicle mass of PM2.5 during an elapsed time span Δt, equal to T_d.

$$\Delta m_{in}[k] = \Delta m_{rc}[k-1] + \Delta m_{oa}[k-1] - \Delta m_{ex}[k-1] \tag{3.2}$$

Introducing the concentration as a density of particle mass per volume, the equation above can be expressed as:

$$V_{cab} \Delta C_{in}[k] = \Delta V \varphi_{rc} C_{in}[k-1] + \Delta V \varphi_{oa} C_{out}[k-1] - \Delta V C_{in}[k-1] \tag{3.3}$$

Depending on the position of each flap, φ_{rc} for the RC duct flap and φ_{oa} for the OA duct flap, the air flow rate might increase, as the relation $\varphi_{rc} + \varphi_{oa} = 1$ is not compulsorily true. As this is a vehicle-specific behaviour, there is no general solution to this issue. For further details on how this issue is resolved in this study, see section 3.4.1.
So far, this expression represents a basic model, incorporating ventilation speed, circulation mode and some vehicle-specific characteristics. In an attempt to improve this model, several other effects have to be taken into consideration. As one distinctive feature this study is trying to incorporate is the usage of an electret fine dust fibre filter, the effect of the filter has to be embedded in the model. Thus, the so-called filter efficiency η_{filt} is introduced, defined as the ratio of particle concentration downstream the filter to particle concentration upstream the filter. The evaluation of this parameter is subject to extensive research, as already discussed in section 2.6. Ideally the filter is installed in an airtight manner in the duct. However, under real conditions and considering the fact that the filter has to be exchanged as it is a wearing part, this will not be the case. Hence, in addition to the filter efficiency, the ventilation speed-dependent filter leakage p_{leak} is introduced. Strictly, it represents not only the penetration due to leakage of the filter, but also incorporates the ventilation speed-variable part of the filter efficiency. This results from the experiment it is obtained with, as will be shown in subsection 3.2.1. Assuming that filter efficiency and filter leakage at time kT_d are known, they can be incorporated as the fraction of particular mass that is trapped inside the HVAC system.

$$\begin{aligned} V_{cab}\Delta C_{in}[k] = &\left[\Delta V \varphi_{rc}\left(1 - \eta_{filt} + p_{leak}\right) - \Delta V\right] C_{in}[k-1] \\ &+ \Delta V \varphi_{oa}\left(1 - \eta_{filt} + p_{leak}\right) C_{out}[k-1] \end{aligned} \tag{3.4}$$

As the outcome of the model should be the in-vehicle concentration at time kT_d, some minor reshaping has to be applied. Using the relation that $\Delta C_{in}[k] = C_{in}[k] - C_{in}[k-1]$ an expression for $C_{in}[k]$ is obtained.

$$\begin{aligned} C_{in}[k] = &\left[1 + \frac{\Delta V}{V_{cab}}\varphi_{rc}\left(1 - \eta_{filt} + p_{leak}\right) - \frac{\Delta V}{V_{cab}}\right] C_{in}[k-1] \\ &+ \frac{\Delta V}{V_{cab}}\varphi_{oa}\left(1 - \eta_{filt} + p_{leak}\right) C_{out}[k-1] \end{aligned} \tag{3.5}$$

This expression already delivers rather viable results, yet it is still missing out on some effects. There are different ways outside air can enter the vehicle's cabin, other than via fresh air intake of the vehicle's HVAC unit. Opening windows or doors can cause severe flows of outside air into the car, depending on vehicle speed as well as wind speed and direction. In this case, the inside concentration matches the outside concentration within seconds. In the model, this effect is represented by the air exchange rate due to windows and doors $\zeta_{w,d}$.
However, even with completely shut windows and doors, outside air can still enter the vehicle's cabin. Every vehicle comes with sealing of doors and windows. Unfortunately, even the most high-quality materials can not entirely prevent outside

air from diffusing into the cabin. In order to model this imperfection, the air-exchange rate due to diffusion ζ_{diff} is introduced. It is defined as the fraction of outside concentration C_{out} that diffuses into the cabin (in $^{-1}$). It can be observed that ζ_{diff} increases proportionally with increasing vehicle speed, as a higher air resistance induces a higher dynamic counter-pressure, forcing more air down cracks and gaps in the sealing.
Combining both factors ζ_{diff} and $\zeta_{w,d}$, the total air exchange rate is defined as $\zeta = \zeta_{diff} + \zeta_{w,d}$. As per definition, it is important to understand that ζ can not exceed 1, as this would mean that there is some kind of hidden gain for the concentration of the outside air, amplifying it while entering the vehicle. On another note, ζ does not incorporate leakage of the filter, as this effect is already described by the filter leakage coefficient.
With the assumption of an incompressible gas mixture inside of the cabin still being valid, the same volume entering the vehicle due to ζ, has to leave it. Adding these effects to the mathematical model results in:

$$\begin{aligned} C_{in}[k] = &\left[1 + \frac{\Delta V}{V_{cab}}\varphi_{rc}\left(1 - \eta_{filt} + p_{leak}\right) - \zeta T_d - \frac{\Delta V}{V_{cab}}\right] C_{in}[k-1] \\ &+ \left[\frac{\Delta V}{V_{cab}}\varphi_{oa}\left(1 - \eta_{filt} + p_{leak}\right) + \zeta T_d\right] C_{out}[k-1] \end{aligned} \tag{3.6}$$

The last effect taken into consideration has already been mentioned in section 2.5, in the proposal of Park et al. [31]. As dispersed particulate matter undergoes various transformation processes (see section 2.4), it exhibits a certain volatility. Thus, in an enclosed environment the concentration decreases over time, as particles deposit on the cabin's inside surfaces. Depending on the size of a particle it behaves differently within a stream of air. Bigger particles sink because of their mass and can not follow streamlines because of their inertia. Thus, they are likely to deposit first. Very small particles are subject to Brownian movement, which also increases their probability to get trapped on a surface. However, particles in a certain range in between are very durable and long lasting, as they are relatively unlikely to hit a surface. Eventually they can transform into bigger sized particles, which increases their likelihood of deposition. In order to model these effects of deposition within the cabin, the deposition factor δ is introduced. As δ depends on the size range of particles, it is best to evaluate it for a number of different size ranges. Also, air circulation influences the deposition rate, as particles are more likely to adhere to a surface with an increased flow rate.
Incorporating this in the expression to obtain the in-vehicle concentration, the final form of the model can be obtained:

$$\begin{aligned} C_{in}[k] = &\left[1 + \frac{\Delta V}{V_{cab}}\varphi_{rc}\left(1 - \eta_{filt} + p_{leak}\right) - \zeta T_d - \delta T_d - \frac{\Delta V}{V_{cab}}\right] C_{in}[k-1] \\ &+ \left[\frac{\Delta V}{V_{cab}}\varphi_{oa}\left(1 - \eta_{filt} + p_{leak}\right) + \zeta T_d\right] C_{out}[k-1] \end{aligned} \tag{3.7}$$

The following figure should provide a graphical overview of this (in its final form relatively complex) mathematical model.

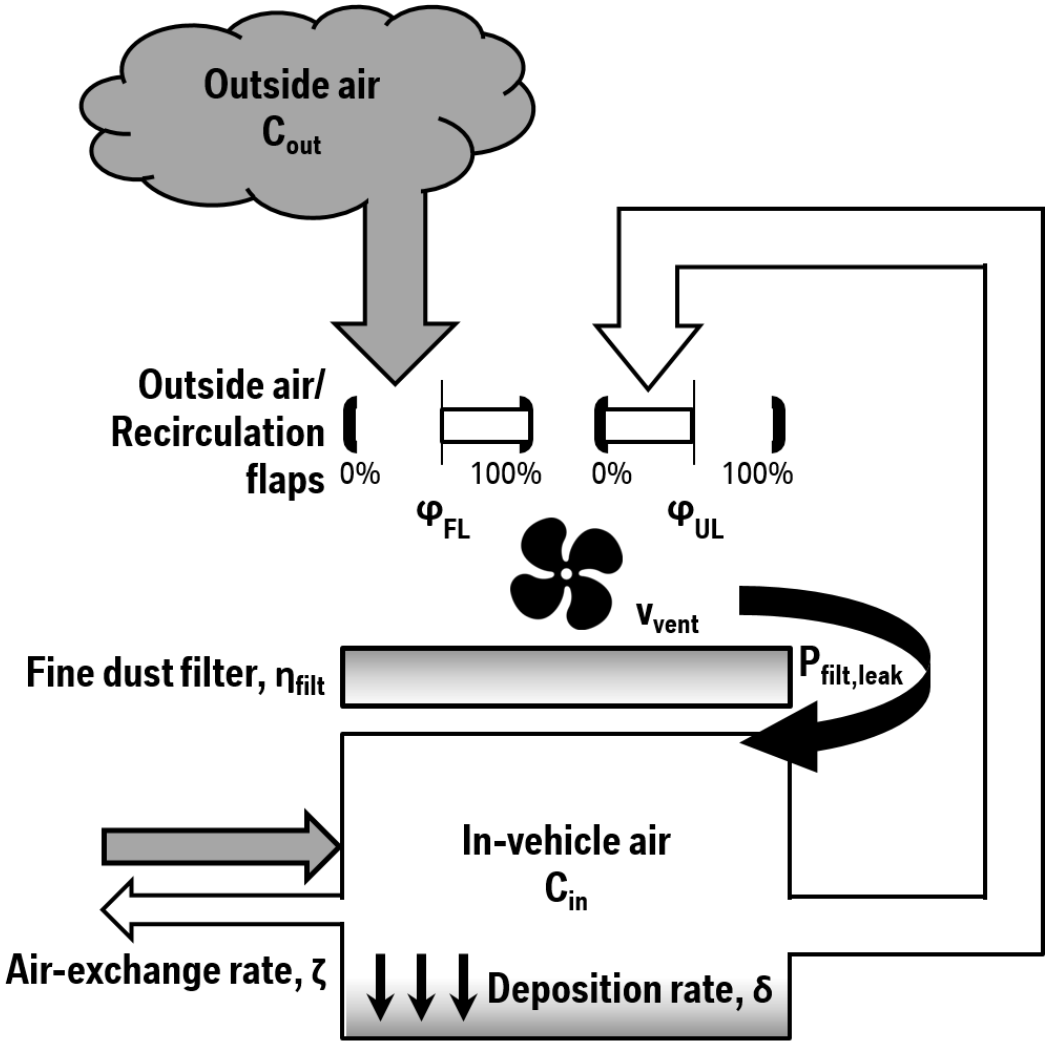

Figure 3.3: Illustration of the in-vehicle PM2.5 model

3.2.1 Model parameter estimation

Based on the model derived in the previous section, there are several parameters that have to be determined in order to apply the model under real conditions. As can be seen in the final model (eq. 3.7), the parameters that have to be identified are the deposition rate δ, the air exchange rate ζ, the filter efficiency η_{filt} and the filter leakage p_{leak}.

Deposition rate δ

In order to determine the deposition rate δ, the vehicle's filters are removed ($\eta_{filt} = 0$, $p_{leak} = 1$). Then, the developing of the inside concentration is measured at standstill. During each test cycle, the ventilation speed has to be kept constant. The recirculation flap must be completely open the whole time, while the outside air flap must be kept

shut ($\varphi_{rc} = 1$, $\varphi_{oa} = 0$). With closed windows and doors and the car in standstill, the air-exchange rate ζ can be neglected ($\zeta \approx 0$). Applying all these constraints to the model from eq.3.7 the following expression is obtained:

$$C_{in}[k] = [1 - \delta T_d]\, C_{in}[k-1] \tag{3.8}$$

Transformed from the discrete time domain into the continuous-time domain, this expression turns into:

$$C_{in}(t) = C_{in,0} \cdot e^{-\delta t} \tag{3.9}$$

As the deposition rate varies for different particle sizes, it is hard to determine a uniform value for δ. However, the equipment available to conduct these experiments is only able to distinguish between PM1 and PM2.5. Using the `fit()` function in Matlab also allows to fit the sum of 2 exponentials to a given curve. Therefore it is possible to compute an estimate for the deposition rate for Nucleation+Aitken mode, Accumulation mode and Coarse mode.
This is done for different ventilation speeds v_{vent}. It was found that the deposition rate can be approximated by a polynomial of 2^{nd} order:

$$\delta_i = c_{\delta,0} + c_{\delta,1} v_{vent} + c_{\delta,2} v_{vent}^2 \tag{3.10}$$

Using `fit()` again provides the coefficients c_i and thus a formula to compute δ_i at an arbitrary ventilation speed v_{vent}. To validate this model, an independent experiment has been conducted. Afterwards the obtained real values were compared to the modelled result by computing and examining the statistical mean and standard deviation.

Filter efficiency η_{filt} & filter leakage p_{leak}
As soon as the deposition rate is determined, estimates for the current filter efficiency η_{filt} and the filter leakage p_{leak} can be obtained. The filter leakage is defined as the fraction of aerosol that passes the filter, depending on the ventilation speed. However, as already discussed in section 2.6.1, the filter efficiency also depends on the ventilation speed. To accurately separate filter efficiency and leakage, a profound analysis under extensively monitored real conditions has to be conducted. However, with the given measuring equipment it was only possible to obtain the total penetration rate p_{tot}, defined as

$$p_{tot} = (1 - \eta_{filt}) + p_{leak} v_{vent} \tag{3.11}$$

This approach is at least valid for a certain mileage, as the filter efficiency is not deteriorating that fast. Thus, it is assumed that these parameters are constant within the time all the experiments have been conducted. To identify η_{filt} and p_{leak} independently from the air-exchange rate ζ, the vehicle has to be in standstill and all windows and doors have to be closed. This way, ζ is negligibly small and the model from eq.3.7 can be written as:

$$\begin{aligned} C_{in}[k] = &\left[1 + \frac{\Delta V}{V_{cab}} \varphi_{rc} p_{tot} - \delta T_d - \frac{\Delta V}{V_{cab}}\right] C_{in}[k-1] \\ &+ \left[\frac{\Delta V}{V_{cab}} \varphi_{oa} p_{tot}\right] C_{out}[k-1] \end{aligned} \tag{3.12}$$

In order to determine p_{tot}, the overall system has to be in a steady state, so that $C_{in}[k] \approx C_{in}[k\text{-}1] = C_{in,ss}$. Also, the steady state for the $C_{in}[k]$ in recirculation is per definition 0, so the experiment has to be done with outside air flap open. Hence, p_{tot} can be obtained as:

$$p_{tot} = \frac{\left(\frac{A}{V_{cab}} v_{vent} + \delta\right) C_{in,ss}}{\frac{A}{V_{cab}} v_{vent} \left[\varphi_{rc} C_{in,ss} + \varphi_{oa} C_{out}[k-1]\right]} \tag{3.13}$$

In outside air mode, it is not possible to keep the outside concentration constant. However, as each experiment only lasts a couple of minutes, the outside concentration is considered constant, measured, filtered and averaged over time, resulting in $C_{out,ss}$. In outside air mode the recirculation flap shuts completely, i.e. φ_{rc}=0. This leads to a simplified form of eq.3.14:

$$p_{tot} = \frac{\left(\frac{A}{V_{cab}} v_{vent} + \delta\right) C_{in,ss}}{\frac{A}{V_{cab}} v_{vent} \varphi_{oa} C_{out,ss}} \tag{3.14}$$

As previously defined, η_{filt} is assumed to be constant, while p_{leak} depends on the set ventilation speed v_{vent}. Using Matlab, a least-square fit can be performed, to obtain the optimal parameters. It was observed that a polynomial of first order is a sufficient approximation:

$$p_{tot} = c_{p,0} + c_{p,1} v_{vent} \tag{3.15}$$

Combining this expression with the definition from eq.3.11 we get:

$$\begin{aligned} \eta_{filt} &= 1 - c_{p,0} \\ p_{leak} &= c_{p,1} v_{vent} \end{aligned} \tag{3.16}$$

And thus a way to estimate η_{filt} and p_{leak}.

Air-exchange rate ζ

The last parameter left to be determined is the air-exchange rate ζ. As discussed in section 3.2, it is composed of the the air-exchange rate due to windows and doors $\zeta_{w,d}$ and the the air-exchange rate due to diffusion ζ_{diff}. The identification of both of those parameters is better done separately, as $\zeta_{w,d}$ is usually a multiple of ζ_{diff} and increases rapidly with the window/door position. To determine ζ_{diff}, test drives are conducted at vehicle speeds of 30, 50, 70 and 100km/h. Afterwards, ζ_{diff} is calculated, again in steady state, where $C_{in}[k] \approx C_{in}[k\text{-}1] = C_{in,ss}$. As all the other parameters should already be determined, ζ_{diff} can be calculated as:

$$\begin{aligned} \zeta_{diff} = &\frac{\frac{A}{V_{cab}} v_{vent} + \delta - \frac{A}{V_{cab}} v_{vent} \varphi_{rc} (1 - \eta_{filt} + p_{leak})}{C_{out}[k-1] - C_{in,ss}} C_{in,ss} \\ &- \frac{\frac{A}{V_{cab}} v_{vent} \varphi_{oa} (1 - \eta_{filt} + p_{leak})}{C_{out}[k-1] - C_{in,ss}} C_{out}[k-1] \end{aligned} \tag{3.17}$$

Again, as every experiment only takes a couple of minutes, the outside concentration can usually be assumed as constant, $C_{out,ss}$, in order to simplify the calculation.

After ζ_{diff} was determined at different vehicle speeds, a least-square fit provides an expression to obtain ζ_{diff} depending on the vehicle's speed v_{veh}:

$$\zeta_{diff} = c_{\zeta,0} + c_{\zeta,1} v_{veh} \tag{3.18}$$

with $c_{\zeta,1}$ and $c_{\zeta,0}$ as the numeric parameters obtained by the least-squares polynomial fit.

To complete the parameter identification, $\zeta_{w,d}$ has to be determined. This happens in two stages: First, the influence of the opening of the doors has to be considered, next the impact of the window opening is modelled. One basic assumption is, that the doors will only open at standstill, or very low speeds. Thus, there is no dependence on the vehicle speed. Due to the limited information about the opening position of the doors, the modelling of the doors was not taken into further consideration. However, as windows can be opened while driving and the position is also obtainable through the windows step motors, the effect of the windows was taken into consideration. The approach was to conduct experiments with one window open as well as both windows open. As the test vehicle's rear windows could not open, these two cases covered all the use-cases. The following table illustrates the different experiments. Each experiment was conducted at 30, 50, 70 and 100km/h.

Experiment	Window opening	Window(s)
1	5cm	passenger
2	10cm	passenger
3	5cm	passenger & driver
4	10cm	passenger & driver
5	completely	passenger & driver

At each experiment the ventilation was shut off, thus its effect can be neglected, simplifying the model from eq.3.7 to:

$$C_{in}[k] = [1 + \zeta T_d - \delta T_d]\, C_{in}[k-1] + \zeta T_d C_{out}[k-1] \tag{3.19}$$

In order to obtain ζ_w this equation can be rewritten as:

$$\zeta_w = \frac{\frac{1}{T_d}(C_{in}[k] - C_{in}[k-1]) + \delta C_{in}[k-1]}{C_{out}[k-1] - C_{in}[k-1]} \tag{3.20}$$

In order to obtain an expression for $\zeta_w(v_{veh}, \varphi_{dw}, \varphi_{pw})$ the following approach was proposed:

$$\zeta_w = a(\varphi_{dw}, \varphi_{pw}) + b(\varphi_{dw}, \varphi_{pw}) v_{veh} + c(\varphi_{dw}, \varphi_{pw}) v_{veh}^2 \tag{3.21}$$

This is due to observations that indicate that at constant window openings φ_{dw} & φ_{pw}, ζ_w is proportional to the square of v_{veh}. In order to obtain the window opening dependent coefficients, observations show that at constant speed, ζ_w is linearly proportional to the sum of both window openings, $\varphi_{dw} + \varphi_{pw}$.

$$a(\varphi_{dw}, \varphi_{pw}) = [a_1(\varphi_{dw} + \varphi_{pw}) + a_0] \tag{3.22}$$

b(φ_{dw},φ_{pw}) and c(φ_{dw},φ_{pw}) are processed the same way. Thus, an expression for ζ_w can be found as:

$$\zeta_w = [a_1(\varphi_{dw} + \varphi_{pw}) + a_0] + [b_1(\varphi_{dw} + \varphi_{pw}) + b_0]v_{veh} + [c_1(\varphi_{dw} + \varphi_{pw}) + c_0]v_{veh}^2 \tag{3.23}$$

Having determined both ζ_{diff} and ζ_w, the total air-exchange rate ζ can now be computed, depending on vehicle speed v_{veh}, window openings φ_{dw} and φ_{pw}, as well as the ventilation speed v_{vent}. As the inside concentration can not be higher than the outside concentration, the air-exchange rate is limited.

$$\zeta_w \leq \frac{1}{T_d} \tag{3.24}$$

3.3 Modelling the aerosol filtration process

For the modelling of the filtration efficiency coefficient η_{filt} there are numerous parameters to be adhered. Before even considering the filtration mechanisms taking place inside the filter itself, the physical characteristics of the aerosol have to be examined.
Theoretical evaluation using the slice model of Thomas et al. [36] was done. However, validating those results under real condition and due to the use of inadequate reference measuring tools was not feasible. As the test vehicle was not explicitly used for the study conducted in context with this thesis, the clogging process was impossible to monitor accurately. Regarding the measurement devices, it would have needed particle sizers able to measure the fraction of mass concentration in terms of particle diameter. Only one of the devices used, the TSI DustTrak DRX, was able to determine the mass concentration for different particle diameter ranges and could only distinguish between PM2.5 and PM1, a rather poor resolution. However, as technology progresses, the author hopes that the proposed approach can still at least provide the basic methodology for further studies conducted on a similar topic.
A promising way to obtain the filter's current efficiency is to derive an expression $\eta_{filt}(m_{load})$ that provides the filter efficiency depending on the captured mass. The captured mass can easily be determined through the in-vehicle concentration model.
Another reason that prevented feasible experimental results, was the fact that few characteristics of the filter itself were known. As will also be discussed in section 3.4.2, the supplier of the used filters was reluctant to release detailed information due to secrecy reasons. These parameters included the filter's fibre diameter as well as the electrical charge of each fibre, necessary to determine the electrostatic collection efficiencies. In order to obtain the fibre diameter(s), an electron microscope could be used. To identify the charge held by a single fibre, more sophisticated measurements would need to be conducted. According to the supplier, not even themselves were able to quantify the charge within the filter.
In summary, it was not possible to conduct experiments to validate the proposed model due to unknown characteristics and insufficient measuring equipment.

3.4 Test vehicle characteristics

The vehicle used to conduct this study was the BMW i3, a fully electric vehicle and the first car utilizing volume produced carbon-fibre-reinforced polymer parts to reduce the overall weight of the car and improve its efficiency. As the vehicle can be seen as a milestone in green technology, it was the perfect choice for this study. Besides, as it is a fully electric car, it is not affected by the local ban-day regulation.

Figure 3.4: Front view of the BMW i3

3.4.1 HVAC unit settings

The HVAC unit of the BMW i3 offers a variety of different settings. Basically, there are two different types of HVAC units available for this car, one with basic air conditioning and the other with a more sophisticated automatic air conditioning unit. In the test vehicle, the latter was installed. The next illustration shows all the different controls on the HVAC panel that can be adjusted by an operator.

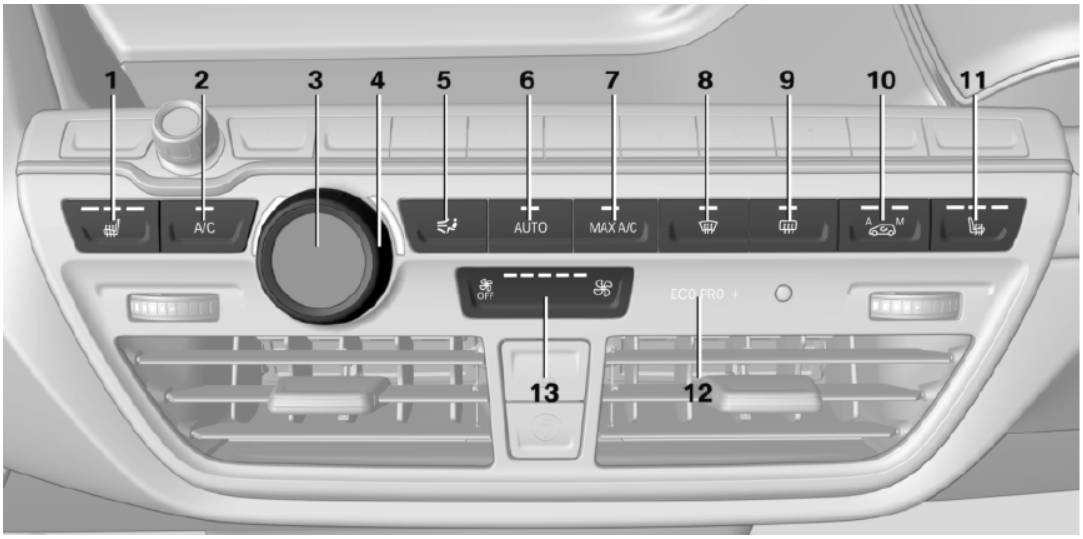

Figure 3.5: Illustration of the installed HVAC panel

1	Integrated seat heating driver	8	Defrost/defog
2	AC on/off	9	Rear window heating
3	Display	10	AUC/Recirculation
4	Set temperature	11	Integrated seat heating passenger
5	Air distribution program	12	ECO PRO mode
6	AUTO mode	13	Ventilation level
7	Max A/C mode on/off		

Integrated seat heating, rear window heating and the heating function of the A/C were not taken into consideration, due to the fact that all the measurements where conducted during the warm seasons in Beijing.
The Defrost/defog option was also kept turned off during the measurements. The AUTO mode is a rather interesting concept as it automatically adjusts ventilation level, air distribution and temperature, depending on the chosen set temperature and the intensity of ventilation (adjusted via ventilation level control). For the modelling itself, this function is rather unpredictable and interferes with most of the measurements. For the validation of the model on the other hand it is useful to activate it, as most customers tend to appreciate the comfortable automatic adjustment.
Air distribution is restricted to the middle ducts, as reference data regarding ventilation air flow per level was only available for this air distribution program. The display constantly shows the set temperature for the AC as well as the chosen air distribution program, the rotary knob is used to adjust the set temperature. The A/C button toggles the cooling function of the HVAC, Max A/C was also only considered for validation purposes, but not directly considered in the modelling (basically this button just temporarily sets the ventilation level to maximum and the set temperature to the minimum of 16°C).
The ECO-PRO mode LED indicates whether the so-called ECO-PRO driving mode is activated. In this mode the vehicle's parameters are adjusted in terms of minimum

power consumption to extend the maximum range of the vehicle. For this work the ECO-PRO mode is generally turned off.

All of those controls described so far are either kept constant or turned off during a test drive, if not specified otherwise. All the other HVAC controls will be discussed in more detail, as it is important to fully understand each of their functionalities. As already elucidated in section 3.2 these parameters need to be evaluated in order to consider the vehicle-specific influence on the model.

The **AUC/recirculation button** allows to switch the air circulation mode from fresh air intake to recirculation or AUC. AUC is the automatic air circulation control mode, where the outside concentration of carbon monoxide and nitrogen oxide is constantly measured and the air circulation mode is automatically switched from fresh air to recirculation mode whenever a noxious concentration level is reached. Unfortunately, this mode is of no help if the outside concentration exceeds harmful PM2.5 concentration levels, as there is no detection so far. Thus, there are only two relevant modes to consider: One is called recirculation (RC) mode, where the inside air is purely recirculated and the outside air is shut out. The other is the outside air (OA) mode, where the HVAC sucks in outside air via fresh air intake and does not recirculate in-vehicle air. If all LED's of the AUC/Recirculation button are off, OA mode is active. If the LED next to the small index M is on, manual recirculation mode is active. This concept may sound rather easy to understand, however there is a tricky logic behind the internal control of the air circulation mode. To control the flow of air from both outside and inside the vehicle, each air duct embodies a flap. In RC mode, the flap for the outside air duct shuts completely, while the flap for inside air opens up completely. In OA mode it's the other way round. In reality there are several functionalities that can transform one or both of the flaps into some intermediate state, for example when humidity inside fogs up the front windshield. To recognise these situations and deal with them accordingly, it is necessary to log the current flap positions using a data logger. Section 3.5 provides further detail on how to do this and which tools have to be used.

Operating the **Ventilation level control** allows to adjust the intensity of the blower fan that generates the air flow inside of the vehicle's cabin, as well as switch off the whole HVAC unit. The operator can choose from 5 different ventilation levels, indicated by the number of illuminated LEDs. From reference measurements conducted by the BMW R&D department, the following table relates the resulting filter face velocities to each of the ventilation settings under both outside air and recirculation setting.

Circulation mode -	Ventilation level -	Face velocity m/s	Flow rate m^3/s
RC	1	0.2852	0.0290
	2	0.3437	0.0350
	3	0.4534	0.0462
	4	0.7166	0.0730
	5	1.0530	0.1072
OA	1	0.2340	0.0238
	2	0.2925	0.0298
	3	0.4183	0.0426
	4	0.6669	0.0679
	5	0.9579	0.0976

As can be seen, face velocity in recirculation mode is slightly higher than in outside air mode, a fact that has to be taken into consideration. To switch off the ventilation and at the same time switch off the whole HVAC unit, the operator can progressively set the ventilation level to 0 (equivalent to no illuminated LEDs on the control) or press and hold the *decrease ventilation level* button. As already mentioned in section 3.2, there could be a situation where, depending on the opening angle of both flaps, the ventilation speed increases, due to a virtually bigger cross-section of the intake ducts. This occurs since the sum of the flap opening angle exceeds 100%. This rare case only occurs in some intermediate modes, as due to flushing cycles and defogging of the windows. It is assumed that the flow rate increases to the same extent then. Another special situation arises when the sum of the flap opening angle is smaller than 100%. However, for the very vehicle used for the test drives in this study, this only occurs in OA mode, to compensate the dynamic pressure generated at higher speeds. Thus, for these situations the OA flap position is manually set to 100% to ensure that the real flow rate is used in the model.

3.4.2 Cabin air filter characteristics

The filter installed in the test vehicle is a so-called combined filter, as it is composed of three layers: the fibrous filter mat, one layer of granular activated carbon (GAC) and another fibrous layer to immobilize the GAC and keep the filter in shape. As for the filtration, only the dedicated fibrous filter mat contributes to the collection of PM2.5, the effect of the other layers is negligible, as GAC only affects particles of a molecular size, being very effective at collecting molecules that may cause unpleasant odours, but rather ineffective on particles that contribute to the mass concentration of PM2.5.

The supplier of the filter states the following geometric specifications:

Dimensions	Length [mm]	246
	Width [mm]	207
	Height [mm]	32
Pleats	Pleat height [mm]	28
	Number of pleats	29
	Media area [mm^2]	6.464
	Pleat distance [mm]	8.5

For the initial pressure drop Δp_0 two reference measurements at different flow rates were conducted.

$\dot{V}$ m^3/h	Δp_0 Pa
225	69
450	192

The most important characteristic is the initial specified filter efficiency. Therefore two test were conducted, one with NaCl and one using Arizona Test Dust A2:

d_p μm	Δp_0 %	Δp_0+25Pa %
0.1 – 0.3	70	56
0.3 – 0.5	72	61

d_p μm	Δp_0 %	Δp_0+25Pa %	Δp_0+100Pa %
0.3 – 0.5	96	84	70
0.5 – 1.0	97	88	82
1.0 – 2.0	98	92	91
2.0 – 5.0	99	97	98
5.0 – 10	99	99	99

The maximum dust holding capacity is specified at 25g, at a pressure drop of Δp_0+100Pa. After request, the supplier specified the packing density α of the filter material to be at 0.14. The fibres are charged using the corona treatment method. Here a "curtain" of corona plasma is formed, by applying a high voltage to an electrode with a sharp tip. Moving the filter material through this curtain enhances the surface charge of it. However, according to the supplier no reference data is available, that quantifies this applied surface charge in any way. Thus, the validation of the filter model is hard to accomplish.
Another key characteristic of the filter that the supplier would not provide due to their non-disclosure policy is the fibre diameter d_f. The only alternative way to obtain it would be by a electron microscope scan. However, this equipment was not available within the facilities of BMW in Beijing, thus the fibre diameter could not be specified.
Figure 3.6 shows the installed filters. Each set of filters contains 2 pieces, both installed in the vehicle.

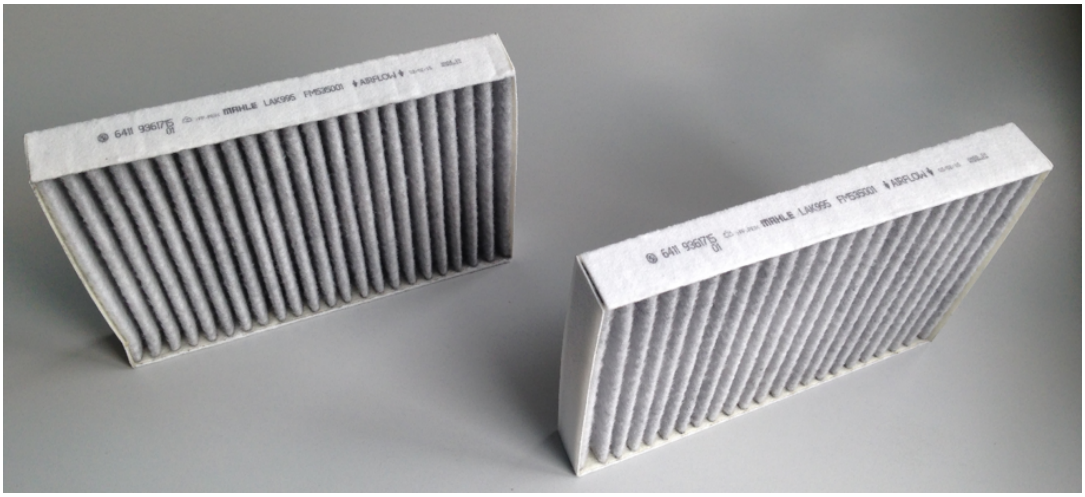

Figure 3.6: Photograph of the installed PM2.5 filters

3.4.3 Other relevant vehicle parameters

Apart from all the HVAC controls, the vehicle offers other useful parameters, that can be obtained via data logging. As discussed in section 3.2 the vehicle's speed greatly influences the air exchange rate ζ. Another essential information is the opening of windows and doors. For the windows, it is even possible to obtain the opening in centimeter based resolution. However, for the car's doors, only the binary information are available, i.e., whether they are open or closed. As the car was not exclusively used for PM2.5 testing purposes and since testing could only be done during times of bad air quality, the mileage was also an important figure to estimate fatigue of the seals and filter. The vehicle's sensor system also constantly measures inside and outside temperature, and provides both of them for logging purposes.
As pointed out in section 3.2, the vehicle cabin's net volume is a major characteristic in modelling the air flow within the cabin. To obtain a rather accurate estimate, the car's interior was virtually split into different modules. The dimensions of these modules were then determined using a tape measure. In the end, after merging all the modules' volumes, the net volume was composed.
The following table shows the volumes of the different modules (rounded to 2 decimals):

Module description -	Volume m^3
Gross volume	4.8
Front seats	0.16
Rear bench seat	0.34
Centre console	0.03
Dashboard	0.27
Net volume	4

To refine the value of the net air volume, one can consider the amount of passengers occupying the car and estimate the volume each of them engages. Sendroy and Collison [41] propose an average volume of 66 litres or 0.066 m^3, respectively. As the BMW i3 does not feature occupancy sensors for the rear bench seats, only driver and passenger seat occupancy can be detected.
An overview of all the static vehicle characteristics of the BMW i3 can be found in the appendix.
An illustration of the vehicle superimposed with the model as in eq.3.7 gives a schematic overview of the whole setup:

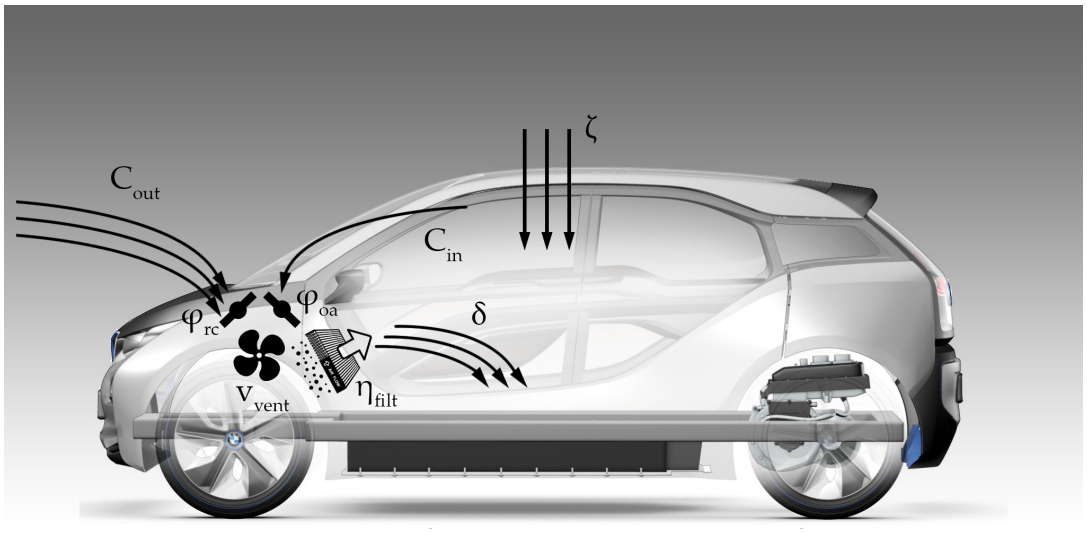

Figure 3.7: Graphic showing the physical representations of the model's parameter within the test vehicle

3.5 Instrumentation and Equipment

The difference of this study compared to most of the previous work was particularly in the detailed recording of vehicle data, as well as inside and outside concentration. Big effort has been put into the time-precise acquisition of vehicle parameters, to get an understanding of which parameters influence the in-vehicle concentration in which way. It was tried to synchronize the timing of each device to one time, provided by the computer used for the logging of the flap position (as the log-file would refer to this time). All the aerosol sampling devices were regularly synchronized using the software provided by TSI. Logging over the on-board diagnosis interface has proven to be a little more problematic. Here the logger was plugged in at a defined time (provided by the computer), which was later used as a reference for the evaluation. This methodology was deemed to be appropriate as a time resolution of a few seconds is sufficient for the model's accuracy.

3.5.1 Aerosol Measurement Devices

For the measurement of inside and outside concentration, two aerosol monitors from TSI have been used, the DustTrak II 8532 and the DustTrak DRX 8533.

Figure 3.8: TSI DustTrak DRX 8533 (left) and TSI DustTrak II 8532 (right)

Both devices rely on the laser photometric measurement method, however, the DustTrak DRX 8533 combines the function of a photometer with that of an optical particle counter. Thus, it is possible to obtain multiple mass fractions of the sampled aerosol. However, only PM2.5 and PM1 are in the scope of this study and can be separated. Devices provided by TSI are calibrated using Arizona Road Dust. This aerosol has a defined bulk density of 2.65 g/cm^2. Empirical studies showed, that this value does not match with air in Beijing, causing an over-estimation of mass concentration for sampled Beijing air [42]. Therefore TSI empirically determined a correction factor of 0.415 for Beijing, meaning that the assumed bulk density of particulate matter in Beijing air is around $1.1 g/cm^2$, which is around standard density ρ_p. This correction factor was set in both devices, accordingly. Moreover, before every test drive or standstill experiment, each device was zero calibrated, as recommended by TSI, to adjust the device to the current concentration range.
In the experiments conducted in the course of this thesis, the DustTrak DRX 8533 was used to measure the inside concentration, as it was more important to have more detailed knowledge about the size distribution inside than outside. The measurement of the outside concentration was done by the DustTrak II 8532 using a tube, fixed perpendicular to the airstream at the test vehicle's inlet in front of the windshield. The device itself was under the bonnet, as the BMW i3's engine is in the rear. Both devices possess an internal flash memory drive and are able to log large amounts of data. Using the USB interface and the provided software, the data can be exported for further processing.

3.5.2 Data Loggers

As already mentioned in section 3.4.1, a way to obtain the test vehicle's parameters during a test drive had to be found. There are several ways to obtain data from a vehicle's sensors and actuators. A lot of parameters can be logged by capturing CAN frames on the OBD (on-board diagnosis) interface of a vehicle. In the experiments conducted for this thesis, this was done using the eDDi logger, produced by Technica Engineering (Figure 3.9).

Figure 3.9: eDDi logger, by Technica Engineering

Figure 3.10: Vector VN1630 logger

To obtain the outside air's and recirculation air's flap position, a direct connection to the infotainment and communication CAN bus had to be installed. Then the CAN frames could be logged using the Vector VN1630 logger plus the Vector software CANape. This had to be done because these parameters are not internally routed to the on-board diagnosis interface.

The complete setup of measurement instrumentation can be seen in figure 3.11:

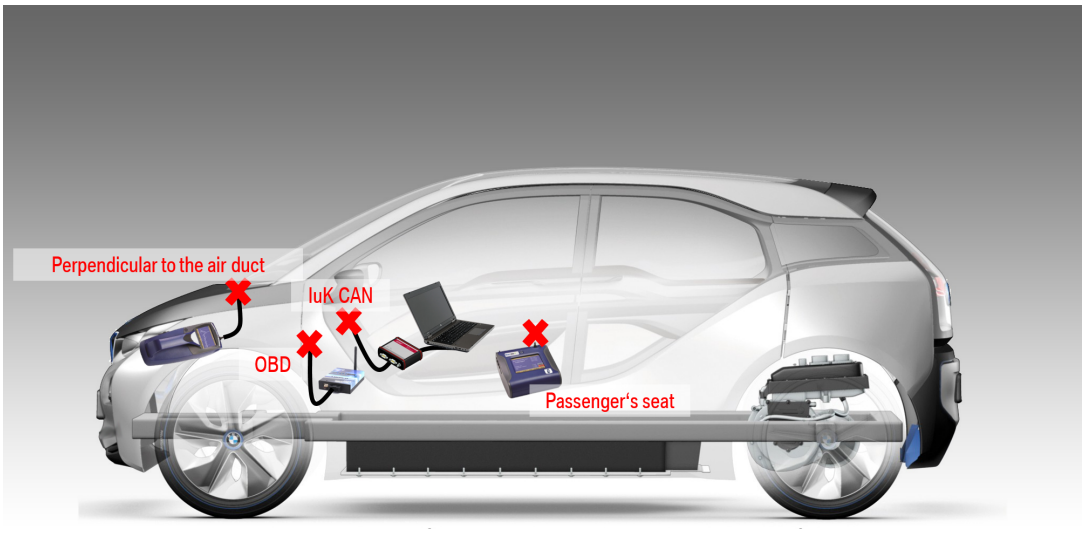

Figure 3.11: Arrangement of measurement instrumentation

To prevent the head wind from distorting the measurement, the measurement tube for the outside concentration was arranged perpendicular to the driving direction. The inside concentration measurement device (the DustTrak DRX) was placed on the passenger's seat. Thus, it has to be noted that the samples were not obtained at the height of the head, but below.

3.5.3 Matlab Evaluation Framework

In order to cluster and be able to process all the accumulated data from a test drive, a sophisticated framework of classes was defined, providing all the relevant data resulting from a single test drive. This data was then evaluated and processed, making use of the framework developed. Each test drive is represented by a single object of the class `TestDrive`. This class is composed of different objects itself, as there are different sources for data. Namely these are: vehicle data, traffic data, meteorological data, AQI data from public stations and data from the reference PM-sensors. The following table illustrates the structure of the `TestDrive` class:

time				
vehicle.	typecode			
	vin			
	chars.	intVol		
		Aface		
		Afilt		
		vvent.	oa	
			rc	
	params.	speed		
		mileage		
		auc		
		humidity		
		doors.	driver	
			passenger	
			driver_rear	
			passenger_rear	
		temp.	inside	
			outside	
		solar.	driver	
			passenger	
		flap.	UL	
			FL	
		ventilation.	circulation	
			setting	level
				autoio
			distribution	prog
				top
				mid
				bottom
		windows.	driver.	status
				position
			passenger.	status
				position
traffic.	occlane.	cong		
		num		
	opplane.	cong		
		num		
meteor.	station[].	name		
		code		
		coords		
		params.	time	
			temp	
			hum	
			windSpeed	
			windDir	
pm25gov.	station[].	name		
		coords		
		params.	time	
			aqi	
			pm25	
refsensor.	outside			
	inside.	pm25		
		pm1		

For every test drive raw data from the eDDi logger, the VN1630 logger, both reference measurement devices, governmental PM2.5-measuring stations, meteorological data from wunderground.com and traffic data from CenNavi are obtained. A simple script extracts this data and creates a single object from the aforementioned class, clustering all this data in a .mat-file which can then be used in a fast way for post-processing. One issue is, that the data is sampled at different frequencies. Thus, a fixed sampling rate is defined and the data is sampled using a simple zero-order hold. This means, that at each time a sample is obtained, the value of the latest available sample is used. For example, if the most current real sample is available for 15:21:31 (in HH:MM:SS) and a sample is drawn at 15:21:35 it takes on the value from 15:21:31. As governmental PM2.5 data is sampled at a rate of only 1 sample per hour, the error in respect to the real value at a certain time is likely to increase as the time difference to the last available sample gets larger. In contrast, data like vehicle speed is available at very high sampling rates, due to their importance in vehicle's on-board software. The smallest feasible sampling rate is at 1 sample per second as this is the minimum sampling rate of both PM2.5 measuring devices.

time contains all the timestamps between start and end time sampled at the defined sample rate.

vehicle contains vehicle identification characteristics (**typecode** e.g. i3 and **vin**, vehicle identification number, a unique, BMW specific number for each produced vehicle), physical characteristics (**chars**) as well as the logged parameters (**params**) during each test drive.
Physical characteristics include the interior volume (**intVol**), the face area of the filter (**Aface**), the filter area (total surface of the filter, larger than Aface due to the pleating) and the vehicle specific ventilation speeds at outside air and recirculation mode, depending on the ventilation level (**vvent**).
The logged parameters are mostly obtained through the eDDi logger, only the flap positions are not routed through the on-board diagnosis interface and thus have to be logged using the Vector VN1630 and Vector's CANape software. The parameters are **speed**, **mileage**, output of the automatic auxiliary air control sensor (**auc**), value of the anti-fog sensor (**humidity**), binary open/close state information for the vehicle's doors (**doors**), measured temperature outside and inside the car (**temp**), values of both solar radiation sensors (**solar**), flap positions for both outside air (**flap.FL**) and recirculation flap (**flap.UL**), relevant ventilation settings, including air circulation mode (**circulation**), ventilation level (**setting.level**), automatic ventilation mode on/off (**setting.autoio**) and air distribution program (**distribution**), as well as position and binary open/closed information for the vehicle's windows (**windows**).

traffic represents the data obtained via CenNavi, namely traffic congestion (**cong**) and lane number (**num**) for both the occupied (**occlane**) and opposite lane(s) (**oppline**).

meteor contains **name**, a wunderground station-specific **code**, coordinates (**coords**) and meteorological parameters (**params**) for a set of **stations**. Meteorological parameters include temperature (**temp**), humidity (**hum**), wind speed (**windSpeed**) and wind direction (**windDir**).

pm25gov provides PM2.5 (**pm25**) and corresponding AQI value (Chinese standard) (**aqi**) for a set of governmental PM2.5 stations.

refsensor clusters the measured PM2.5 concentrations of both TSI measuring devices used to measure **inside** and **outside** concentration. For the in-vehicle concentration there is also a distinct value for PM1 (**pm1**).

After the test drive specific data is stored in a .mat-file, these files can always be loaded in order to evaluate several test drives in order to observe different effects or determine various parameters. Separate scripts were coded to combine results from different test drives in order to obtain parameters like air-exchange rate or deposition rate. Matlab also provides sophisticated ways to plot results, therefore all the results presented in this work were illustrated using Matlab plots.

4 Results

Following the execution and evaluation of the previously discussed experiments, this chapter presents all the results obtained.

4.1 Aerosol characteristics

Section 2.3 presents different approaches on how to describe an aerosol. To get an idea of the extent to which the mentioned parameters change and how sensitive these parameters are to changes in temperature and relative humidity, simulations have been conducted. The scope was defined to be a temperature range of -20 to +50 °C and a range for relative humidity of 0 to 100 %, as these scopes cover nearly all real atmospheric conditions. The results show, that within this scope, the temperature is the parameter with the most impact on each aerosol characteristics parameter.
Using Tsilingiris' formula (eq.2.4), the air density of humid air ρ_m was simulated for steps in relative humidity of 10%:

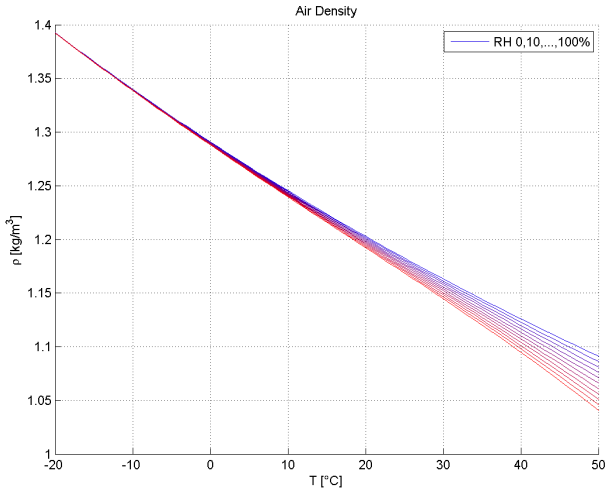

Figure 4.1: Simulation of air density of humid air ρ_m

Referred to the density of dry air (R.H. = 0%), a maximum deviation of 4.35% can be observed, compared to completely saturated air (R.H. = 100%) at the same temperature. The trend shows that this error is increasing at higher temperatures.
Same as for the air density, the dynamic viscosity was computed at different relative humidities with a step size of 10%:

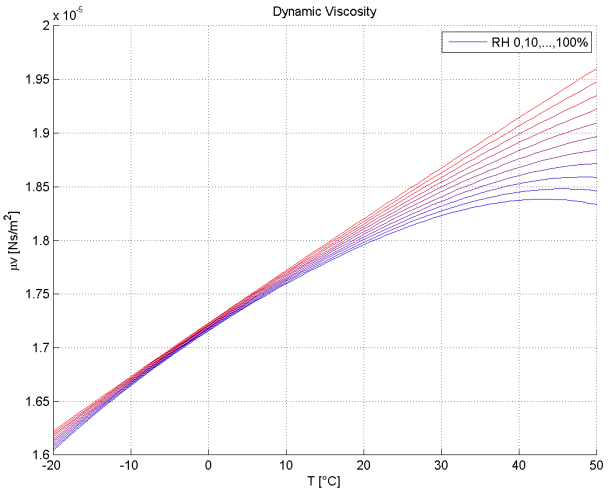

Figure 4.2: Simulation of dynamic viscosity of humid air μ_m

For the dynamic viscosity a maximum deviation of 6.47% can be observed. Again, this deviation increases with temperature.

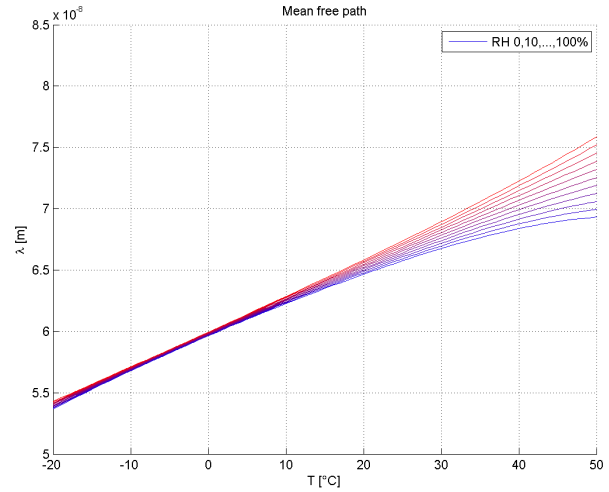

Figure 4.3: Simulation of mean free path of humid air λ_m

The mean free path of air shows the largest dependency on relative humidity, with a relative deviation of around 8.65%.

After having assessed all the carrier gas fluid characteristics of the aerosol, the mean particle size mass distribution in Beijing air was simulated, referring to published data by Wu et al. (see section 2.4.2). As they only consider PM1 in their work, an empirical estimate for the coarse particulate matter of PM2.5 was made, approximating the average fraction of PM1 of PM25 with 80%. Thus, the fraction of particles larger than 1μm is assumed to be uniformly distributed. As Wu et al. published different data for each season of the year, figure 4.4 compares these seasonal distributions.

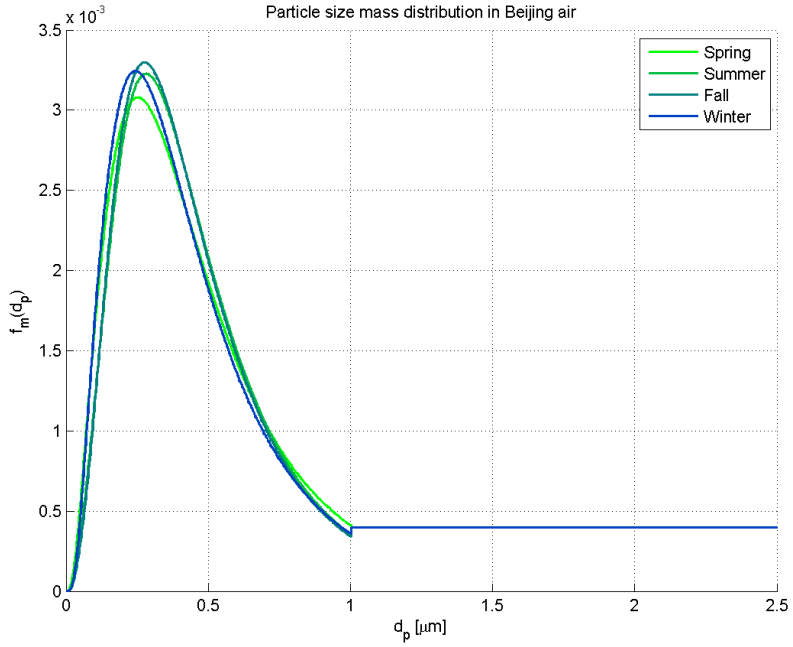

Figure 4.4: Comparison of seasonal variety of the average PM2.5 distribution in Beijing

As can be seen, the mean particle size mass distribution is only slightly varying over the year. Without the possibility of determining the true particle size distribution, one of these distributions can be used as a regional reference for the Beijing area. As already shown before, the bin size can have a significant effect on the accuracy of models sensitive to particle sizes. Therefore, figure 4.5 shows the distribution in summer for different bin sizes.

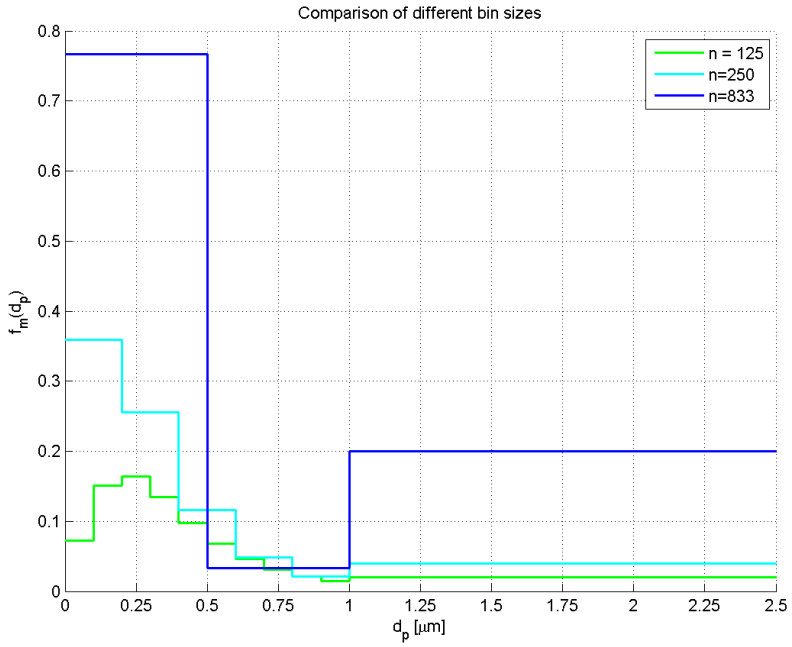

Figure 4.5: Comparison of different choices of bin size n

As this curves represents distributions, the sum over all bins must not exceed unity. For the in-vehicle PM2.5 model, due to a lack of particle sizing equipment, a bin size of 833 (equal to dividing the PM2.5 range into 3 subranges) was the highest resolution used.

4.2 Model parameter estimation

The model parameter estimation was done in Matlab, using data obtained from data loggers and measuring devices. In order to identify all the parameters, different experiments were conducted, as described in section 3.2.1. All the data resulting from those experiments was clustered and processed in Matlab, using the testing framework as developed in section 3.5.3.

Deposition rate δ

The deposition rate δ was obtained in standstill experiments. One experiment was conducted on July 29^{th}, the other on August 03^{rd}. As already mentioned in section 3.2, it is important that, in order to not corrupt the measurement, the flaps are in recirculation mode. This means that, ideally, the recirculation flap is completely open during each experiment and the outside air flap is completely shut. However, as mentioned in section 3.4.1, there are certain functions implemented in the used test vehicle that might control the flaps and change their position. Thus, the flap position during each measurement has to be monitored closely.

The following figures show the real measured in-vehicle concentration versus the modelled in-vehicle concentration of PM2.5 and PM1 over time. Figure 4.6 illustrates the in-vehicle deposition at perfect measuring conditions:

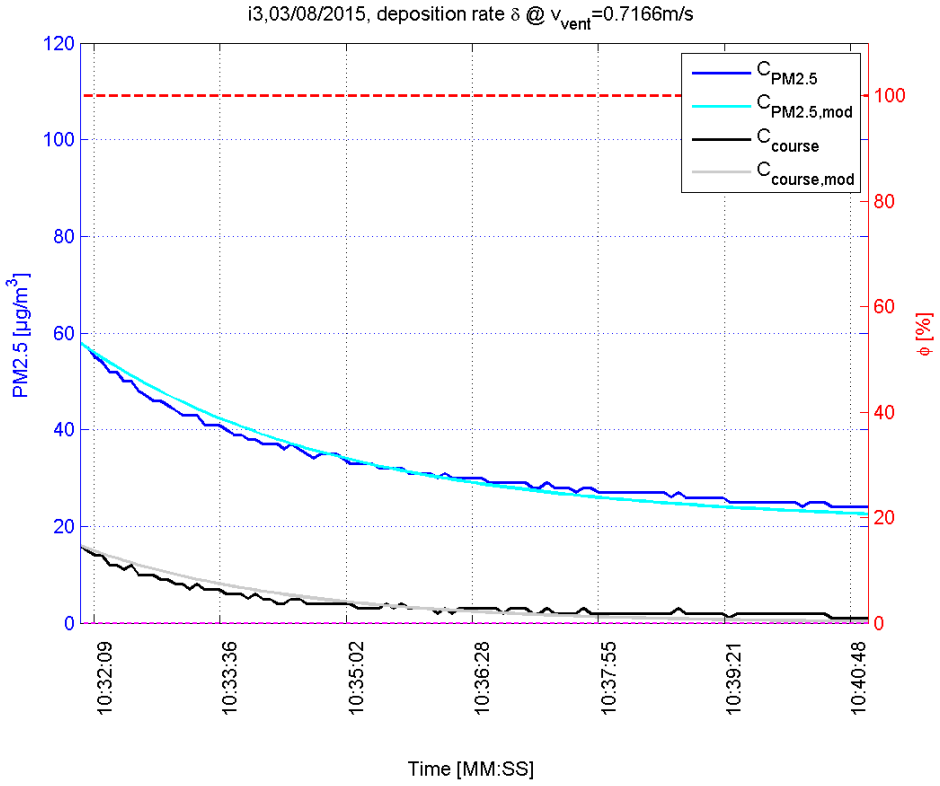

Figure 4.6: Deposition at ventilation level 4

As can be observed the model is a rather perfect fit to the real deposition process. However, figure 4.7 shows the impact of a slightly opened outside air flap:

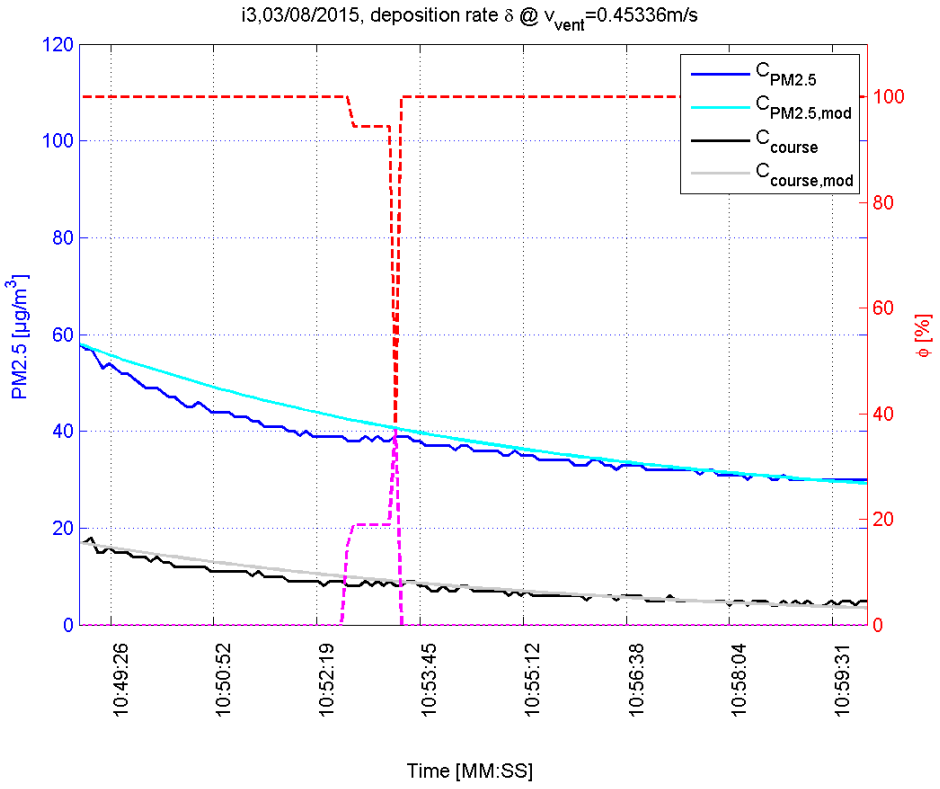

Figure 4.7: Deposition at ventilation level 3

Here, the process can not be fit by the sum of three exponentials, thus this measurement is not to be considered in order to obtain an expression for $\delta(v_{vent})$.
Performing this fit at all ventilation levels provides a set of six 3x1-vectors $\underline{\delta}$. This set was then also fit by a 2^{nd} – order polynomial depending on the ventilation speed v_{vent}. Plots 4.8 – 4.10 compare the experimentally obtained values for $\underline{\delta}$ at each ventilation level with the 2^{nd}–order fit.

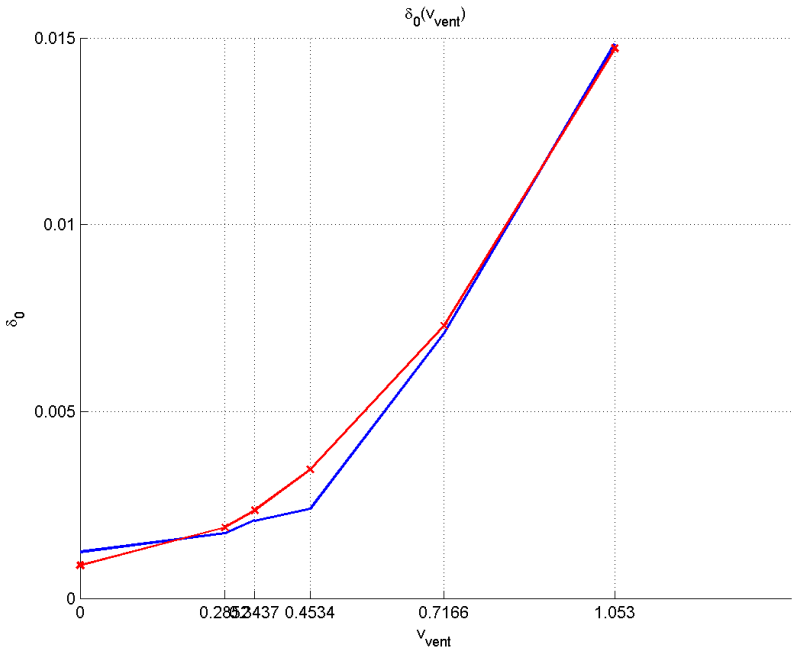

Figure 4.8: Deposition rate for Aitken+Nucleation mode particles, δ_0.

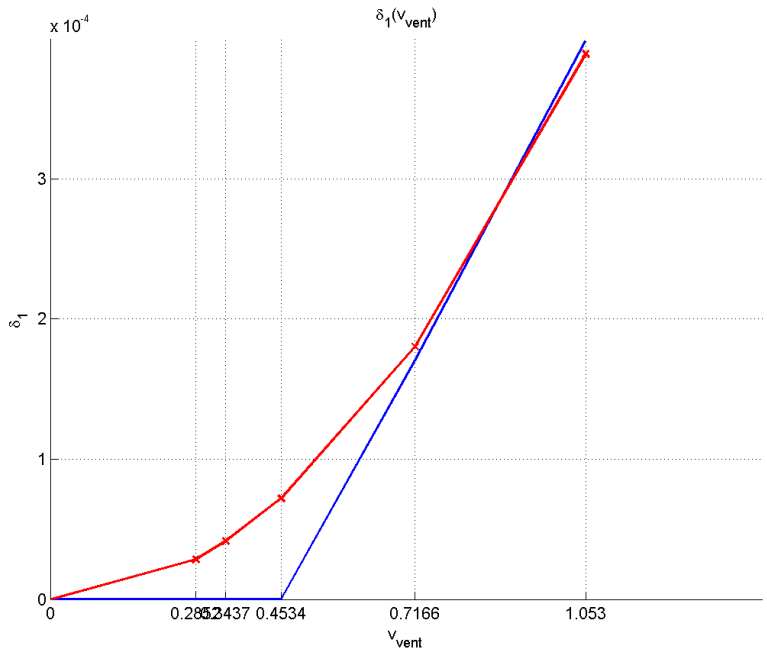

Figure 4.9: Deposition rate for Accumulation mode particles, δ_1.

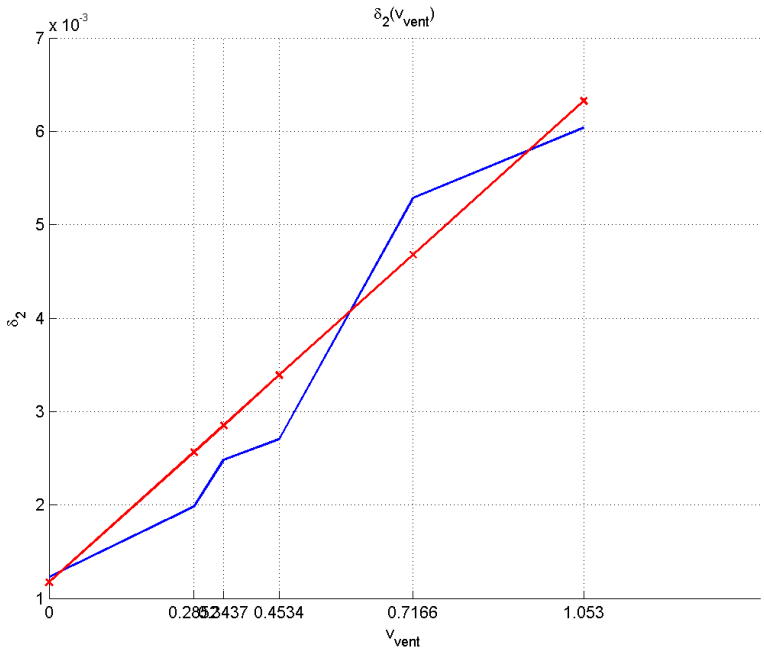

Figure 4.10: Deposition rate for coarse mode particles, δ_2.

In order to validate the obtained values, a second experiment was conducted, under similar circumstances as the first one. Figure 4.11 depicts a perfect test cycle, with a completely shut outside air flap. Figure 4.12, on the other hand, is a good example for the impact of an open outside air flap. As the flap is 25% open for about one minute, the assumption of no outside concentration being introduced into the cabin is violated, which corrupts the validation.

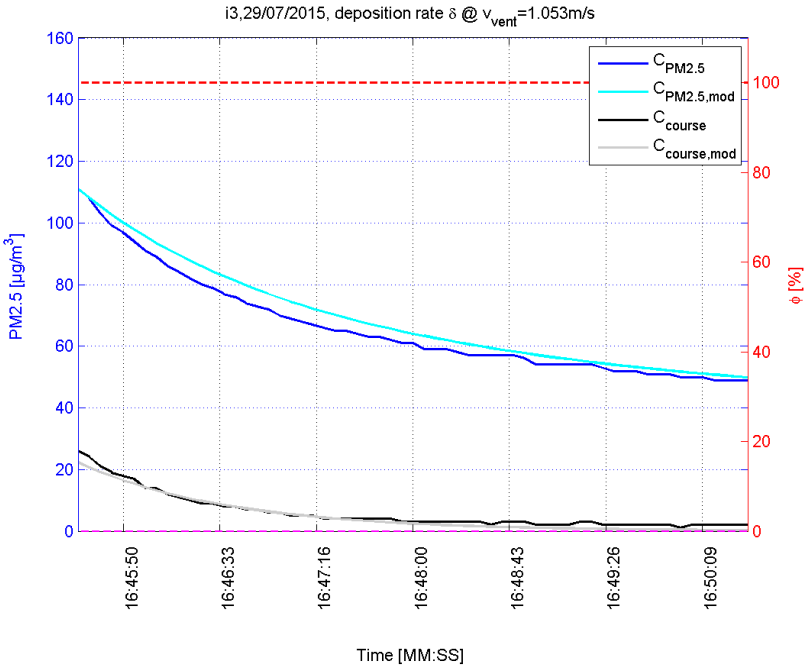

Figure 4.11: Deposition at ventilation level 5

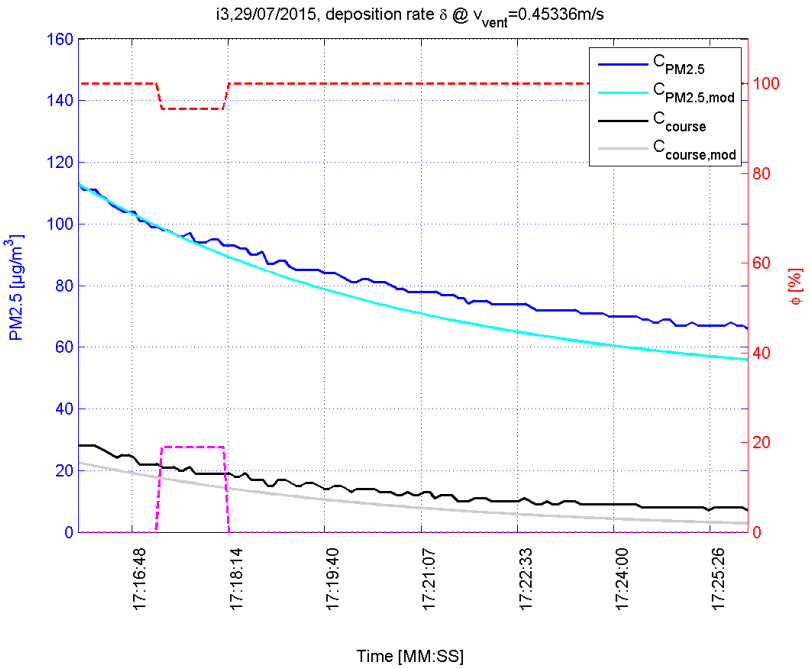

Figure 4.12: Deposition at ventilation level 3

In order to get a conclusion about the performance of the deposition model, a statistical evaluation of the error of the model compared to the data obtained in the validation tests has been made. The error is defined as:

$$e = C_{in} - C_{in,mod} \tag{4.1}$$

Thus, a negative value for e means an overestimation of the model, while a positive value for e means an underestimation of the model compared to the real concentration. The following table shows the mean of the average error $\bar{e}$, the relative error in relation to the real value $\bar{e}\%$, as well as the standard deviation of the error σ_e.

	$\bar{e}$ $\mu g/m^3$	$\bar{e}_{\%}$ %	σ_e $\mu g/m^3$
off	-6.8081	-7.3769	1.2850
1*	3.0753	3.0613	1.7831
2*	1.4051	1.5538	3.9929
3*	6.0932	7.4457	3.6260
4**	-	-	-
5	-3.2128	-4.8667	1.7295

An asterisk* indicates that these validation cycles have also been corrupted by the outside air flap opening for a short time. However, the results are still of acceptable accuracy, given that the reference tool's uncertainty specified at is around 20 % itself. The double asterisk** indicates that the measurement was corrupt in a way that it was not possible to evaluate it properly, due to technical issues.
For the coefficients $\underline{c_\delta}$ for each $\underline{\delta}$ the following values were obtained

	$\delta_{ait,nuc}$	δ_{acc}	δ_{coarse}
$c_{\delta,0}$	0.012	0	0.0009
$c_{\delta,1}$	0.0049	0	0
$c_{\delta,2}$	0	0.0004	0.0125

Filter efficiency η_{filt} & filter leakage p_{leak}
After the deposition rate is determined, the filters can be reinstalled and filter efficiency and leakage can be identified. As already discussed in section 3.2.1, both parameters are obtained through the total penetration rate p_{tot} at each ventilation speed. Thus, five standstill test runs have been conducted, varying the ventilation level from 1 to 5. Moreover, all measurements have been done in outside air circulation mode. This means that the flap position does not have to be monitored, as outside air mode overrides any logic from ECUs and the flap is only regulated at high vehicle speeds to keep the air flow of the fresh air intake constant.
Figure 4.13 shows the penetration rate at each ventilation level and the linear fit that has been made. As can be observed, the assumption of a linear dependency of ventilation speed is appropriate.

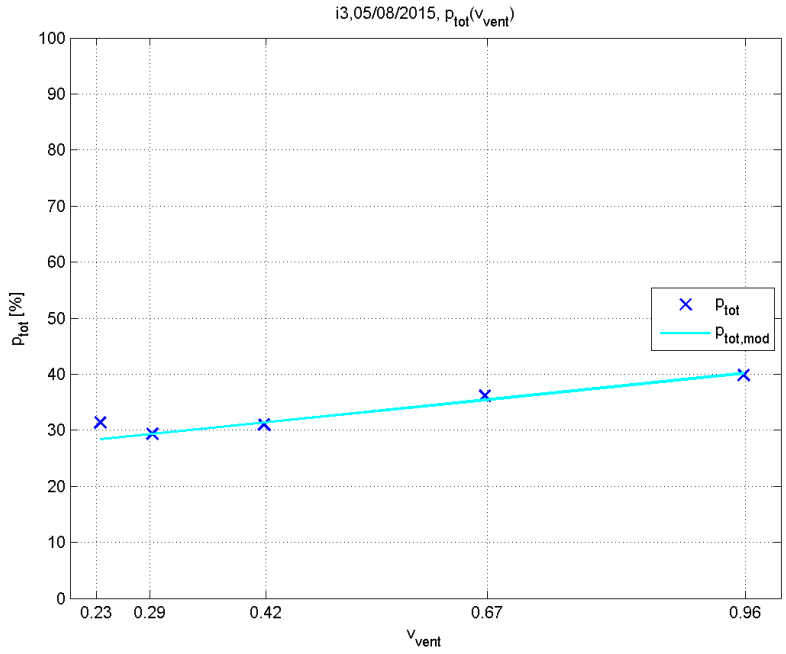

Figure 4.13: Trend of the real in-vehicle concentration vs. model-based trend at ventilation level 2

Given the total penetration rate at each ventilation level, filter efficiency η_{filt} and filter leakage p_{leak} can be determined, using a simple first order polynomial fit.
The Matlab evaluation of the test data provided the following coefficients $\underline{c}_p$:

$c_{p,0}$	$c_{p,1}$
0.1542	0.2310

Once inserted into the model, the model can be executed and compared to the real trend of PM2.5 concentration at standstill, measured using the reference tools. At ventilation level 2, the following curve was obtained:

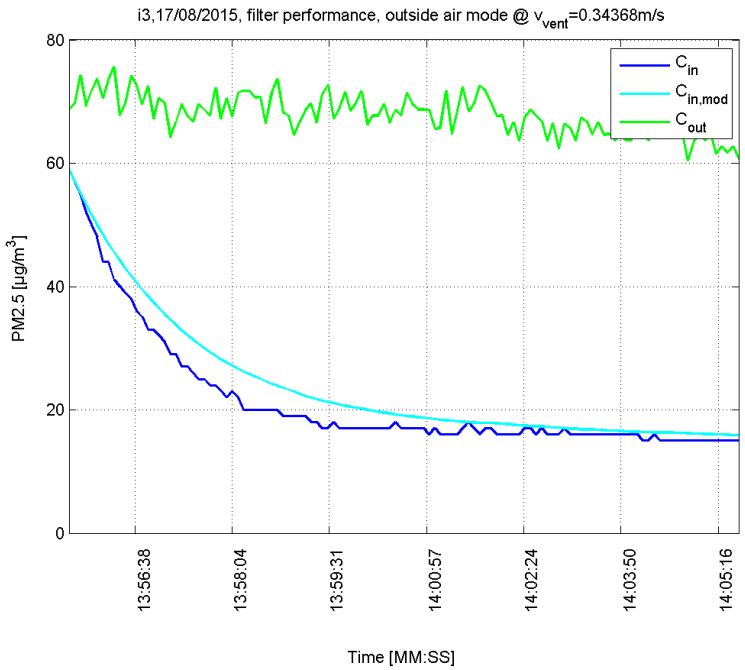

Figure 4.14: Trend of the real in-vehicle concentration vs. model-based trend at ventilation level 2

Air-exchange rate ζ

The last parameter that had to be determined in order to complete the proposed model was the air-exchange rate ζ. As already mentioned in section 3.2.1, the total air-exchange rate ζ is composed from both the air-exchange rate due to doors and windows $\zeta_{w,d}$ and the air exchange rate due to diffusion ζ_{diff}. Given that δ, η_{filt} and p_{leak} are known, ζ_{diff} can be obtained by conducting steady state experiments at different vehicle speeds v_{veh}, in order to obtain an expression $\zeta_{diff}(v_{veh})$. Following the methodology given in the previous chapter, ζ_{diff} was evaluated at vehicle speeds of 30, 50, 70 and 100km/h. Next, an expression $\zeta_{diff}(v_{veh})$ was calculated, using the `fit()` function again. It was found that a first order polynomial is a good approximation (see figure 4.15).

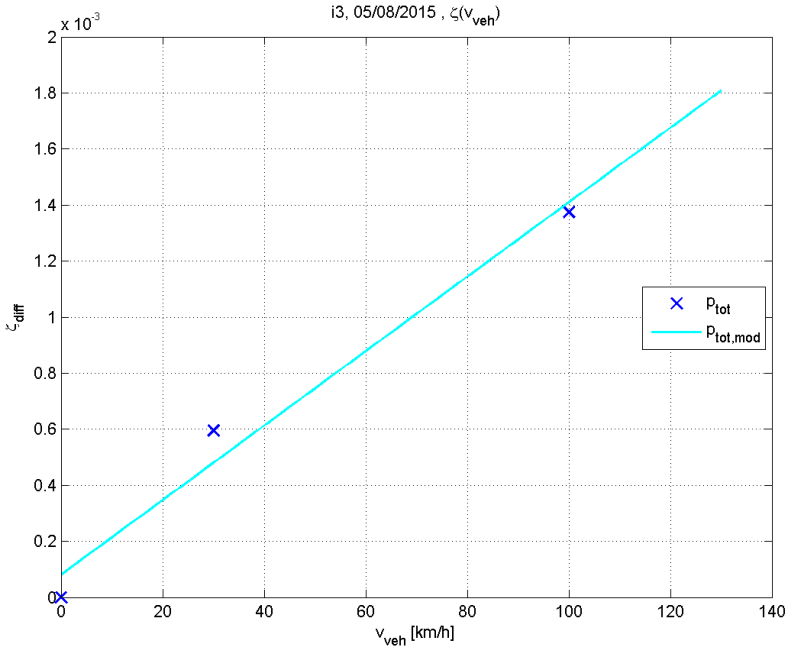

Figure 4.15: ζ_{diff} at different vehicle speeds v_{veh}

The coefficients for $\zeta_{diff}(v_{veh})$ were determined to be:

$c_{\zeta,0}$	$c_{\zeta,1}$
$1.33\ 10^{-}05$	$8.12\ 10^{-}05$

For the air-exchange rate due to window opening ζ_w 14 experiments were conducted as discussed in section 3.2.1. As ζ_w is a two-dimensional function of the window openings φ_{dw} and φ_{pw}, as well as the vehicle speed v_{veh}, it is difficult to choose the right approach. Thus, two plots were studied, the first one (fig. 4.16) shows ζ_w among different vehicle speeds v_{veh}, the second one (fig. 4.17) shows ζ_w among different cumulated window openings $\varphi_{dw} + \varphi_{pw}$.

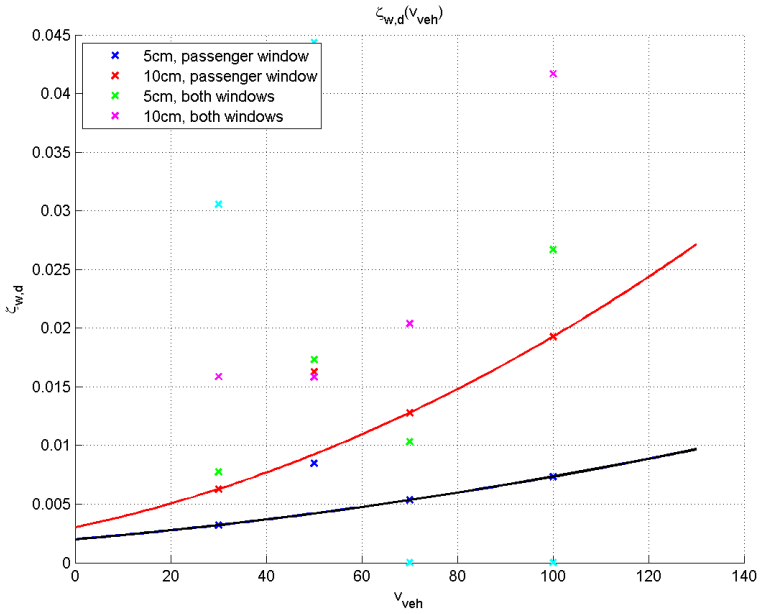

Figure 4.16: ζ_w at different vehicle speeds v_{veh}

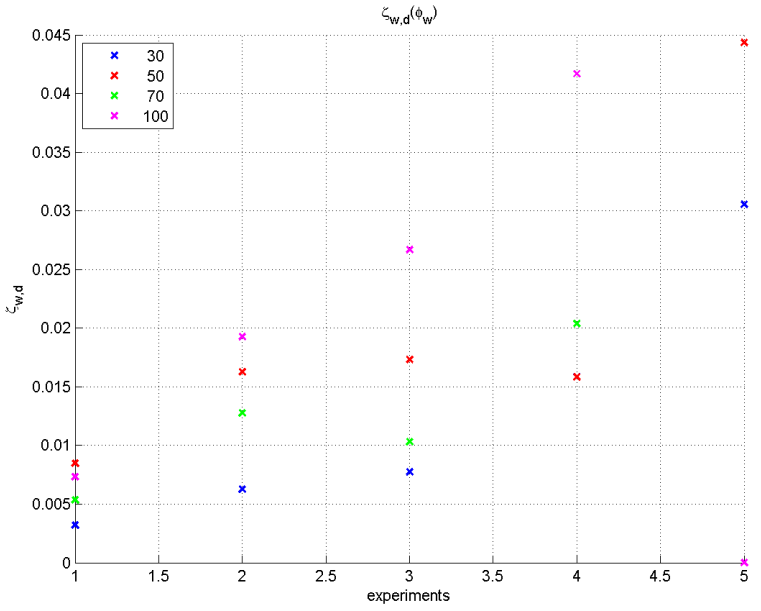

Figure 4.17: ζ_w at different vwindow openings φ_{dw} and φ_{pw}

As already stated, it seems that ζ_w is proportional to the square of v_{veh}, therefore a second order least square fit provides values for $a(\varphi_{dw}, \varphi_{pw})$, $b(\varphi_{dw}, \varphi_{pw})$ and $c(\varphi_{dw}, \varphi_{pw})$, referring to eq. 3.22.

Using these values, the coefficients a_0, a_1, b_0, b_1, c_0 and c_1 can be determined by computing a first order fit among the cumulated window openings $\varphi_{dw} + \varphi_{pw}$ as in eq.3.22.

a_0	a_1	b_0	b_1	c_0	c_1
0.0209	0.00094	0.001	-1.54 10^{-5}	1.17 $10^{-}5$	-4 10^{-7}

4.3 In-vehicle model validation

After all parameters were obtained, the model was validated by conducting real conditioned test drives and applying the model to the formerly conducted test drives (i.e. those to determine the parameters). The result was then compared to the reference values and the quality of the model estimation was quantified by the mean value and the standard deviation of the model error e. A perfect model would have a mean $\bar{e}$ and a standard deviation σ_e of naught. In this thesis, the model error e was defined as:

$$e = C_{in,real}[k] - C_{in,mod}[k] \tag{4.2}$$

Figure 4.18 shows one of these real condition test drives.

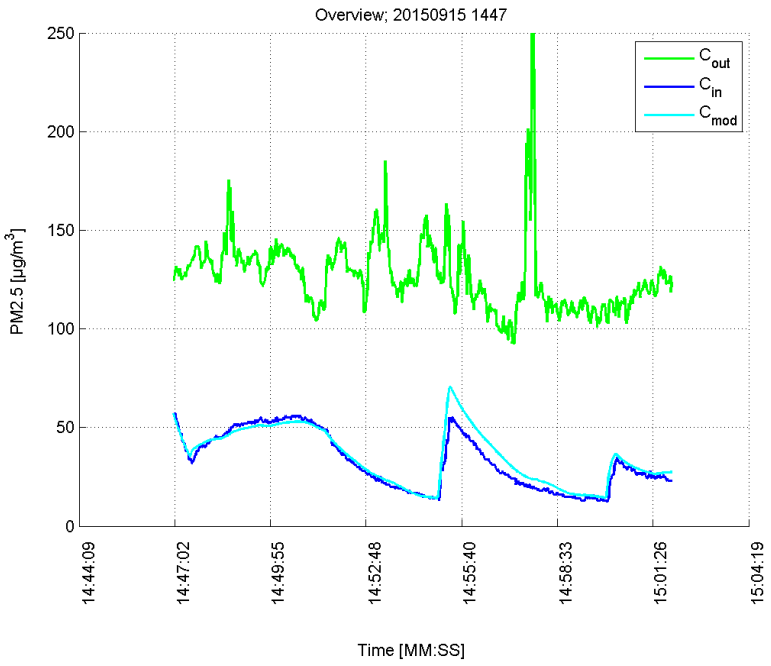

Figure 4.18: Validation test drive comparing the real in-vehicle concentration ($C_{in,real}$) with the modelled in-vehicle concentration ($C_{in,mod}$) using the outside concentration C_{out} sampled with 1s.

As can be seen, the fit the model provides seems to be of good quality. To quantify this quality the statistical parameters of the model were obtained as:

$\bar{e}$	σ_e
-2.259	4.145

This can be interpreted as an average overestimation of in-vehicle concentration, with 63% of the error e lying in the interval ($\bar{e}$-σ_e;$\bar{e}$+σ_e). Also, in this case the model uses the reference values for the outside concentration in every timestep. Using a lower sampling rate for the outside concentration, the result changes. Figure 4.19

shows the effect of a downsampled outside concentration C_{out} on the model. The sampling time here was set to 10min, each sample was computed of the average of a 10s interval measurement.

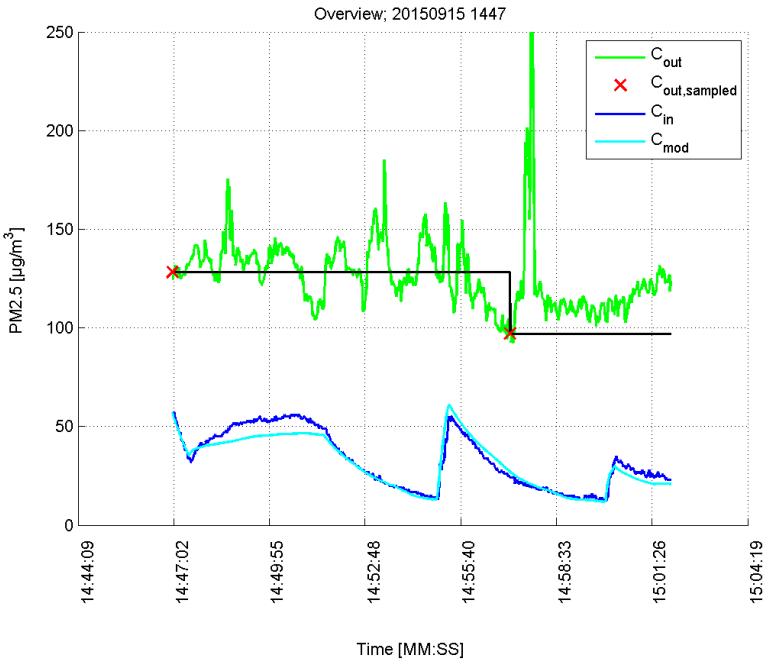

Figure 4.19: Validation test drive comparing the real in-vehicle concentration ($C_{in,real}$) with the modelled in-vehicle concentration ($C_{in,mod}$) using the outside concentration C_{out} sampled with 10min.

The statistical characteristics of the model error e here were computed to be:

$\bar{e}$	σ_e
1.631	4.046

As can be observed, the quality of the model fit did not change significantly. Thus, for well-predictable use-cases, it is assumed that a reduction in sample-rate does not excessively deter the model's prediction.

5 Conclusions

After the results were obtained in the previous chapter, this chapter tries to provide a discussion regarding methodology and tries to answer the research questions stated in chapter 1. Next, implications and conclusions are made, based on the given results. Limitations and constraints are discussed and suggestions for future improvements are made. Finally, this chapter provides an outlook on how the model can be used in a real environment and in which ways it can support in-vehicle PM2.5 measurement.

5.1 Discussion

In order to discuss the experimental results, the four research questions stated in the beginning are considered and attempted to be answered:

1. **Is there a way to model the in-vehicle concentration of PM2.5?**
   As discussed in chapter 2, there has already been research on modelling the in-vehicle air quality in the past. Based on these publications, a new model was derived. Concluding from the reviewed literature, this model is supposed to be the first of its kind, as it incorporates detailed knowledge about the specific characteristics of the vehicle used. This was possible because of data logging technology, logging parameters in real time. A difference between modelling the PM2.5 concentration inside and outside the vehicle has to be made. This thesis assumes knowledge of the outside quality in order to estimate the in-vehicle concentration. However, in order to achieve a model that can work completely without locally installed supporting sensors, a feasible model or source for the outside concentration would have to be found. Also, the deterioration of the filter is still to be modelled; a very complex task which is still to be resolved by science. In summary, the research question can be affirmed, the results show that a model can provide predictions of the in-vehicle PM2.5 concentration.

2. **How can the parameters of that model be determined in practice?**
   In subsection 3.2.1 a framework for estimating the model parameters is proposed. Thus, an easy-to-understand guideline should be provided that can be followed step-by-step. It has to be highlighted that the parameter determination would have to be done for each type of car (i.e. for BMW: 1series, 3series, 5series etc...). This results in a multiplicity of measurements, repeating for each car model. It is yet to be seen if a generic way can be found in order to calculate the parameters for different car types, based on experimental parameter estimation for only one or a few other types of cars. A future goal could be an improved parameter estimation framework, providing precise

model parameters depending on a few key characteristics of the car, that can be obtained by only a few reference measurements.

3. **Can the model provide feasible estimates under real conditions?**
   The qualitatively good results provided in section 4.3 further verify that the in-vehicle air quality can be modelled rather accurately. In terms of feasibility, the model is yet to be verified using different car models and in different ambient conditions (rain, cold weather). Combined with an on-board PM2.5 sensor, the model can also be exploited in other ways, creating new possibilities and use-cases.
4. **How can the obtained model be used in a real-world application?**
   In course of the thesis, numerous ways of exploiting the model were found, as will be discussed in section 5.4. A sensor-based filter deterioration detection indicates when the customer should change his filter. Furthermore, the model is able to detect non-official BMW products with a lower performance and the customer is protected from low-quality fake products (especially relevant in China).

5.2 Limitations

The proposed model tries to incorporate as many variables as possible, however it is yet far from perfect. Limitations of different source constrain the model's prediction, some easy to incorporate in future work, some taking more effort to attain. The following list shows already incorporated parameters (✔), parameters that have yet to be included in the model (❑), as well as parameters that have to be subject of excessive further research or are not able to be obtained under the given premisses (✘).

- ✔ different air circulation modes
- ✔ different ventilation speeds
- ✔ window opening
- ❑ sun roof opening
- ❑ door opening
- ❑ validation using other vehicles
- ❑ influence of heating mode (detour of air flow over heat exchanger)
- ✘ individual customer behaviour
- ✘ incorporation particle size distribution of the ambient aerosol
- ✘ filter deterioration model

While the parameters already obtained have been sufficiently discussed, other parameters yet to be incorporated limit the model and should therefore be subject of this section.
As the sunroof behaves similarly to the side windows, its effect on the in-vehicle PM2.5 concentration can be modelled using the same approach. To illustrate how the model in its current form would react to an open sunroof, figure 5.1 shows a test drive with a temporarily open sunroof.

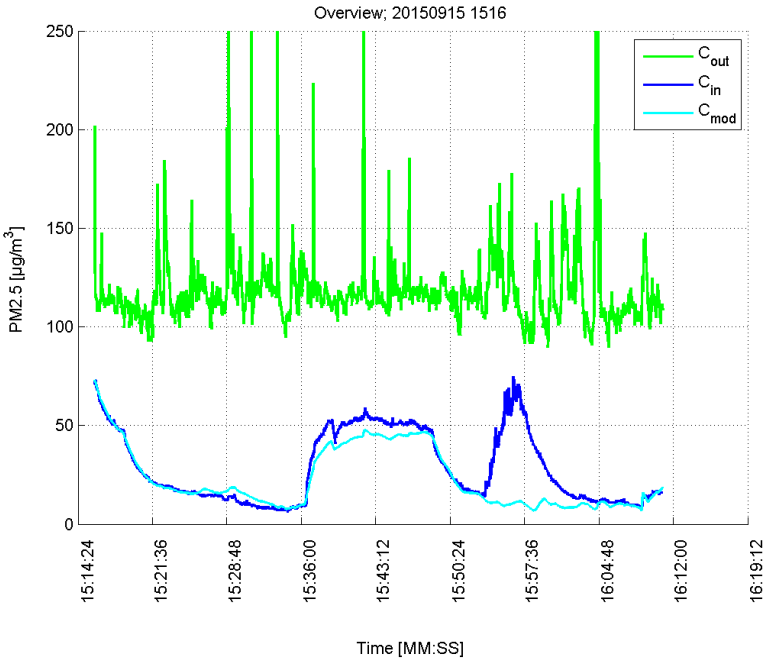

Figure 5.1: Effect of a temporary open sunroof on the predicted in-vehicle PM2.5 concentration

As can be seen, the model does not recognize the change in concentration, as it does not incorporate the sunroof. Opening the doors of the car leads to a similar behaviour. Because the state of the doors is only registered binary (open/closed) in most vehicle's software systems, it is hard to feasibly model the effect of door opening on the in-vehicle concentration. However, as the doors usually open only in standstill, this use-case occurs rather rarely. It is therefore recommended to continuously measure the inside concentration with the sensor, while the vehicle's doors are detected in an open state. Due to the season these experiments were conducted in, the effect of the heat exchanger could not be determined in a reasonable use-case, as the ambient weather did not require for the heating to be activated. In general, for the used test vehicle the ventilation speed decreases to about half of the original speed at each ventilation level. Whether there is any significant difference due to heating-up the air is yet to be examined.

5.3 Suggested improvements

As already discussed in various sections in chapter 2, the behaviour of particulate matter in an aerosol is closely linked to its composition in respect to its particle size distribution. As especially filter mechanisms are more effective for particles in a certain size range, splitting up the model into more dimensions can greatly enhance the performance of the model proposed in eq.3.7. Rather than modelling the in-vehicle mass concentration of PM2.5 in total, it is thus recommended to model

the mass concentration of particulate matter for different size ranges.

$$\begin{aligned} C_{i,in}[k] = &\left[1 + \frac{\Delta V}{V_{cab}}\varphi_{i,rc}\left(1 - \eta_{i,filt} + p_{i,leak}\right) - \zeta_i T_d - \delta_i T_d - \frac{\Delta V}{V_{cab}}\right] C_{in}[k-1] \\ &+ \left[\frac{\Delta V}{V_{cab}}\varphi_{i,oa}\left(1 - \eta_{i,filt} + p_{i,leak}\right) + \zeta_i T_d\right] C_{out}[k-1] \end{aligned} \tag{5.1}$$

However, the benefit of increased accuracy comes with the disadvantage of more computing complexity as well as more effort in parameter identification. Depending on the chosen resolution for the particle size range, the number of parameters increases significantly.
With public PM2.5 data sources increasing in number and time resolution, there may also be a feasible way to accurately estimate the outside PM2.5 concentration in the future. Irrespectively, further research on estimating the outside concentration can gradually improve the proposed model. A similar conclusion is drawn for the estimation of filter efficiency. There has been extensive research on this quantity in the past, yet the gap between theory and reality is still existing. Several approaches from different articles were merged into one model to predict the development of the filter efficiency over time. Due to a lack of precise measurement tools, facilities and material specifications, the model could not be applied and verified under real conditions. It remains to be seen whether there will be a way to model the deterioration of the filter without using specific sensors in the near past. On the other hand, if car manufacturers decide to include pressure drop sensors in their filter systems, it would also be easier to estimate the filter's fatigue. However, as will be discussed in the final section, the proposed model itself, in combination with PM2.5-sensors, can be used to estimate the filter's performance.
Regarding the multiplicity of car models today, it would also be necessary to further investigate the possibility of obtaining the mathematical model's parameter without the need of performing time-consuming parameter determination experiments for **each** car model. Here, HVAC system, interior geometry and other characteristics might be used to derive a generic parameter determination procedure.
Finally, as all the results here have been obtained in a specific geographical region and its typical weather conditions, it would be useful to improve the model by taking changes in humidity and temperature into consideration and validate the model accordingly.

5.4 Outlook

The model proposed in this thesis seems to offer qualitatively feasible results within its scope. However, as discussed in the previous section, there is still potential for further improvement. That said, the model in its current form can already be used as a foundation to conduct further research in order to generate customer benefits. Based on the observations from the conducted experiments, five use-cases for the model are implied:

Sensor-based filter deterioration detection Using a similar approach as for the original determination of the filter efficiency (see section 3.2.1), the integrated PM2.5 sensor enables a periodical determination of the filter efficiency η_{filt}. It is assumed that p_{leak} is constant over lifetime and only the filter efficiency η_{filt} is decreasing with lifetime. Given the measured average $C_{out,ss}$ of the outside concentration during the phase of steady in-vehicle concentration $C_{in,ss}$, the total penetration in outside air mode can be calculated as:

$$p_{tot} = \frac{\left(\frac{A}{V_{cab}} v_{vent} + \delta\right) C_{in,ss}}{\frac{A}{V_{cab}} v_{vent} \left[\varphi_{oa} C_{out}[k-1]\right]} \tag{5.2}$$

Based on the definition of p_{tot} (see eq.3.11) and making use of the aforementioned assumption of a constant p_{leak}, η_{filt} can be calculated as:

$$\eta_{filt} = (1 - p_{tot}) + p_{leak} v_{vent} \tag{5.3}$$

Figure 5.2 shows an example for a detection procedure in outside air mode.

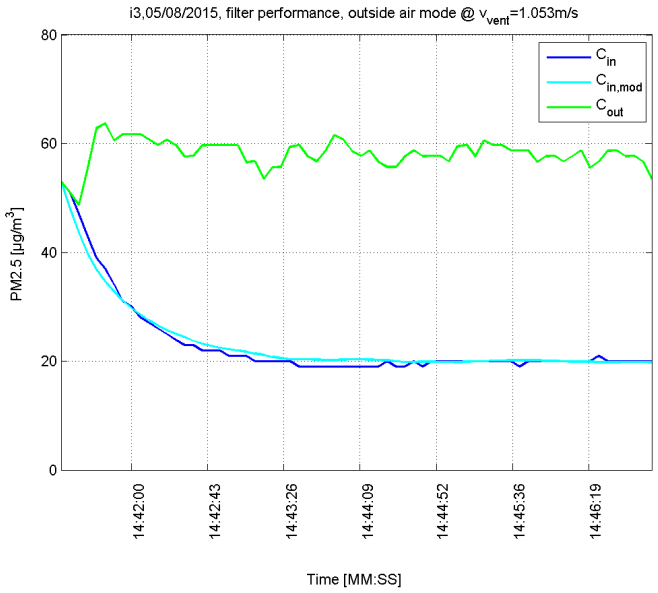

Figure 5.2: Trend curve used for the filter deterioration detection

The idea is to perform these calculations in periodical intervals of mileage, for example every 1000km of mileage since the last change of filter. This could either be done automatically in the background or by requesting the customer to confirm the execution of the detection procedure. Figure 5.3 illustrates how a pop-up in the central information display of a BMW could look like, urging the customer to change the cabin air filter.

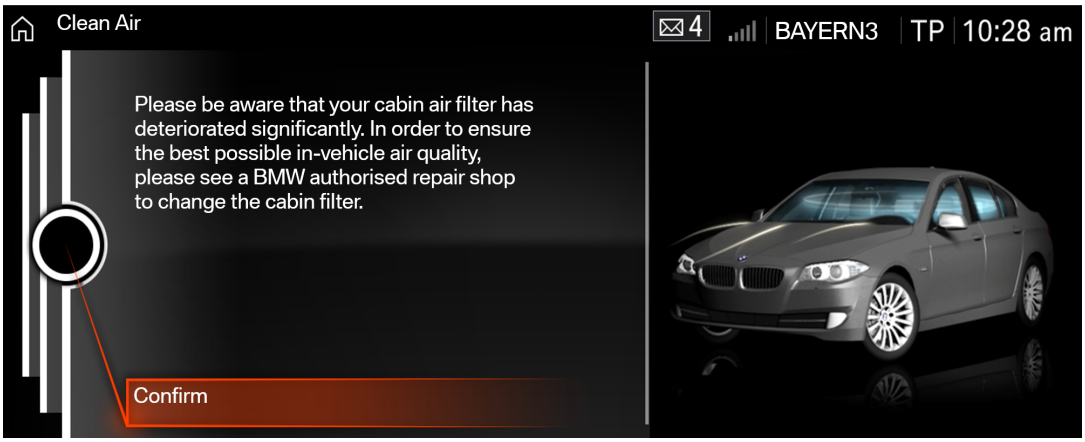

Figure 5.3:

It should be noted that as this approach would mean that the detection has to be executed in outside air mode, the passengers inside of the vehicle are exposed to a higher concentration than when in recirculation mode. In general, it would also be possible to calculate the filter deterioration in recirculation mode, but here no steady state consideration can be found and therefore it is harder to realize. Another benefit of periodical filter performance detection lies in detecting fake or low-quality replicas in order to protect the customer's health. Especially in China, it is often hard to tell if a product is authentic. Therefore, a detection of the true filter performance would create awareness for replica filters with low-efficiency.

Reducing energy consumption and enhancing lifetime of the PM2.5 sensor As already mentioned in section 4.3, the model allows to change the sampling rate at which inside and outside concentration are measured by the installed PM2.5 sensor. According to the current driving situation, the certainty of the model can be rated and the sampling rate could be adjusted accordingly. For example, blind spots of the model that are not modelled can be compensated by continuous measurement during that phase of uncertainty. As for now the impact of open doors is not modelled, however, the state of doors can be detected. A logic that increases the sampling rate of the sensor can be implemented, quasi-continuously measuring the inside concentration. After the doors are closed and the vehicle moves with windows shut, the sampling rate could be decreased, as the concentration can be estimated with a higher confidence.

Problematic situations occur whenever the customer activates a finedust source inside of the vehicle. A classic example here would be smoking. However, it is deemed to be very unlikely that a passenger smokes with closed windows. Further research on customer behaviour would have to be conducted in order to address this topic.
As a result, a decreased sampling rate of the sensor helps to reduce both fatigue and energy consumption of the sensor system. Thus, the sensor's lifetime increases or, from a different point of view, lower quality parts can be used in order to obtain the same lifetime, leading to a cost reduction.

Prediction of minimum attainable in-vehicle concentration Another possibility of exploiting the model is in using it to educate the customer. Whenever the customer chooses vehicle-specific settings that downgrade the in-vehicle air quality, a predicted minimum attainable concentration value can signal him that his behaviour is not optimal. For example, the predicted minimum attainable concentration can be presented on the same screen that shows the current in-vehicle and outside concentrations. Figure 5.4 shows the conceptual design of how this could be implemented.

Figure 5.4: Concept of how to signal the predicted best attainable in-vehicle air quality

Additionally, this concept could involve a button that automatically adapts the vehicle's settings to attain the best in-vehicle air quality. In combination, this would be a comfortable way to achieve clean air inside of the vehicle.

Qualitative monitoring and cross-validation of the PM2.5 sensor Finally, the prediction of the model can be compared to the sensor-measured results over a longer period of time, in order to implement some kind of watchdog function for the sensor. However, customer-individual behaviour could mislead this watchdog function, as the sensor may measure the true concentration, altered by the customer. Thus, further research would have to be conducted in order to find a feasible solution to use the model for this purpose.

Bibliography

[1] WHO. *Air pollution*. 2015. URL: http://www.who.int/topics/air_pollution/en/ (cit. on p. 1).

[2] "Moderate exercise: No pain, big gains". In: 11 (May 2007) (cit. on p. 1).

[3] WHO. *Life expectancy Data by country*. 2013. URL: http://apps.who.int/gho/data/node.main.688 (cit. on p. 1).

[4] Ki-Hyun Kim, Ehsanul Kabir, and Shamin Kabir. "A review on the human health impact of airborne particulate matter". In: *Environment International* 74 (2015), pp. 136–143. ISSN: 0160-4120. DOI: http://dx.doi.org/10.1016/j.envint.2014.10.005. URL: http://www.sciencedirect.com/science/article/pii/S0160412014002992 (cit. on pp. 3, 5, 6).

[5] Günter Oberdörster, Eva Oberdörster, and Jan Oberdörster. "Nanotoxicology: An Emerging Discipline Evolving from Studies of Ultrafine Particles". In: *Environ. Health Perspect.* 113 (2005), pp. 823–839. URL: http://www.ncbi.nlm.nih.gov/pmc/articles/PMC1257642/ (cit. on p. 4).

[6] WHO. *7 million premature deaths annually linked to air pollution*. 2014. URL: http://www.who.int/mediacentre/news/releases/2014/air-pollution/en/ (cit. on p. 5).

[7] Robert A. Rohde and Richard A. Muller. "Air Pollution in China: Mapping of Concentrations and Sources". In: (2015) (cit. on p. 7).

[8] WHO. *Ambient (outdoor) air pollution in cities database 2014*. 2014. URL: http://www.who.int/phe/health_topics/outdoorair/database/cities/en (cit. on p. 7).

[9] World Bank Group. *The Little Green Data Book*. Tech. rep. 2015. URL: https://openknowledge.worldbank.org/bitstream/handle/10986/22025/9781464805608.pdf (cit. on p. 7).

[10] MEP. *The State Council Issues Action Plan on Prevention and Control of Air Pollution Introducing Ten Measures to Improve Air Quality*. 2013. URL: http://english.mep.gov.cn/News_service/infocus/201309/t20130924_260707.htm (cit. on p. 9).

[11] World Steel Association. *World Steel in Figures*. Tech. rep. 2015. URL: https://www.worldsteel.org/dms/internetDocumentList/bookshop/2015/World-Steel-in-Figures-2015/document/World%20Steel%20in%20Figures%202015.pdf (cit. on p. 10).

[12] Reuter's David Stanway. *China's Hebei province says paying 'huge price' in war on pollution*. 2015. URL: http://www.reuters.com/article/2015/03/09/us-china-parliament-hebei-idUSKBN0M51M820150309 (cit. on p. 10).

[13] HJ 633–2012. *Technical Regulation on Ambient Air Quality Index (on trial)*. Tech. rep. in mandarin. 2012 (cit. on p. 11).

[14] EPA-454/B-13-001. *Technical Assistance Document for the Reporting of Daily Air Quality–the Air Quality Index (AQI)*. Tech. rep. 2013. URL: http://www.epa.gov/airnow/aqi-technical-assistance-document-dec2013.pdf (cit. on p. 11).

[15] ISO 6976:1995. *Natural gas - Calculation of calorific values, density, relative density and Wobbe index from composition*. Tech. rep. 1995. URL: http://www.iso.org/iso/iso_catalogue/catalogue_tc/catalogue_detail.htm?csnumber=13531 (cit. on p. 13).

[16] Dietrich Sonntag. "Important New Values of the Physical Constants Of 1986, Vapour Pressure Formulations Based on the ITS-90 and Psychrometer Formulae". In: *Z.Meteorol.70* (1990), pp. 340–344 (cit. on p. 13).

[17] P.T. Tsilingiris. "Thermophysical and transport properties of humid air at temperature range between 0 and 100 C". In: *Energy Conversion and Management* 49.5 (2008), pp. 1098–1110. ISSN: 0196-8904. DOI: http://dx.doi.org/10.1016/j.enconman.2007.09.015. URL: http://www.sciencedirect.com/science/article/pii/S0196890407003329 (cit. on p. 14).

[18] T.F. Irvine and P. Liley. "Steam and gas tables with computer equations". In: (1984) (cit. on p. 14).

[19] S.G Jennings. "The mean free path in air". In: *Journal of Aerosol Science* 19.2 (1988), pp. 159–166. ISSN: 0021-8502. DOI: http://dx.doi.org/10.1016/0021-8502(88)90219-4. URL: http://www.sciencedirect.com/science/article/pii/0021850288902194 (cit. on p. 15).

[20] William C. Hinds. *Aerosol Technologies - Properties, Behavior, and Measurement of Airborne Particles*. 2. Edition. John Wiley and Sons, Inc., 1999 (cit. on pp. 16, 19–21, 23, 28–32, 38).

[21] John H. Seinfeld and Spyros N. Pandis. *Atmospheric Cheistry and Physics: From Air Pollution to Climate Change*. 2. Edition. John Wiley and Sons, Inc., 2006 (cit. on p. 18).

[22] Zhijun Wu et al. "Particle number size distribution in the urban atmosphere of Beijing, China". In: *Atmospheric Environment* 42.34 (2008), pp. 7967–7980. ISSN: 1352-2310. DOI: http://dx.doi.org/10.1016/j.atmosenv.2008.06.022. URL: http://www.sciencedirect.com/science/article/pii/S1352231008006213 (cit. on p. 18).

[23] Scott A. Fruin et al. "Predictive Model for Vehicle Air Exchange Rates Based on a Large, Representative Sample". In: *Environmental Science & Technology* 45.8 (2011). PMID: 21428392, pp. 3569–3575. DOI: 10.1021/es103897u. eprint: http://dx.doi.org/10.1021/es103897u. URL: http://dx.doi.org/10.1021/es103897u (cit. on p. 24).

[24] Neelakshi Hudda et al. "Vehicle and Driving Characteristics That Influence In-Cabin Particle Number Concentrations". In: *Environmental Science & Technology* 45.20 (2011). PMID: 21928803, pp. 8691–8697. DOI: 10.1021/es202025m. eprint: http://dx.doi.org/10.1021/es202025m. URL: http://dx.doi.org/10.1021/es202025m (cit. on p. 24).

[25] N. Hudda and S. A. Fruin. "Models for Predicting the Ratio of Particulate Pollutant Concentrations Inside Vehicles to Roadways". In: *Environmental Science & Technology* 47.19 (2013). PMID: 23957386, pp. 11048–11055. DOI: 10.1021/es401500c. eprint: http://dx.doi.org/10.1021/es401500c. URL: http://dx.doi.org/10.1021/es401500c (cit. on p. 24).

[26] Lianfa Li et al. "Modeling the Concentrations of On-Road Air Pollutants in Southern California". In: *Environmental Science and Technology* 47.16 (2013). PMID: 23859442, pp. 9291–9299. DOI: 10.1021/es401281r. eprint: http://dx.doi.org/10.1021/es401281r. URL: http://dx.doi.org/10.1021/es401281r (cit. on p. 24).

[27] Pouyan Joodatnia, Prashant Kumar, and Alan Robins. "Fast response sequential measurements and modelling of nanoparticles inside and outside a car cabin". In: *Atmospheric Environment* 71 (2013), pp. 364–375. ISSN: 1352-2310. DOI: http://dx.doi.org/10.1016/j.atmosenv.2013.02.028. URL: http://www.sciencedirect.com/science/article/pii/S1352231013001295 (cit. on p. 24).

[28] Xiaozhen Liu and H. Christopher Frey. "Modeling of in-vehicle human exposure to ambient fine particulate matter". In: *Atmospheric Environment* 45.27 (2011), pp. 4745–4752. ISSN: 1352-2310. DOI: http://dx.doi.org/10.1016/j.atmosenv.2011.04.019. URL: http://www.sciencedirect.com/science/article/pii/S1352231011003888 (cit. on pp. 24, 46).

[29] Wayne Ott, Neil Klepeis, and Paul Switzer. "Air change rates of motor vehicles and in-vehicle pollutant concentrations from secondhand smoke". In: *Journal of Exposure Science and Environmental Epidemiology* 18 (2007), pp. 312–325 (cit. on pp. 24, 46).

[30] Ryan Allen et al. "Evaluation of the recursive model approach for estimating particulate matter infiltration efficiencies using continuous light scattering data". In: *Journal of Exposure Science and Environmental Epidemiology* 17 (2006), pp. 468–477 (cit. on p. 25).

[31] Jae Hong Park et al. "Removal of PM2.5 entering through the ventilation duct in an automobile using a carbon fiber ionizer-assisted cabin air filter". In: *Journal of Aerosol Science* 41.10 (2010), pp. 935–943. ISSN: 0021-8502. DOI: http://dx.doi.org/10.1016/j.jaerosci.2010.07.005. URL: http://www.sciencedirect.com/science/article/pii/S0021850210001655 (cit. on pp. 25, 37, 48).

[32] I. B. Stechkina, A. A. Kirsch, and N.A. Fuchs. "Studies on Fibrous Aerosol Filters–IV. Calculation of Aerosol Deposition in Model Filters the Range of Maximum Penetration". In: *Ann. Occ. Hyg.* 12 (1969), pp. 1–8 (cit. on p. 30).

[33] J. A. Hubbard et al. "Fibrous Filter Efficiency and Pressure Drop in the Viscous-Inertial Transition Flow Regime". In: *Aerosol Science and Technology* 46 (2012), pp. 138–147 (cit. on p. 30).

[34] T. Frising et al. "Influence of Filter Fibre Size Distribution on Filter Efficiency Calculations". In: *Chemical Engineering Research and Design* 81.9 (2003). 9th Congress of the French Society of Chemical Engineering, pp. 1179–1184. ISSN: 0263-8762. DOI: http://dx.doi.org/10.1205/026387603770866353. URL: http://www.sciencedirect.com/science/article/pii/S0263876203724149 (cit. on p. 33).

[35] A. Joubert et al. "Modelling the pressure drop across {HEPA} filters during cake filtration in the presence of humidity". In: *Chemical Engineering Journal* 166.2 (2011), pp. 616–623. ISSN: 1385-8947. DOI: http://dx.doi.org/10.1016/j.cej.2010.11.033. URL: http://www.sciencedirect.com/science/article/pii/S1385894710011174 (cit. on p. 33).

[36] D. Thomas et al. "Clogging of fibrous filters by solid aerosol particles Experimental and modelling study". In: *Chemical Engineering Science* 56.11 (2001), pp. 3549–3561. ISSN: 0009-2509. DOI: http://dx.doi.org/10.1016/S0009-2509(01)00041-0. URL: http://www.sciencedirect.com/science/article/pii/S0009250901000410 (cit. on pp. 34, 35, 54).

[37] R.C. Brown. "Capture of dust particles in filters by linedipole charged fibres". In: *Journal of Aerosol Science* 12.4 (1981), pp. 349–356. ISSN: 0021-8502. DOI: http://dx.doi.org/10.1016/0021-8502(81)90024-0. URL: http://www.sciencedirect.com/science/article/pii/0021850281900240 (cit. on p. 36).

[38] Myonghwa Lee et al. "Prediction of Collection Efficiency of High-performance Electret Filters". In: *JOURNAL OF CHEMICAL ENGINEERING OF JAPAN* 35.1 (2002), pp. 57–62. DOI: 10.1252/jcej.35.57 (cit. on p. 36).

[39] J.H. Ji et al. "Effect of particle loading on the collection performance of an electret cabin air filter for submicron aerosols". In: *Journal of Aerosol Science* 34.11 (2003), pp. 1493–1504. ISSN: 0021-8502. DOI: http://dx.doi.org/10.1016/S0021-8502(03)00103-4. URL: http://www.sciencedirect.com/science/article/pii/S0021850203001034 (cit. on p. 38).

[40] TSI PD-001. *Getting data you need with particle measurements*. Tech. rep. 2012 (cit. on pp. 39, 40).

[41] Julius Sendroy Jr. and Harold A. Collison. "Determination of human body volume from height and weight". In: *Journal of Applied Physiology* 21.1 (1966), pp. 167–172 (cit. on p. 61).

[42] TSI EXPMN-007. *Rationale for programming a photometer calibration factor (PCF) of 0.38 for ambient monitoring*. Tech. rep. 2013 (cit. on p. 62).

List of Figures